ROLE OF BINDER COMPOSITIONS AND CARBONATE POLYMORPHS ON THE PERFORMANCE OF CARBONATION ACTIVATED CEMENTITIOUS COMPOSITES

by

MOHAMMAD RAKIBUL ISLAM KHAN

Presented to the Faculty of the Graduate School of
The University of Texas at Arlington in Partial Fulfilment of
the Requirements for the Degree of

DOCTOR OF PHILOSOPHY
THE UNIVERSITY OF TEXAS AT ARLINGTON

December 2021

THE UNIVERSITY OF TEXAS AT ARLINGTON

GRADUATE SCHOOL STATEMENT OF COMMITTEE APPROVAL

Dr. Warda Ashraf, Chair

Assistant Professor, Civil Engineering Department, University of Texas at Arlington

Dr. Surendra P Shah

Professor, Civil Engineering Department, University of Texas at Arlington

Dr. Nur Yazdani

Professor, Civil Engineering Department, University of Texas at Arlington

Dr. Frank W Foss

Professor, Chemistry and Biochemistry Department, University of Texas at Arlington

ABSTRACT

Title of Dissertation: Role of Binder Compositions and Carbonate Polymorphs on The Performance of Carbonation Activated Cementitious Composites

Mohammad Rakibul Islam Khan, Ph.D.

The University of Texas at Arlington, 2021

Supervising Professor: Dr. Warda Ashraf

The most energy-intensive manufacturing industry in the US is the Ordinary Portland Cement (OPC) industry. This industry is responsible for 5-8% of global CO_2 emissions caused by humans. The calcination of limestone to produce high lime calcium silicate and high manufacturing temperature (1450°C) are responsible for this significant amount of CO_2 emissions. This CO_2 footprint of the cement-based composites can be decreased by utilizing cementitious materials with low-lime calcium silicate. Low-lime calcium silicates are typically semi-hydraulic or non-hydraulic. As a result, it is necessary to activate those materials in order to increase their reactivity. Alkali activators, carbonation curing (CO_2 curing), and other techniques have been shown in recent investigations to substantially increase the reactivity of those materials.

Calcium silicate combines with CO_2 in the presence of water to produce $CaCO_3$ and calcium-modified silica gel during the carbonation curing procedure. As a result of this technique, low-lime calcium silicate can now be used as an OPC replacement.

This study looked into the specifics of effective carbonation curing and reaction kinetics for hydraulic, semi-hydraulic, and non-hydraulic calcium silicate. The influences of minerals and biopolymers on the carbonation curing phase were also investigated in this study.

In order to construct the new binder composition successfully, an in-depth investigation into the performance of the OPC-slag blended system due to carbonation curing was conducted. This detailed investigation revealed that slag might replace 65% of OPC without degrading compressive strength. Slag accelerates the carbonation process. Slag carbonation also improves the concrete's durability by reducing permeability. Silica gel polymerization was enhanced by increasing the amount of slag and the carbonation duration. This research also shows that pre-hydration curing prior to carbonation improves mechanical and microstructural properties.

The impacts of biopolymers on carbonation-activated binders were investigated in this study. When biopolymers like dopamine hydrochloride come into contact with hydraulic/semi-hydraulic calcium silicate, they polymerize and produce polydopamine. Polydopamine has a greater affinity for Ca^{2+} and prevents amorphous $CaCO_3$ from clustering together. As a result, when dopamine is incorporated into a carbonate matrix, more amorphous $CaCO_3$ is produced than calcite. The effects of cellulose nanofibers were also studied. Cellulose nanofibers can significantly improve the early age strength gain and flexural strengths of carbonated composites.

Finally, the impacts of MgO-based cementitious materials on carbonated semi-hydraulic and non-hydraulic systems were studied in this section. This extensive investigation discovered that MgO-based cement produced more hydro-magnesite when mixed with non-hydraulic calcium silicate during carbonation curing. It's worth noting that hydrated magnesium carbonate has a 600% higher solid volume than magnesium oxide. Because of the substantial volume increase, the microstructure has significantly densified, and the critical pore size distribution has changed. As a result, adding MgO improves mechanical performance substantially. It also helps to increase CO_2 sequestration.

ACKNOWLEDGMENTS

All praise to Allah, for giving me the resilience to accomplish this dissertation.

I would like to convey my heartfelt gratitude to Prof. Warda Ashraf, my Ph.D. supervisor, whose outstanding mentoring was vital in the completion of this dissertation. I will be eternally grateful to her for her kind support and encouragement during my graduate studies. I genuinely admire her kind intention to infuse creativity into the minds of her students. Her supervision and guidance facilitated the development of my research skills and increased my confidence. Her insightful comments were extremely beneficial to my academic progress.

I would like to thank the members of my dissertation committee, Prof. Surendra P Shah, Prof. Nur Yazdani, and Prof. Frank W Foss, for their insights and helpful suggestions in enhancing the effectiveness of my research.

I like to thank Dr. Jiechao Jiang for always having his door open for me.

I would like to acknowledge funding support from the following sources:

- Transportation Infrastructure Durability Center at the University of Maine, USA
- University of Texas at Arlington's faculty start-up grant to Dr. Warda Ashraf
- National Science Foundation (NSF)
- Defense Advanced Research Projects Agency (DARPA), Young Faculty Award

My deepest gratitude goes to all my family members, friends, and lab mates.

DEDICATION

Dedicated to my parents, in laws, wife, daughter, and sister for their unconditional love and support.

LIST OF FIGURES

LIST OF TABLES

TABLE OF CONTENT

Chapter 1: Research Background, Objectives, and Organization

1.1 Introduction

Concrete is the world's second most consumed material in terms of total volume, after water. One of the most important components in concrete is ordinary Portland cement (OPC). Portland cement contains more than two-thirds of calcium silicates (tricalcium silicate (C_3S) and dicalcium silicate (C_2S))[1], calcium aluminate, and calcium aluminoferites [1]. Calcium comes from natural raw materials like limestone, marl, and seashells, while silica comes from clays and shales. As shown in Figure 1.1, these natural minerals are mixed and calcined at 1450 to 1500°C to produce OPC. During the calcination ($CaCO_3 \rightarrow CaO + CO_2$) process, a significant amount of CO_2 is released into the atmosphere. The combination of this released CO_2 and increased OPC usage accounts for 5-8% of global man-made CO_2 emissions from the cement industry [2]. The increased CO_2 emissions raise greenhouse gas levels and contribute to global warming. The cement and concrete industry is interested in finding alternative cementitious materials that will offer a lower carbon footprint compared to OPC. Portland Limestone Cement (PLC) [3,4], Alkali activated materials (including geopolymers) [5], OPC with high volume SCMs [6,7], and Carbonation-activated binders [8,9] are potential examples of cementitious materials with a low carbon footprint. Among these options, carbonation activated binders are the most recently developed material that, in addition to reducing the carbon emissions from the production process, can further sequester a significant portion of CO_2 during the hardening process. The primary goal of this thesis is to

[1] C=CaO, S=SiO_2

identify the potential routes for enhancing the mechanical performance and CO_2 sequestration capacity of calcium silicate-based carbonation-activated binders. This chapter presents a review of the background knowledge on this topic, identifies the knowledge gaps, and specifies the research objectives of the thesis.

1.2 Background

During the carbonation process, calcium silicates react with CO_2 in the presence of water and form $CaCO_3$ and Ca-modified silica gel. Calcite, aragonite, and vaterite are different crystal polymorphs of $CaCO_3$ that result from the carbonation curing of calcium silicate [10]. Carbonated binders can be formed using hydraulic (e.g., alite, belite, etc.) and/or semi-/non-hydraulic low-lime calcium silicate (i.e., wollastonite, rankinite, slag) [11]. Semi-/non-hydraulic calcium silicates show increased reactivity in the presence of CO_2 [12]. This binder accounts for 70% fewer carbon footprints compared to traditional binders [11]. These carbonated binders are showing a new path in cement materials research. The idea behind carbonation-activated binders is that certain raw materials can be hardened by carbonation curing. Low lime semi-/non-hydraulic binders can be hardened using the 'mineral carbonation' principle, which is one of the safest long-term CO_2 sequestration solutions. CO_2 reacts with minerals containing calcium or magnesium to form stable carbonate in mineral carbonation. Carbonated cementitious binders have received a lot of attention in recent years, owing to their rapid strength gain and CO_2 sequestration when exposed to a CO_2-rich environment.

1.2.1 Carbonation curing

The invention of ordinary Portland cement (OPC) in the early nineteenth century set a new standard for hydraulic binders, on which today's giant concrete industry is built. Cement hydration

is accomplished through wet or sealed curing of freshly cast concrete, which results in hydrated products such as $Ca(OH)_2$ and calcium silicate hydrate (C-S-H) gel.

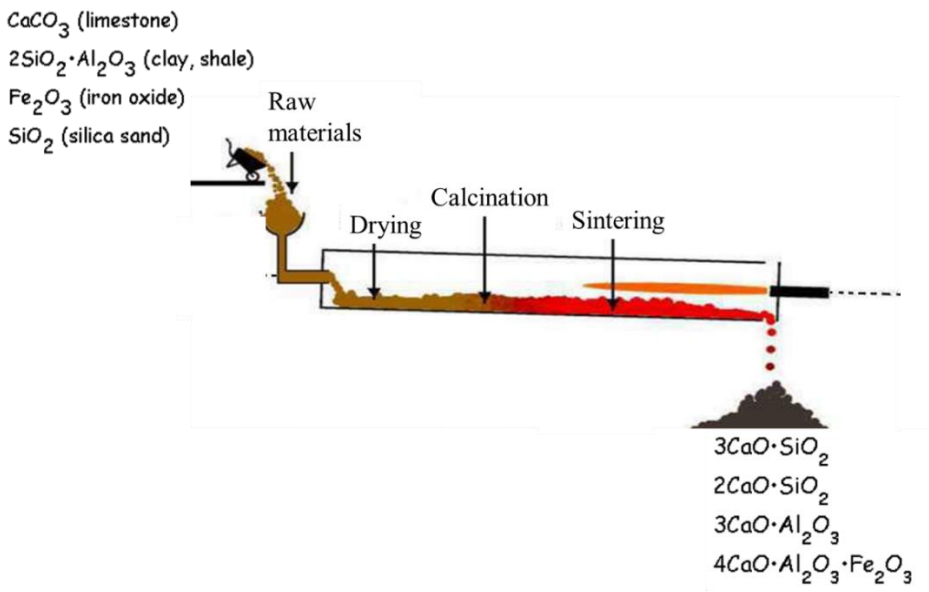

Figure 1.1: Portland cement manufacturing process

The concept of using CO_2 to cure cementitious material was first suggested in the 1970s [13]. In recent years, the carbonation curing of cement-based materials has received a lot of attention, particularly in light of new carbon-reduction initiatives. Carbonation curing has emerged as a promising technology in the cement-based composite industry, owing to three advantages: i) significant CO_2 consumption and storage potential; ii) property enhancement for cement-based composite products, and iii) economic advantages for the precast industry [14]. Carbonation curing of cementitious composites has been investigated for its ability to accelerate strength gain and integrate carbon dioxide in the cementitious matrix. The use of CO_2 in construction materials is not a new phenomenon. It all started in Ancient Rome when a mortar made of lime, sand, and water was revealed to have enhanced binding strength after steadily reacting with CO_2 in the atmosphere [13]. The mortar used in the building of China's Great Wall had a similar enhancement effect. Carbonation cure approaches have been debated with trepidation due to the high cost of

pure CO_2 production and the negative effects of weathering carbonation. Weathering carbonation is the adverse effect of atmospheric CO_2 on mortars and concrete caused by the decalcification of C-S-H gel. However, after the 2000s, the importance of reducing carbon emissions rekindled interest in carbonation curing [15]. Carbonation curing at an early age (0 to 7 days after mixing and casting) engages anhydrous binder minerals to generate a binding matrix as compared to 'weathering carbonation' wherein hydration products are damaged by atmospheric CO_2. Instead of acting as a catalyst, CO_2 gas serves as a reactant, resulting in a binding matrix that differs from that obtained through traditional hydration.

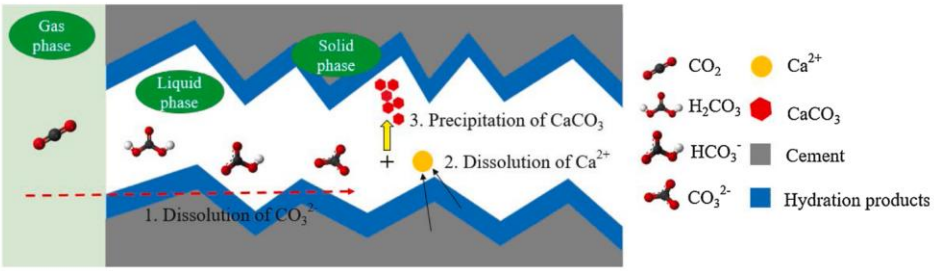

Figure 1.2: Carbonation mechanism of cement-based materials. Adopted from [14].

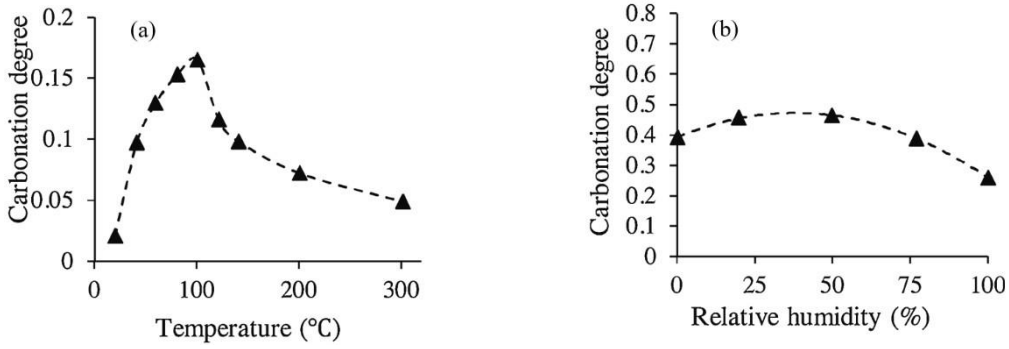

Figure 1.3: Relationship between carbonation degree with (a) Temperature, (b) Relative humidity. Adopted from [14]

Figure 1.2 depicts the carbonation curing procedure where CO_2 is transported and dissolved first, resulting in carbonate ions. Then, Ca^{2+} ions release from cement-based materials, followed by a reaction between Ca^{2+} ions and carbonate ions.

Early-age carbonation curing of OPC-based materials is normally carried out at room temperature (20–25 °C) in most studies. Additionally, the temperature can influence the reaction rate in a variety of ways. Higher temperatures facilitate CO_2 diffusion and ion migration while decreasing aqueous solubility. Furthermore, it enhances water evaporation. To compensate for water evaporation during high-temperature carbonation curing, researchers suggested soaking the sample for 1 minute after certain intervals [14]. The effect of temperature on the degree of carbonation is shown in Figure 1.3 (a). It indicates that the amount of carbonation reaction increases until the temperature reaches 100°C, after which it begins to decrease. Higher temperature increases early compressive strength in an OPC-slag blend system [16]. Qian et al. demonstrated that the optimal temperature for an OPC-Slag blend carbonation system is 60°C. Optimal CO_2 diffusion and thus carbonation reaction commonly prefer ambient range relative humidity (RH). RH of 50-70% is commonly used in studies on carbonation curing of OPC. In situations where the temperature is high or the w/s ratio is low, a RH of about 90% is often used to avoid water evaporation. However, carbonation curing is primarily studied on a laboratory scale due to two major challenges that must be overcome before it can be widely used in industrial-scale production: (a) because of the limitation of CO_2 diffusion into the matrix during carbonation curing, CO_2 sequestration rates remain low, ranging between 20% and 50% of theoretical capacity; and (b) the impact of carbonation curing on the durability of cement-based composites, as well as the mechanisms underlying it, remains unknown, particularly for some critical aspects such as alkali-silica reaction, corrosion, and sulfate attack.

1.2.2 Chemical reactions in carbonation cured system

More than 60% of the volume of hydraulic OPC or semi-hydraulic slag is calcium silicate ($CaO.SiO_2$), which is mainly responsible for the engineering properties of concrete products. In a hydrated system, calcium silicate reacts with water (H_2O) to form calcium hydroxide ($Ca(OH)_2$) and calcium silicate hydrate (C-S-H) gel, as shown in eqn. 1. Similarly, calcium silicate reacts with CO_2 in the presence of moisture (H_2O) to produce $CaCO_3$ and C-S-H gel during carbonation curing as shown in eqn. 2. As eqn. 3 shows, further carbonation of C-S-H results in decalcification and subsequent transformation to silica gel and $CaCO_3$. Although the formation of C-S-H from carbonation itself is controversial, definitive proof points to a gel-like amorphous phase with a lower CaO/SiO_2 ratio than C-S-H produced hydraulically from calcium silicates. This gel phase is also known as decalcified C-S-H gel or polymerized silica gel in some studies [17]. The formation of $CaCO_3$ and Ca-modified silica gel is the main binding phase in the carbonation cured system. $CaCO_3$ formed during carbonation has many polymorphs, including calcite, vaterite, aragonite, and amorphous. The presence of a ^{13}C CP/MAS NMR signal in carbonated C_3S, C_2S, and C_3S_2 phases can be due to the formation of amorphous calcium carbonate (ACC) [17]. The strength of carbonated calcium silicate matrices is increased by the existence of poorly crystallized forms of $CaCO_3$. Furthermore, due to the presence of different polymorphs of $CaCO_3$ crystals, the elastic modulus of $CaCO_3$-rich binders can vary across a broad range.

$$CaO.SiO_2 + H_2O \rightarrow Ca(OH)_2 + C-S-H \quad \text{eqn. 1}$$

$$CaO.SiO_2 + H_2O + CO_2 \rightarrow CaCO_3 + C-S-H \quad \text{eqn. 2}$$

$$C-S-H + CO_2 \rightarrow CaCO_3 + SiO_2 + H_2O \quad \text{eqn. 3}$$

1.2.3 Ca- and Mg- based carbonation activated binders

Carbonation of non-hydraulic or slowly hydrated minerals opens the door to use CO_2-activated binders that need less energy. Belite (β-C_2S) and wollastonite (CS), both calcium-silicate minerals, have been evaluated as possible OPC substitutes. Tricalcium silicate (C_3S), β-dicalcium silicate (β-C_2S), γ-dicalcium silicate (γ-C_2S), tricalcium disilicate (C_3S_2), and monocalcium silicate (CS) can react with CO_2 and form strong monolithic matrices. Belite-rich (C_2S) cement has a greater impact on mechanical properties as it is more reactive to CO_2 than alite-rich (C_3S) cement. At an early age, carbonation curing accelerated belite reaction and improved flexural strength and toughness. CO_2 can activate all polymorphs for strength gain, as shown in eqn. 2. Calcium silicate minerals such as wollastonite, in addition to C_3S and C_2S, achieve strength by reacting with CO_2 and H_2O. Ashraf & Olek showed that the degree of polymerization of Ca-modified silica gel (which is determined by the inverse of the Ca/Si ratio) is nearly identical for all of the carbonated calcium silicates, with the exception of carbonated C_3S, which has a slightly lower degree [17]. Figure 1.4 depicts the aqueous CO_2 reactivity of minerals studied in cement-based materials in a simplified ternary phase diagram.

Recently, MgO has been used as an SCM and cured by carbonation in cementitious materials, which has piqued the interest of researchers. MgO has a high CO_2 sequestration potential and a lower calcination temperature (700–1000 °C for $MgCO_3$ versus 1450 °C for $CaCO_3$) [14]. Calcite, aragonite, C-S-H, magnesium calcite, and nesquehonite all coexisted in the MgO-OPC system. The densification of pore structure and increased microhardness were attributed to these identified components. As compared to portlandite carbonation, brucite carbonation seems to have contributed more to compressive strength [18].

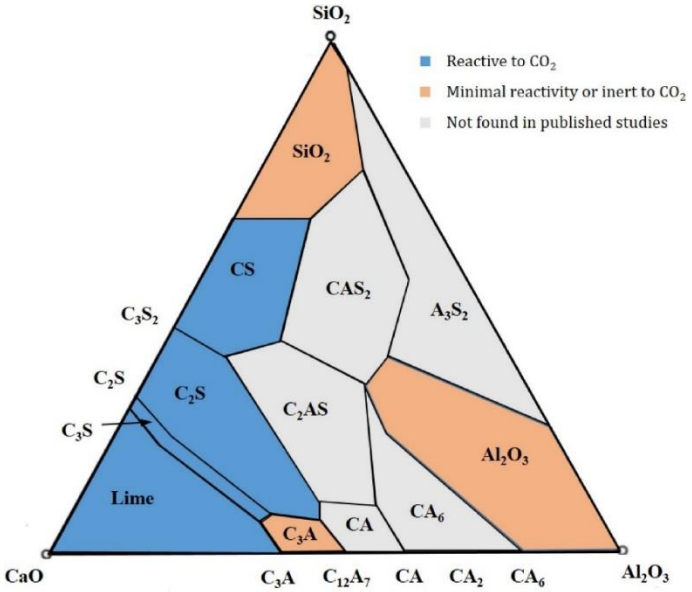

Figure 1.4: Simplified CaO-SiO-Al_2O_3 ternary phase diagram depicting aqueous CO_2 reactivity of minerals studied in cement-based materials, adopted from [13].

Walling and Provis investigated the chemistry of producing magnesia-based cement and found that carbonation was the best option [19]. The reactivity was reported to be temperature sensitive during synthesis [20]. MgO reacts with H_2O to form $Mg(OH)_2$. The strength of hydrated $Mg(OH)_2$ is minimal. When CO_2 is incorporated, such as in eqn. 5, magnesium carbonate hydrate is formed, which is the primary binding agent. CO_2 concentration and relative humidity affect the carbonation reaction in magnesia-based cement. The densification of materials caused by the formation of nesquehonite ($MgCO_3.3H_2O$), dypingite ($Mg5(CO_3)_4(OH)_2.5H_2O$), and artinite ($Mg_2(OH)_2CO_3.3H_2O$) increases the compressive strength of magnesium-rich cement. In carbonated magnesia-based binders, nesquehonite has been described as the primary binding phase.

$$MgO + H_2O \rightarrow Mg(OH)_2 \qquad \text{eqn. 4}$$

$$Mg(OH)_2 + CO_2 + (n-1)H_2O \rightarrow MgCO_3.nH_2O \quad \text{eqn. 5}$$

Supplementary cementitious materials such as slag and fly ash are reactive to carbonation. Other SCMs, such as silica fume and metakaolin, are inert to carbonation, but their presence can influence carbonation activity by acting as a nucleation site, facilitating $CaCO_3$ precipitation. Those industrial wastes follow this mineral composition requirement, prompting several studies to look at the use of such waste materials in construction and envisioning alternative concrete raw materials with a low carbon footprint [13].

1.2.4 Slag as a carbonation activated binder

Infrastructure, cars, buildings, industrial facilities, and a variety of other daily necessities all necessitate the supply of essential materials, which the iron and steel manufacturing industries provide. In 1967, global steel production was less than 500 million tonnes, compared to 1599.5 million tonnes in 2015. Steel production increased significantly in 2016, with a total of 1666.2 million tonnes recorded [21,22]. This massive volume of steel processing also results in a significant amount of waste materials (i.e., slag). Slag is a byproduct of the incineration processing of a variety of ores. The global production of slag is estimated to be 1600 million tonnes per year [23]. Research is going on to find a way to deal with the massive amount of slag that has accumulated. The use of slag as supplementary cementitious material is environmentally, economically, and technically viable and attractive, as it has the ability to minimize material usage, energy costs, and waste storage areas. Globally, 5–10% of slag is reused as cement additives [24].

The three primary areas of slag reuse research include slag usefulness as a construction material, metal recovery from slag, and slag use in environmental remediation applications. Slag's chemical composition illustrates its mechanical strength. The higher the alkalinity content of the slag, the

higher the hydraulic property. Hydraulic calcium silicates (C_3S, β- C_2S), non-hydraulic calcium silicates (e.g., γ-C_2S, CS), and free CaO are all components of slag that can react with CO_2. Calcium carbonate (calcite and aragonite) is the main carbonate product formed.

Carbon sequestration by industrial wastes such as slags and fly ash has been the subject of extensive research. Monkman and Shao compared the carbonation of EAF slag, GGBF slag, and CaO-rich fly ash compacts and found that carbonated EAF slag had the highest CO_2 absorption and intensity [25]. Mahoutian et al. investigated ladle slag and found a compressive strength of 35 MPa on compacted mortars after a 24-hour cure [26]. Carbonation of KOBM slag was investigated by Ghouleh et al., who found that this C_2S-rich material was extremely CO_2 reactive, achieving compressive strength of 80 MPa in 2 h due to γ-C_2S carbonation [27].

1.2.4.1 CO_2 Sequestration

More recently, a global study found that 4.5 Gt of CO_2 had been absorbed into existing cement from 1930 to 2013, offsetting 43% of CO_2 emissions due to cement output over the same time span [28]. Mahoutian and Shao went one step further, replacing OPC as the binder for CMU production with steel slag. The cement-free unit could have a net CO_2 footprint of less than 0.23 kg, making it a CO_2-negative product [29]. In Hong Kong, Xuan et al. looked into concrete blocks for the local market and estimated that using carbonation curing could sequester 4900t of CO_2, which would offset 0.13-0.35 percent of CO_2 produced annually by Hong Kong's cement manufacturing industries [30]. If carbonation curing could be justified on precast reinforced concrete, this capability could be increased even further.

If the amount of slag in the concrete increases, the gas permeability of the concrete increases, and the carbonation reaction in slag-containing concrete cause the pore structure to coarsen, allowing

more CO_2 to enter the concrete more easily [31]. The carbonation reaction increases with increasing slag content. Monkman and Shao demonstrated that in the presence of slag, dispersed OPC particles carbonated further. According to them, slag facilitated intensive carbonation of OPC particles by allowing CO_2 to penetrate deeper into the sample before being slowed by carbonation products [32].

The compressive strength behavior was accompanied by a carbon dioxide absorption study, as predicted by the researchers. CO_2 uptake was higher in samples that developed a high compressive strength [27].

1.2.4.2 Durability

Carbonation of slag improves early strength and long-term durability, even though research on the reliability of a carbonated slag system is still scarce. The denser microstructure imparted by carbonation curing improves concrete toughness noticeably. Carbonated areas have very low permeability, according to measurements of surface air permeation and electrical resistivity [33]. Furthermore, rapid chloride permeability and natural chloride ingress after wet-dry exposure show that carbonation-cured concrete has a higher resistance to chloride permeation. It's also said to be more resistant to freeze-thaw degradation. The effects of sulfate attacks are also reduced. Metal ions were also found to be less soluble in carbonation-cured cement pastes in previous studies. The carbonated rim surrounding the cement grains, where the immobile metal ions become confined, was blamed for the reduced leaching activity. Other studies involving the carbonation of hydrated cement materials, on the other hand, recorded a decrease in overall leaching but a possible increase in calcium ion leaching. Dissolution erosion can occur due to the high solubility of $Ca(OH)_2$ and CSH gel. Carbonation transforms highly soluble $Ca(OH)_2$ (approximately 1.2 g/L) to less

soluble/insoluble $CaCO_3$ (approximately 4 x 10-3 g/L). As a result, carbonation curing effectively prevents dissolution degradation and improves durability [16].

1.2.4.3 Effects on microstructure

Despite morphological similarities between carbonation-cured and normal moist-cured specimens, $CaCO_3$ precipitation creates a denser microstructure in carbonated OPC-slag paste. As a result, total and capillary porosities are reduced, modifying the paste's transport properties to show lower absorption and permeability on concretes [34]. The amount of densification depends on the clinker's mineral composition. Jang et al. stated that the carbonation of belite produced less pore volume and connectivity than that of alite [35].

Carbonation curing at higher temperatures increases the C_3S peak in XRD, implying that the early and later hydration reaction is also increased [16]. Carbonation curing also improves the crystal structure of $Ca(OH)_2$. Carbonation of C_3S and C_2S results in an 11.5% rise in volume, which compensates for shrinkage during carbonation [36].

The surface of the specimen subjected to carbonation curing has fewer cracks than the surface subjected to hydration curing. The carbonation-cured surface has a thick shell of rubbly $CaCO_3$ with particle sizes ranging from 1 to 8 μm [16]. This fine particle size creates micro aggregation, which improves the compactness of the carbonated matrix by providing nucleation points for C_3S. This type of structure has high mechanical properties.

$CaCO_3$ appears in a variety of shapes and sizes, including spherical vaterite, needle-shaped aragonite, and rhomboidal calcite, with calcite being the most stable. El-Hassan et al. discovered the coexistence of calcite, vaterite, and aragonite in a carbonated matrix, as well as a 50-80% transformation of amorphous to stable calcite [37]. As shown in Figure 1.5, carbonated C-S-H gel

has a higher degree of polymerization than hydrated C-S-H gel. Interlayer Calcium is extracted, and Si-OH is concentrated into Si-O-Si during the carbonation process. As a result, C-S-H gel decalcification occurred, and silicate chain lengthening occurred.

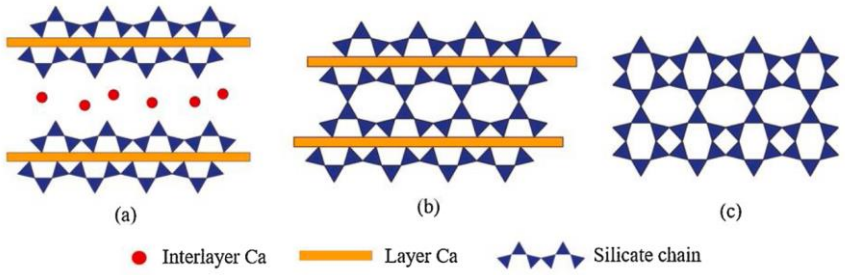

Figure 1.5: CSH structure in carbonation curing: (a) CSH from hydration, (b) decalcified CSH, (c) silica gel formation [14].

As shown in Figure 1.6, the inclusion of fiber in the cementitious matrix increases the formation of $CaCO_3$ and increases the high-density region.

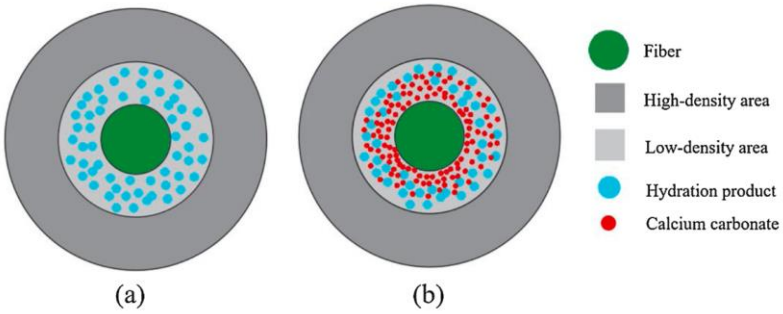

Figure 1.6: Effects of carbonation on fiber-matrix interface (a) uncarbonated, (b) carbonated [14]

1.3 Research objectives and thesis organization

Based on the previous studies, it is evident that the carbonation cured calcium silicate represents an environmentally friendly binder system that can offer similar performance as traditional OPC

binders. However, as a relatively new type of binder, how different curing regimes, supplementary cementitious materials, and organic additives affect the performance of this binder remains unexplored. With the primary goal of providing a fundamental understanding of how CO_2 sequestration and mechanical performance of the carbonation cured calcium silicates can be enhanced, the followings are the specific research objectives of this thesis.

Research objective 1: Understand how the combination of hydraulic calcium silicates (i.e., OPC) and semi-hydraulic calcium silicates (i.e., slag cement) can be capitalized to enhance the microstructure, mechanical performance, durability performance, and CO_2 sequestration capacity of carbonated cured binders. The research activities associated with this objective are presented in Chapter 2 of the thesis.

Research objective 3: Investigate if the application of biopolymers as an organic admixture can lead to superior mechanical performance and CO_2 sequestration of carbonation calcium silicate binders. The research activities corresponding to this objective are presented in Chapter 3 of the thesis.

Research objective 2: Investigate how the Mg-based supplementary cementitious material affects the mechanical performance and CO_2 sequestration capacity of carbonation cured calcium silicate binders. The research activities corresponding to this objective are presented in Chapter 3 of the thesis.

As discussed above, in this dissertation, three novel routes for improving the overall performance of carbonation-cured calcium silicates were investigated. While the primary goal was to improve the performance of the binder, comprehensive experimental plans were executed to understand the role of microscopic phase formation in the carbonation cured system for each of the selected routes.

These three routes were selected based on an extensive literature survey, which is discussed in the corresponding chapters.

This dissertation follows the article-based dissertation wherein chapters 2, 3, and 4 contain a full individual manuscript. Co-author Muhammad Intesarul Haque helped to perform durability tests in chapter 2 and nanoindentation for chapters 3 and 4. Prof. Ashraf supervised and reviewed all the experimental works and writings.

Chapter 2: Binary cement containing Slag and Portland Cement for Optimum Carbonation Curing

This work will be submitted for publication as bellow:

Rakibul I. Khan, Warda Ashraf, Muhammad Intesarul Haque, "Blended Slag Cement and Ordinary Portland Cement for Optimum Carbonation Curing".

2.1 Abstract

The use of accelerated carbonation curing is a promising way to reduce the carbon footprint of concrete. This article presents an investigation into the potential use of ground granulated blast-furnace slag cement (SC) as a replacement to Ordinary Portland Cement (OPC) in carbonation cured cement-based materials. To investigate the effects of carbonation on mechanical performances and microstructures, 0%-100% OPC was replaced with slag cement. Thermogravimetric analysis and Fourier transformed infrared (FTIR) spectra were utilized to investigate the carbonation reaction extent rate and microstructural phase formations. Slag cement was found to improve the efficiency and rate of carbonation. This study revealed that a minimum of 72 hours of carbonation in a CO_2-containing environment yields better mechanical performance compared to the traditional curing method. Specifically, the incorporation of 72 hours of carbonation curing was observed to increase the strength of concrete up to 30% after 28 days of total curing duration (carbonation and hydration). The chloride permeability of the carbonation cured samples was observed to reduce by 80% due to the addition of SC. Finally, slag cement was found to increase the degree of silicate polymerization in the CSH gel and reduce the amount of $Ca(OH)_2$ present in the carbonation-cured blended cement pastes.

Keywords: Carbonation curing, Portland cement, slag cement, microstructure

2.2 Introduction

Slag cement (SC) is a supplementary cementitious material produced as a byproduct of the steel industry [38]. This semi-hydraulic and calcium-rich amorphous material are found to demonstrate higher carbonation reactivity as it often contains hydraulic calcium silicate (Ca_3SiO_5, β- Ca_2SiO_4), non-hydraulic calcium silicate (γ-Ca_2SiO_4), and portlandite in addition to the amorphous calcium-alumina-silica phase [38,39]. SC has latent hydraulic properties and demonstrates longer initial and final setting times [31]. The carbonation-curing helps to increase the early strength gain of slag cement. Boone et al. (2014) reported that carbonation of SC significantly reduced pore size and pore volume [40]. This densification had a considerable influence on compressive strength [38]. Previous studies also discussed that shrinkage of the carbonation-cured mortar containing SC was lower compared to the traditional OPC mortar [41]. The long-term durability of these materials is still being debated. This is the most important issue to address in order to gain the acceptance and confidence that these alternative materials can be used in large-scale applications. This research also explores the durability of a carbonation-cured OPC-slag system.

Despite the fact that multiple studies on SC carbonation have been conducted in which researchers performed carbonation curing from 2 hours to 672 hours, some questions remain unexplored [31,42–44]. The majority of researchers focused on pressurized carbonation curing at various temperatures [32,38,45,46]. Carbonation under atmospheric pressure at ambient temperature is beneficial for the application of carbonation curing on an industrial scale. In this research, a potential hybrid curing (carbonation and hydration) was investigated, and it was discovered that hydration curing prior to carbonation yielded better performance. This research also provides

information on the required minimum carbonation duration for the enhanced mechanical performance of the concrete. The specific objectives of this study were to determine the synergic effects of SC and OPC carbonation on i) carbonation rate, ii) carbonation efficiency, iii) microstructures, iv) silica gel polymerization, v) compressive strength, and vi) durability of cement-based materials including paste and concrete. The findings of this study will help to better understand the mechanism of SC-OPC interaction in carbonated systems.

2.3 Materials and Methods

2.3.1 Materials

In this study, the raw materials used are OPC, Ground Granulated Blast Furnace Slag (addressed as 'slag cement' or SC), sand, and gravel. Slag cement (SC) was supplied by Dragon Products Company. Based on the X-ray fluorescence measurement, the OPC contained 20.1% SiO_2, 63.7% CaO, 4.7% Al_2O_3, 3.5% Fe_2O_3 and the SC contained 34.72% SiO_2, 13.68% Al_2O_3, 0.88% Fe_2O_3, 42.28% CaO, 5.62% MgO, 1.71% SO_3. River sand with 2.61 finesse modulus (FM) was used as fine aggregates and gravel was used as coarse aggregates. The particle analyses of the OPC and SC were performed by Malvern Mastersizer 2000 using a 1.63 refractive index and deionized water as a solvent. The mean particle sizes of the OPC and SC were 20 μm and 14 μm, respectively. Figure 2.1 shows the particle size distribution.

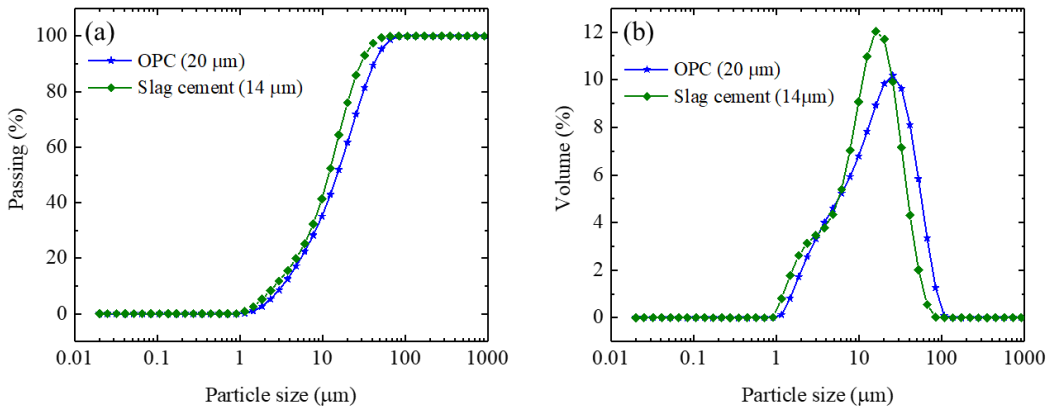

Figure 2.1: Particle size distribution of Ordinary Portland Cement (OPC) and Slag cement (SC)

2.3.2 Sample preparation

Two categories of samples were prepared for this study as shown in Figure 2.2. The first category of samples included thin (2~3 mm) paste samples prepared without compaction for microstructural analysis. In the first category of samples, the carbonation throughout the cross-section of the sample can be considered uniform. This category of samples was used for carbonation reaction kinetics and Fourier Transform-Infrared Spectroscopy (FTIR) measurements. The second category included 100 mm × 200 mm cylindrical concrete samples for mechanical performance and durability testing. This category of samples was prepared for the compressive strength and rapid chloride penetration (RCPT) tests.

For the first category, five different paste mixtures were prepared by replacing OPC with 0%, 45%, 55%, 80%, and 100% by weight of SC. SC and OPC were mixed using a 'Renfert Twister Evolution' mixer with a w/b ratio of 0.40. The ASTM C305 [47] standard was followed during mixing.

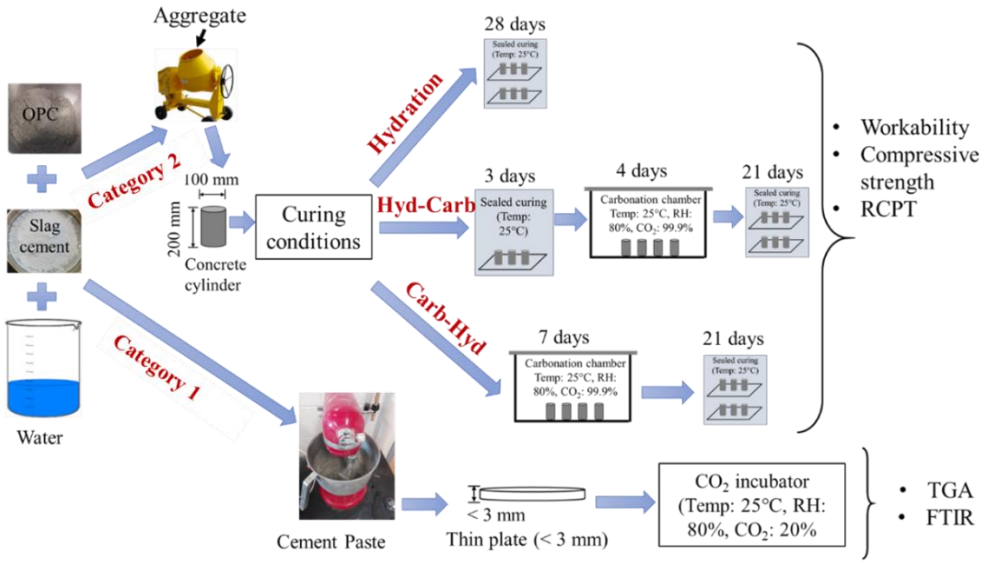

Figure 2.2: Schematic presenting the cement paste and concrete sample preparation. Hyd-Carb and Carb-Hyd present 'hydration followed by carbonation' and 'carbonation followed by hydration' curing conditions.

For the second category of samples, six different concrete mix designs were adopted for the preparation of concrete cylinders using a constant w/b ratio of 0.40. In these samples, OPC was replaced by 0%, 20%, 45%, 65%, 80%, and 100% by weight of SC. For the remainder of this article, the mixer of 100% OPC or 0% SC content will be called the control batch. Concrete mixing was performed in a large mechanical mixer in accordance with the ASTM C192 [48] standard. A fine aggregate and coarse aggregate proportion of 38% and 62%, respectively, was used for the second category of concrete sample. The binder (OPC + SC) and aggregate contents of the mixtures were 400 kg/m^3 and 1890 kg/m^3, respectively. Using this mixture, 100 mm by 200 mm cylinders were prepared for mechanical and durability testing. The cylinders were prepared into three layers using a mechanical vibrator and a tamping rod. Each layer was vibrated for 45 seconds for compaction. After casting, the cylinders were kept under different curing conditions as described in section 2.3.2.1 Cylinders were demolded after 24 hours of casting.

Slump tests to measure the workability of each batch of concrete were performed with freshly mixed concrete using ASTM C143 [49].

2.3.2.1 Curing condition

For the first category of samples (thin paste), carbonation curing was adopted. After mixing (w/b ratio of 0.4), the paste was spread over a plate with a thickness and diameter of less than 3 mm and 10 mm, respectively, and kept in 'VWR Air Jacket CO_2 Incubators' for carbonation curing. A temperature of 25°C, relative humidity (RH) of 80%, and a CO_2 concentration of 20% were maintained inside the carbonation chamber. Any possible compaction was also avoided in order to eliminate the effect of CO_2 diffusion across the sample. Carbonation-curing was performed until 300 hours. At regular intervals (such as 0.5, 3, 6, 10, 24, 72, 145, 200, and 300 hours), a small quantity of samples was collected for microstructural analysis. It was assumed that carbonation was not hampered during the sample collection process as relative humidity, temperature, and CO_2 concentration remained constant inside the carbonation chamber.

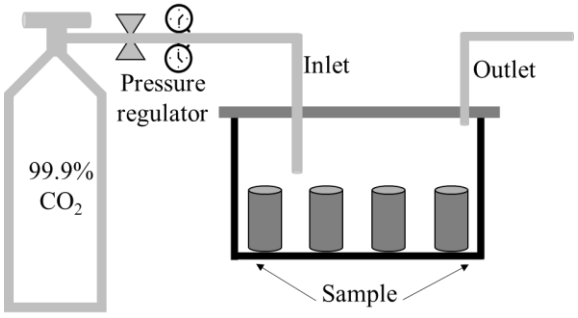

Figure 2.3: Customized carbonation setup

In the second category of samples, three different curing conditions were used, including hydration curing, hydration-carbonation curing, and carbonation-hydration curing, as shown in Figure 2.3. In the hydration curing condition, cylinder samples were kept in a sealed condition for 28 days. In

the hydration-carbonation curing condition, the cylinder samples were kept in a sealed condition for 3 days and afterward kept in an unsealed condition in a customized carbonation chamber (Figure 2.3) for carbonation curing for 4 days at 99.9% CO_2 concentration, then returned to the sealed condition for 21 days. For the carbonation-hydration curing condition, cylinder samples were stored in an unsealed condition in a customized carbonation chamber (at 25°C, 80% RH, and 99% of the CO_2 was purged) for 7 days, and then kept in a sealed condition in a moist curing room for 21 days. A reduced CO_2 concentration was used for the first category of samples, compared to the second category, to ensure that the carbonation reaction would be slow enough to effectively monitor microscopic phase formation over time.

2.4 Results and discussions

2.4.1 Polymerization of the calcium-silica gel product

The peaks in the wavenumber, ranging from 800 cm^{-1} to 1200 cm^{-1}, were due to the asymmetric and stretching vibration (ν_3) of the Si-O bond [17,50]. The exact location of these peaks depends on the Ca/Si ratio [17]. The band of calcium silicate hydrate (C-S-H) gel can be observed at around 950 cm^{-1}, and this was due to the Si-O stretching vibration (ν_3) of the Q^2 tetrahedron [17,41,51,52]. Hydrated OPC primarily contains a C-S-H gel consisting of Q^1 and Q^2 tetrahedrons in ^{29}Si NMR [8]. Details of Q^0 to Q^4 arrangements of silica tetrahedra can be found elsewhere [8].

The absorbance band at and below 800 cm^{-1} was due to out-of-plane and in-plane skeletal (ν_4) vibrations of Si-O [17] and was not studied here. The band range from 1400 cm^{-1} to 1500 cm^{-1} was due to asymmetric stretching (ν_3) of CO_3^{2-} and the 872cm^{-1} band was due to out-of-plane bending vibration (ν_2) of CO_3^{2-} [50,53]. The $Ca(OH)_2$ and chemically bound water were responsible for the

bending peak vibration at around 1639 cm^{-1} [50,54]. A previous study reported that this peak shifted to a higher wavenumber due to carbonation [50].

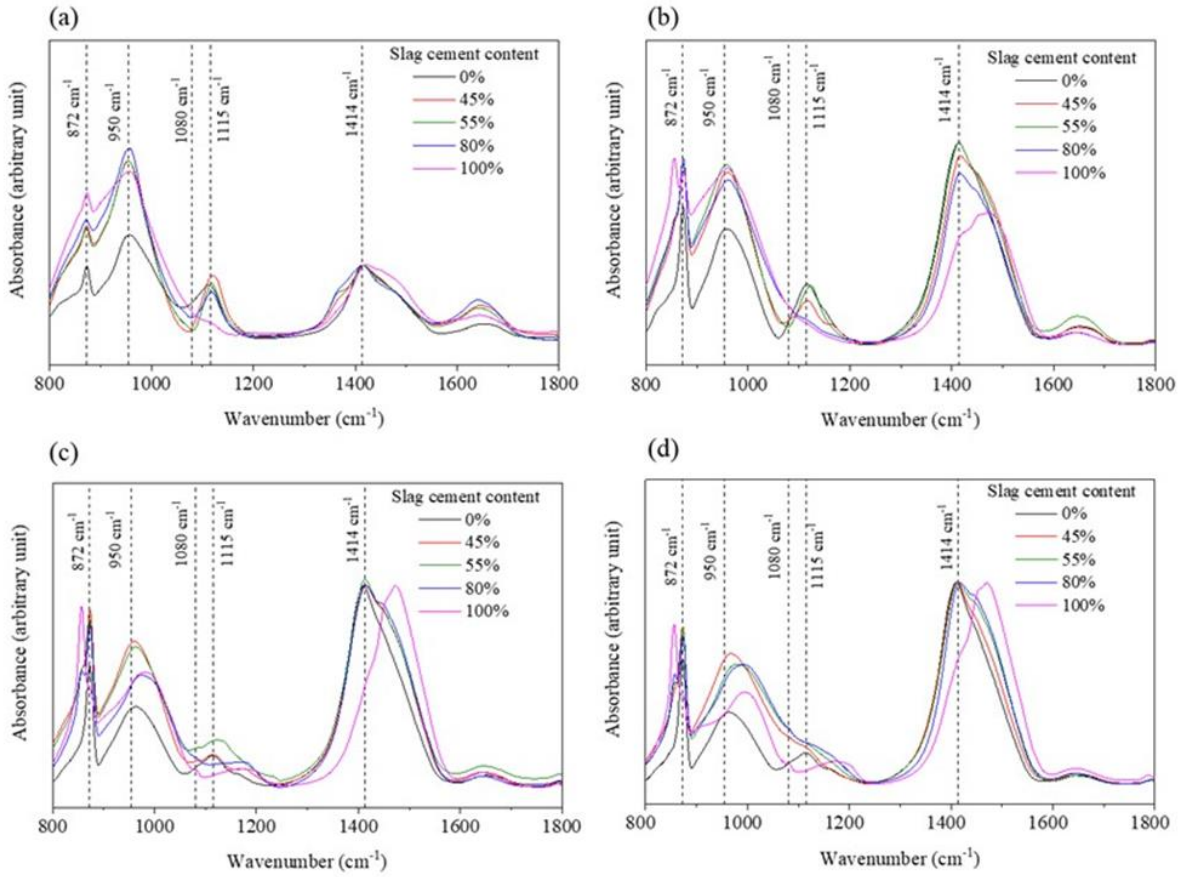

Figure 2.4: Normalized FTIR spectra of the OPC-SC carbonated paste after (a) 0.5 hour, (b) 24 hours, (c) 145 hours, and (d) 300 hours of carbonation

The main focus of this part of the study was to analyze the peaks ranging from 800 to 1800 cm^{-1} to study the calcium-silica gel polymerization. The shift of the 950 cm^{-1} band to a higher wavenumber was due to the increasing degree of silica gel polymerization and the higher bond strength of Si-O [17,50,55,56]. Figure 2.4 shows the FTIR spectra for different carbonation durations for different SC content. The out-of-plane vibration (ν_2) of CO_3^{2-} at 872 cm^{-1} was due to the calcite [50,53]. The calcite peak increased in intensity with carbonation duration [Figure 2.4

(a-d)], indicating higher amounts of calcite formation. Figure 2.4 (a) shows the 950 cm^{-1} peak, due to the Si-O bond in C-S-H gel, after 0.5 hours of carbonation curing [57]. This peak at 950 cm^{-1} decreased and shifted to higher wavenumbers with increasing carbonation and with higher SC content. This is due to silica gel polymerization and the formation of Ca-modified silica gel from the C-S-H gel during carbonation. Due to the silica gel polymerization, additional peaks were observed to form around 1080 and 1115 cm^{-1}, as shown in Figure 2.4 (c, d). These peaks were assigned to Q^3 and Q^4 sites for wavenumbers of around 1089 cm^{-1} and 1135 cm^{-1}, respectively. The formation of these peaks indicates the decalcification of C-S-H gel and the presence of higher amounts of silica gel [58]. The decalcification of C-S-H and subsequent polymerization of silica gel during the carbonation of the OPC-SC blends were observed by the reduced intensity of Q^2 and increased intensity of Q^3 and Q^4 peaks (Figure 2.4). The sharp ν_3 peak at around 1414 cm^{-1} was due to calcite formation [59], and the overlapped stretching vibrational peak at about 1490 cm^{-1} was due to vaterite formation [54,60]. As observed from Figure 2.4, an increased amount of SC resulted in higher amounts of vaterite formation during carbonation.

The FTIR spectra were deconvoluted using commercially available software (OriginPro 2017) for quantifying the peaks due to the C-S-H gel and Ca-modified silica gel. A small peak at around 1080 cm^{-1} was due to aragonite and vaterite [17] for the 100% SC batches and it was ignored during the deconvolution. The deconvolution results of the various SC content batches carbonated for 300 hours are shown in Figure 2.5. The Si-O bond shifted to 968cm^{-1} and another peak at 1114 cm^{-1} was formed due to the silica gel polymerization of the 0% SC batch, as shown in Figure 2.5 (a). For the 45%, 55%, 80% and 100% SC batches, the Si-O bonds shifted to 966, 979, 991, and 993 cm^{-1}, respectively. This indicates that with increasing SC content, the silica polymerization in the calcium-silica gel increased. The Q^3 peaks were at 1064, 1102, 1139, 1167 cm^{-1} for the 45%,

55%, 80%, and 100% SC batches, respectively, further indicating that the final calcium-silica gel hydration product in SC batches has a higher degree of silica polymerization.

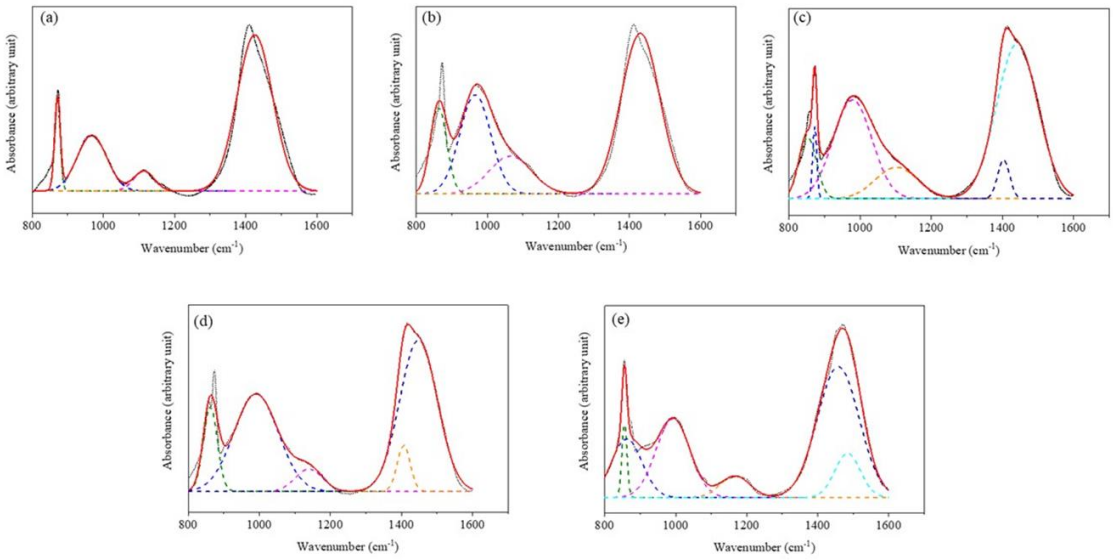

Figure 2.5: Deconvolution of FTIR spectra of 300 hours of carbonation, (a) 0% SC content, (b) 45% SC content, (c) 55% SC content, (d) 80% SC content, (e) 100% SC content. Dotted line, solid line and dashed line represent experimental FTIR spectra, simulated spectra and deconvoluted absorbances bands, respectively.

The mean wavenumber due to Si-O bond was calculated based on eqn. 6 [17].

$$I_{mean} = \frac{I_i A_i + \cdots + I_N A_N}{A_i + \cdots + A_N} \qquad \text{eqn. 6}$$

Here, I_{mean} is the mean wavenumber of Si-O (ν_3) vibration. $I_i \ldots I_N$ are the wavenumbers corresponding to the bands i...N. $A_i \ldots A_N$ represents the area under the bands of $I_i \ldots I_N$. The mean wavenumbers of different SC contents for 300 hours of carbonations have been plotted. Figure 2.6 shows the variation of wavenumbers corresponding to the Si-O ν_3 vibration bond with various SC contents. The linear fit line shows the gradual shifting of the Si-O bond to higher wavenumbers with increasing SC contents. Although the actual minimum and maximum wavenumbers were 964

cm^{-1} and 1139 cm^{-1}, the average minimum and maximum wavenumbers were 991 cm^{-1} and 1021 cm^{-1}, respectively. This implies that there were a higher number of Q^3 tetrahedron sites in the carbonated matrix.

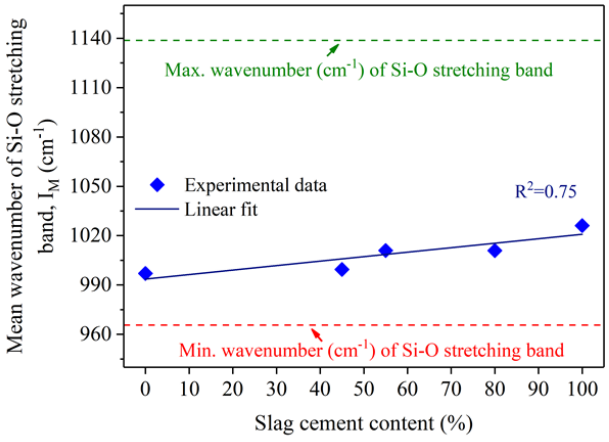

Figure 2.6: Mean wavenumber of Si-O stretching band with slag cement content

2.4.2 Workability

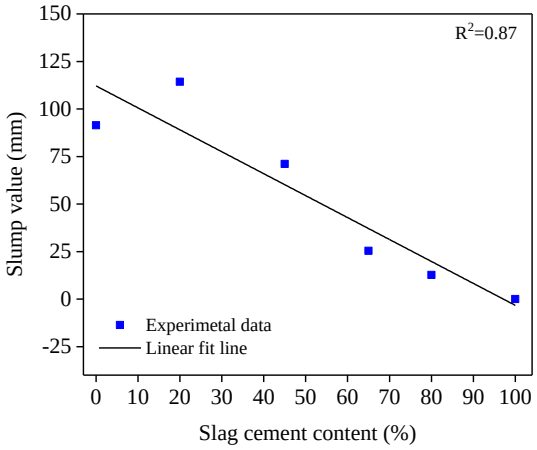

Figure 2.7: Concrete workability (i.e., slump) due to the addition of slag cement

The slump of the freshly made concrete samples is shown in Figure 2.7. The slump value of the control batch was measured to be 92 mm. The workability of the 20% SC batch was increased by 25% over the control batch. On the other hand, workability decreased by 22%, 72%, 86%, and

100% for the 45%, 65%, 80%, and 100% SC batches, respectively. This finding is similar to the previously reported data [61–64]. That is due to the vitreous appearance of SC, when a small amount of OPC was replaced by SC, the workability increased by improving the dispersion of the particle [65]. On the contrary, since SC has a smaller particle size than OPC, the higher amount (more than 45%) of OPC replacement by SC reduced its workability due to the increase in surface area and decrease in the inter-particle distance [63]. The angular shape of the SC particle is another possible reason for decreased workability [62].

2.4.3 Compressive strength

The results of the cylinder compressive strength of the different curing conditions are shown in Figure 2.8. The compressive strength of concrete samples after 3 days, 7 days, and 28 days of hydration curing is given in Figure 2.8 (a). The 20% SC batch achieved the same compressive strength as the control batch (100% OPC) after 3 days of hydration curing. Concrete batches containing 45%, 65%, 80%, and 100% of slag cement provided compressive strengths that are 19%, 13%, 35%, and 82% lower, respectively, compared to the control batch. After 7 days of hydration curing, the 45% SC batch showed the highest compressive strength at 5% higher than the control batch. The other batches, i.e., 20%, 65%, 80%, and 100% SC batches, showed a decrease in compressive strength of 5%, 6%, 32%, and 80%, respectively. After 28 days of hydration curing, the 45% SC batch showed a 16% increase in compressive strength, and the 20% and 65% SC batches were the same as the control batch. The 80% and 100% SC batches showed a reduction in compressive strength of 21% and 63%, respectively. Based on these results, it can be concluded that 45% of OPC can be replaced with SC cement without any detrimental effect on the mechanical performance in the case of hydration curing.

Figure 2.8 (b) shows the compressive strengths of concrete cylinders cured in the hydration-

carbonation condition. The results of the first three days of compressive strength were the same as for the hydration curing as, in both cases, the cylinder samples were under a sealed condition in a moist curing room. After 7 days of curing, the 20%, 45%, and 65% SC batches showed a 10%, 6%, and 12% increase in compressive strength, respectively. The 80% and 100% SC batches showed a 20% and 74% decrease in compressive strength compared to the control batch. After 28 days, the 80%, 20%, 45%, and 65% SC batches showed 9%, 12%, 19%, and 30% higher compressive strength, respectively. The 80% and 100% SC batches showed a 15% and 68% decrease in compressive strength compared to the control batch. Therefore, in the case of the hydration-carbonation curing condition, the optimum SC content is 65%.

Figure 2.8 (c) shows the compressive strengths of concrete cylinders cured in carbonation-hydration conditions. After 3 days of curing, the 20% SC batch showed a 5% increase in compressive strength. The 45%, 65%, 80% and 100% SC batches showed a 12%, 9%, 28% and 81% decrease in compressive strength, respectively, compared to the control batch. After 7 days of curing, the concrete batches with 0%, 20%, 45% and 65% SC provided a 4%, 6%, 15%, 14% increase in compressive strength, respectively. The 80% and 100% SC batches provided 22% and 76% less compressive strength, respectively. After 28 days, the 0%, 20%, 45%, and 65% SC batches provided a 12%, 17%, 16%, and 10% increase in compressive strength, respectively, compared to the control batch (hydration-cured 100% OPC batch). The 80% and 100% SC batches provided 20% and 70% less compressive strength, respectively. Therefore, in the case of the carbonation-hydration curing condition, the optimum SC content is 45%.

Figure 2.8 (d) – (f) show the percentage changes in compressive strengths of the concrete samples with respect to the control batch due to different SC contents, curing conditions, and curing durations. The concrete batch with 100% OPC which was subjected to hydration only was

considered as the control batch. As observed from Figure 2.8 (d), after 3 days of curing, almost all the batches containing SC showed a lower compressive strength compared to the control batch. This is expected due to the slow reactivity of slag. Nonetheless, the concrete batch containing 20% SC shows slightly higher compressive strength compared to the control batch when subjected to carbonation curing. All the carbonation-cured batches also showed higher strength compared to the batches subjected to hydration only. After 7 days [Figure 2.8 (e)], incorporation of carbonation curing resulted in a higher compressive strength compared to the control batch. At this stage, the 'carbonation-hydration' curing condition resulted in higher strengths compared to the 'hydration-carbonation' curing condition. Further, it is evident from the plot that both 'hydration-carbonation' or 'carbonation-hydration' curing conditions will allow up to 65% cement to be replaced with SC without degrading the strength. Based on the 28 days strength results [Figure 2.8 (f)], incorporation of carbonation curing still provides superior strength compared to the control batch, even after replacing up to 65% of cement with SC. It is worth noting that for both the 7-day and the 28-day compressive strength results, incorporation of carbonation resulted in a higher increase in strength, up to 65% SC content, compared to the batch with 0% SC. Therefore, the efficiency of carbonation curing is enhanced when a higher amount (up to 65%) of SC is used in the concrete mixture. However, as observed from the compressive strength test results, the strength of the 0% slag was not the highest. This indicates that not only the extent of the reaction but also the types of reaction products play a crucial role in the mechanical performance of carbonated matrixes. Based on the results, a balance of $Ca(OH)_2$ and $CaCO_3$ results in high strength.

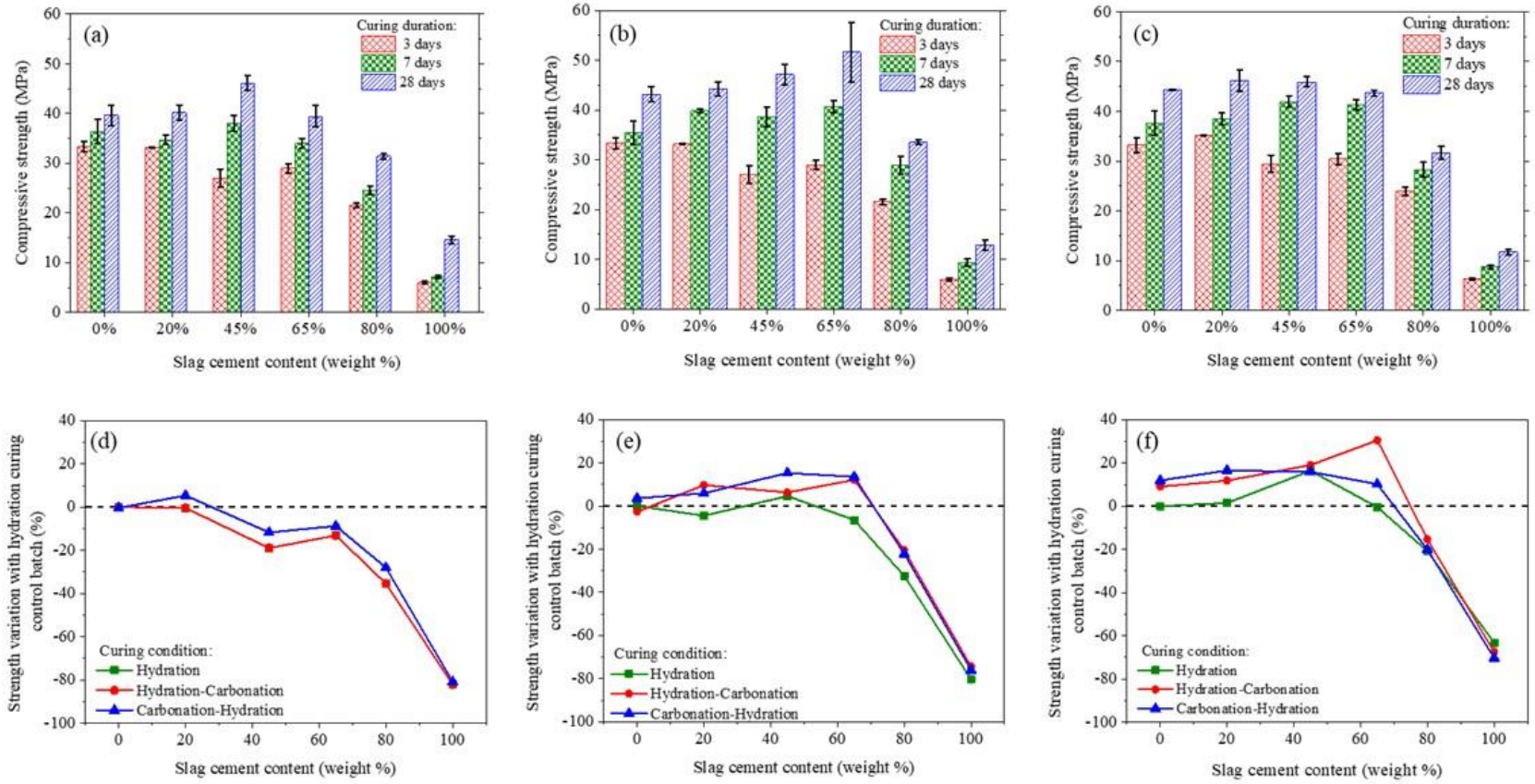

Figure 2.8: Cylinder compressive strength test of curing condition (a) hydration, (b) hydration-carbonation, (c) carbonation hydration.

Strength variation with respect to control batch of hydration curing for curing duration of (d) 3 days, (e) 7 days, and (f) 28 days.

2.4.4 Testing of concrete resistivity against chloride ions

For cement concrete systems, the durability of concrete plays a significant role in controlling the service life [66]. Importantly, the durability of concrete mainly depends on the capacity to resist fluid penetration into the microstructure of the concrete, which is called permeability [66]. Concrete permeability has a close relationship with the intensity of microcracks at the aggregate-cement paste interface [67]. Therefore, the rapid chloride permeability test (RCPT) test was performed to monitor the effects of carbonation curing on the durability performance of concrete.

Figure 2.9 (a) shows the plot of the total charge passed versus the slag cement content. From the standard, it is known that, based on the amount of charge passed, there are five categories of chloride ion permeability. They are: high (>4000C), moderate (2000C-4000C), low (1000C-2000C), very low (100C-1000C) and negligible (<100C). Among the batches, the higher slag content ones had lower total charge passed into their system. Furthermore, in the case of the curing conditions, it was found that the hydration-carbonation batches exhibited the lowest number of charges among the three curing conditions. These results showed relevance combined with the compressive strength results, for which the hydration-carbonation batches exhibited the highest strength. The more compressive strength indicates a denser matrix in the system which allows less charge to penetrate. The 0% SC batch exhibited the least resistance to charge, and it fell under the moderate range. The hydration and carbonation-hydration batches of 20% and 45% SC content fell under the low range, whereas the hydration-carbonation batches of the same SC content fell under the very low range. From the previous section 3.4, the 65% SC batch showed the highest strength, and here it showed the most resistance to charge passing.

Although taking data from the rapid chloride penetration test at short time intervals (here 30 minutes) can erase the temperature effect on the passing charge, this method may not always

portray a correct assessment of chloride ion permeability because concrete with low resistivity does not necessarily have a high chloride ion diffusivity [68]. Thus, it can be misleading to consider passing charges only to determine chloride ions' penetrability in concrete. That is why a further investigation was conducted by extending the RCPT test. Once the rapid chloride penetration test ended, the average chloride ion penetration depth was determined, from which chloride ion diffusion due to non-steady-state migration was calculated using eqn. 7 [69].

$$D = \frac{0.0239(273+T)*L}{(V-2)*t}\left(X_d - 0.0238\sqrt{\frac{(273+T)*L*X_d}{V-2}}\right) \qquad \text{eqn. 7}$$

Where D = non-steady-state migration coefficient (x10^{-12} m^2/s),

V = applied voltage (V),

T = average value of initial and final temperatures in the anolyte solution (°C),

L = thickness of the specimen (mm),

X_d = average value of penetration depth (mm), and

t = time (hour).

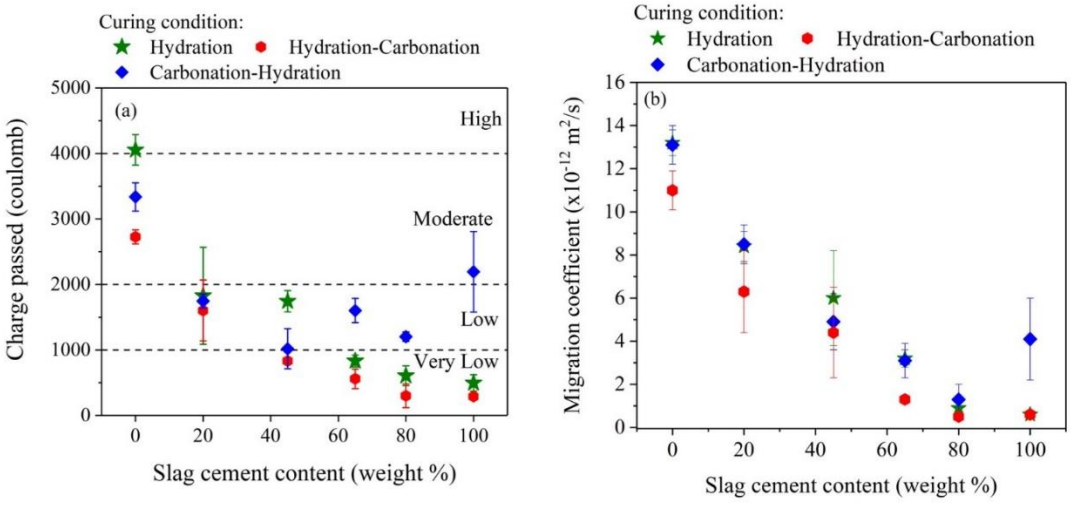

Figure 2.9: (a) Rapid chloride permeability test (RCPT) results; (b) Non steady state migration coefficient

Figure 2.9 (b) exhibits the plot of migration coefficients versus slag cement content, where the correlation was observed that the more charge passed, the more chloride ion diffusion in the system. As the penetration depth was measured at four spots due to its non-uniformity, the standard deviation was found to be slightly higher. It was found that for 45% SC content with the hydration-carbonation curing condition, the diffusion coefficient was 27% lower than for the hydration-only curing batches. For 65% SC content, the coefficient for the hydration-carbonation curing was reduced by 60% compared to the hydration-only batch. Apart from these two superior batches, the other slag cement content batches also had lower diffusion coefficients compared to the hydration-only and carbonation-hydration curing condition batches. The samples with the lowest charge consumption still showed the best resistance to chloride ion diffusion.

2.5 Conclusions

This article presented a study on the synergy between OPC and SC for carbonation systems. In summary, the following observation can be made based on this study,

(1) Concrete cylinder compressive strength was measured in three curing conditions. Among those three curing conditions, the highest compressive strength resulted from 28 days of hydration-carbonation curing, which consisted of three days of hydration, four days of carbonation, and then the remaining 21 days of hydration. Therefore, accelerated carbonation curing is advantageous when the concrete is allowed to briefly hydrate first.

(2) TGA results showed that the chemically bound water and $Ca(OH)_2$ content remained the same after 72 hours of carbonation up to 300 hours of carbonation. Even after 300 hours of carbonation, blended batches containing less than 80% SC were found to have uncarbonated $Ca(OH)_2$.

(3) The actual amount of $CaCO_3$ formed in OPC-SC blended systems was higher than the theoretical value, indicating that the addition of SC improves the carbonation efficiency of the OPC-SC blended system.

(4) The polymerization of calcium-silica gel products formed during the carbonation of OPC-SC blend systems varies depending on the blend ratio. Specifically, increasing SC content increases the silica polymerization of the gel.

(5) Increasing SC content in the OPC-SC blend was found to result in higher amounts of vaterite compared to the 100% OPC which only had calcite.

(6) Incorporation of carbonation curing helps achieve higher mechanical performance from OPC-SC blended systems after both seven days and 28 days of curing. An SC content in the range of 45% to 65% was found to result in maximum benefit, with a 65% replacement level resulting in the highest mechanical strength using the hydration-carbonation curing regime.

Chapter 3: The effects of natural biopolymers in carbonated cementitious system

This work will be submitted for publication as bellow:

Rakibul I. Khan, Warda Ashraf, Muhammad Intesarul Haque, "The effects of natural biopolymers in carbonated cementitious system".

3.1 Abstract

This study investigated the application of two different biopolymers; polydopamine and cellulose nanofibers, as a performance-enhancing additive in carbonation cured OPC-slag blended composites. Carbonation cured OPC-slag blended composites were found to generate stable $CaCO_3$. Dopamine hydrochloride, on the other hand, facilitated the formation of metastable $CaCO_3$. The inclusion of cellulose aided in increasing the reinforcing potential of this carbonated system. The incorporation of dopamine and cellulose nanofibers reduced the critical pore size and total porosity, resulting in a 36% and 66% increase in compressive and flexural strength, respectively. The effects of cellulose were found to be physical, whereas the effects of dopamine hydrochloride were found to be chemical in the OPC-Slag composites.

Keywords: Cellulose nanofibers, Dopamine hydrochloride, Carbonation, Slag, Calcium carbonate

3.2 Introduction

Sustainable construction materials can be achieved by using clinker-free binder materials, which significantly reduce CO_2 emissions associated with Ordinary Portland Cement (OPC). As an

alternate cementitious material, industrial byproducts such as ground granulated blast furnace slag (referred to as "slag") can be utilized. Slag has a latent hydraulic feature that prevents it from gaining early strength. It reacts slowly and gains strength through the pozzolanic activity as it grows older. However, slag can be activated by carbonation curing, resulting in enhanced early strength.

In carbonation curing, calcium silicate reacts with CO_2 in the presence of water to produce $CaCO_3$ and Ca-modified silica gel. The primary binding phases in this matrix are $CaCO_3$ and Ca-modified silica gel. CaCO3 polymorphs (i.e., calcite, vaterite, aragonite, and amorphous CaCO3 (ACC)) control the composites' mechanical performance [70]. Amorphous $CaCO_3$ is produced first, then more stable polymorphs such as aragonite, vaterite, and finally calcite are formed. To control the formation of those polymorphs, a variety of bio-additives can be used. A few studies in cementitious composites used different inorganic materials to regulate the formation of polymorphs and investigate the effects of such polymorphs on mechanical performance. In a carbonated wollastonite system, Khan et al. utilized amino acids to control the polymorphs of $CaCO_3$ [70]. This study showed that metastable CaCO3 significantly improves the strength and microstructure of carbonated composites. The application of dopamine showed a similar effect on the crystallization of $CaCO_3$ polymorphs [71]. Saleh et al. utilized dopamine hydrochloride in a hydraulic OPC and investigated its effects on the hydration system [72]. Additionally, cellulose nanomaterials were used in the past with amorphous calcium carbonate to produce composite materials with superior properties [73]. Although cellulose nanofibers (CNF) were used in hydration-based cementitious materials in previous research [74], the application of this biopolymer in carbonation-based composites remains unclear. With the goal of providing a fundamental understanding of the interaction between dopamine and cellulosic biopolymers with

carbonated cementitious composites, the specific research objectives of this study are as follows:

(i) Understand how the presence of dopamine and CNF affects the formation of carbonated phases in CO_2 cured calcium silicate composites.

(ii) Investigate the effects of the biopolymers on the microstructural phase formation in CO_2 cured calcium silicates composites.

(iii) Investigate the effects of the biopolymers on the macroscale performance (i.e., shrinkage, compressive strength, flexural strength) of the CO_2 cured calcium silicates composites.

3.3 Materials and methods

3.3.1 Materials

Samples were prepared using Ordinary Portland Cement (OPC, type I/II), Ground Granulated Blast Furnace Slag (addressed to as slag), and ASTM standard sand. Table 3-1 summarizes the chemical compositions of OPC and slag. Cellulose nanofibers (addressed as 'CNF') were supplied by a commercial company, 'Cellulose Lab'. The CNF was extracted from bleached sulfate hardwood pulp. The supplied CNF was in slurry form, containing 1% by weight concentration of fibers in 99% water. The average width and length of the fiber were reported to be 10-60 nm and 800-3000 nm, respectively. Dopamine hydrochloride ($C_{18}H_{11}NO_2$-HCl) (addressed as Dopamine) was purchased from VWR.

Table 3-1: Composition of OPC and slag

	SiO_2	CaO	Al_2O_3	Fe_2O_3	MgO	SO_3	MnO
OPC (%)	20.1	63.7	4.7	3.5	1.11	2.83	0.1

Slag (%)	34.72	42.28	13.68	0.88	5.62	1.71	0.24

3.3.2 Sample preparation

For the preparation of all paste and mortar samples, 50% OPC and 50% slag were mixed with constant water to binder ratio of 0.40. Based on the CNF and dopamine dosages, three distinct batches of paste samples were prepared for mechanical and microstructural investigation. In the first batch, 0% (control), 0.05%, 0.1%, and 0.3% CNF by weight of binder were added to mixtures of 50% OPC and 50% slag. In the second batch, 0.05%, 0.10%, and 0.30% Dopamine hydrochloride by weight of binder were added to the paste mixture. In the third batch, the paste combination contained 0.05%, 0.1%, and 0.3% CNF and dopamine hydrochloride (50% CNF and 50% Dopamine) by weight. The batch that does not contain any bio-additive is referred to as the 'control' batch. Those doses were determined based on earlier research that showed that lesser doses of bio-additives effectively improve the performance of cementitious composites [72,75–79].

The following procedures were used for mixing pastes: (i) For homogenization, CNF slurry/Dopamine hydrochloride was mixed with water for 2 minutes, (ii) cement and slag were added to this suspension and mixed for 2 minutes at a speed of 140 r/min, (iii) after 30 sec of rest, the mixer was again mixed for 1 minute at a speed of 285 r/min, (iv) the paste mixture was used to cast 25 mm x 25 mm cubes and 40 mm x 20 mm x 15 mm beams in two layers on a vibrator table. Immediately, following the casting of the beams and cubes, the samples were placed in a moist curing room with a temperature of 25 degrees Celsius and a RH of 80%. After 24 hours, the beams and cubes were demolded and placed in a carbonation chamber with a 20% CO_2 concentration, 80% RH, and a temperature of 50°C. Flexural and compressive strengths of beam and cube samples were determined after 3 days, 7 days, 14 days, and 28 days of curing from the

date of casting. The tested samples were immersed in isopropanol for 24 hours to allow for solvent exchange before being dried in a vacuum desiccator. These dried samples were used for additional microstructural investigation, including TGA, FTIR, XRD, MIP, SEM, and DVS.

Mortar samples were used to monitor the length change in accordance with the ASTM C 157 standard [80]. CNF/Dopamine was first homogenized with water for 2 minutes before being used in the mortar samples. Following that, OPC and slag were mixed with the suspension for 2 minutes at a speed of 140 r/min. After the initial 30 seconds of mixing, ASTM standard sand was added for 30 seconds, and the mixing was continued for another 1 minute. Following a 30-second break, the mixer was mixed for 1 minute at a speed of 285 r/min. The mixed mortar samples were used to cast 25 mm x 25 mm x 285 mm prims. Those prisms were prepared in three layers per the standard. The prisms were immediately placed inside the above-mentioned moist room after being cast. After 24 hours, the prisms were demolded and placed in the previously stated carbonation chamber, where length variations were observed for up to 56 days.

3.4 Results and Discussions

3.4.1 Mechanical performances

Figure 3.1 (a) depicts the effects of Dopamine on the compressive strength of an OPC-slag carbonated system with a w/b ratio of 0.40. The alkalinity of the OPC-slag system acts as an activator in the polymerization process of dopamine hydrochloride [72]. The polymer continues to develop a network within the binder matrix and propagate through the solid phases in alkaline conditions. This alkaline state allows for the deprotonation of the phenolic groups found in dopamine hydrochloride molecules, resulting in negatively charged sites along the polymer's backbone. During the polymerization process, negatively charged sites preferentially bond

electrokinetically to positively charged sites within the binder structure, such as Ca^{2+} and Al^{3+} sites, forming an interconnected network of polymer-binder composites. This integrated network contributes to a denser microstructure and higher mechanical performance. This improved mechanical performance could be attributed to the strong chemical interaction between the polymer backbone and the binder matrix, as well as the intrinsic higher strength of polydopamine fibers. After 3 days and 28 days of carbonation curing, adding 0.05% by weight of dopamine binder increases compressive strength by 20% and 4%, respectively, compared to the control batch. After 3 days, 7 days, 14 days, and 28 days of carbonation curing, 0.1% by weight of the binder dopamine yields 34%, 3%, 17%, and 36% increased compressive strength, respectively. However, a higher concentration of dopamine can bind more Ca^{2+} and impede the hydration and carbonation processes. As a result, less hydration and carbonation products are generated, resulting in lesser compressive strength. As a result, the addition of 0.3% dopamine results in lower compressive strength than the control batch. As observed, the 0.1% dopamine-containing batch yields higher compressive strength.

The effect of CNF on carbonated OPC-slag binder composites is presented in Figure 3.1 (b). Addition of 0.05% and 0.1% CNF aid to boost early compressive strength (3 days of curing) by 34% and 35%, respectively. After 28 days of carbonation curing, the addition of 0.1 % CNF enhanced compressive strength by up to 8%. This improved strength was attributable to the effects of CNF's internal curing. Internal curing results in denser microstructures with decreased porosity, resulting in higher compressive strength. CNF also serves as a nucleation site for hydrated and carbonated products in cementitious systems, which aids in the enhancement of compressive strength. Kavya et al. showed reduced compressive strength at later ages as a result of CNF degradation under elevated alkalinity conditions [76]. In this investigation, carbonation curing was

used, which reduced the alkalinity of the binders and the degradation of CNF compared to conventional cement paste.

The combined effects of CNFs and dopamine on the compressive strength of an OPC-slag blended system are depicted in Figure 3.1 (c). It shows that 48% and 43% higher compressive strength is achieved for 0.05% and 0.1% CNF-Dopa after 3 days of carbonation curing, respectively. After 28 days of curing, 0.3% CNF-Dopa had a 10% increase in compressive strength. The combination of CNF and Dopa aids in the reduction of compressive strength for higher doses.

Figure 3.1 (d) represents the effect of Dopamine on flexural strength. Previous research showed that polydopamine possesses higher tensile strength due to its polymer chain and side chains of polymerizable catechol monomers [81]. Due to this polymerization, 18%, 48%, and 55% higher flexural strength can be achieved for 0.05% dopamine inclusion within 7 days, 14 days, and 28 days of carbonation curing, respectively. A decreased in flexural strength was observed for higher doses of dopamine content.

Figure 3.1 (e) shows the flexural strength of the OPC-slag binder with the addition of CNF. 23%, 39%, and 36% higher flexural strength were achieved in 3 days of carbonation curing for 0.05%, 0.1%, and 0.3% by wt.% addition of CNFs respectively. The maximum increase of flexural was achieved by 34%, 62%, and 66% after 28 days of curing for 0.05%, 0.1%, and 0.3% CNF addition, respectively. The higher flexural strength was due to the crack-bridging capacity of CNF [74]. So, CNF can be used as a nano-reinforcing material. Figure 3.1 (f) depicts the combined effects of CNF and Dopa. 55% higher flexural strength was achieved after 28 days of curing for 0.05% and 0.1% addition of CNF-Dopa. It is worth noting that combining CNF with dopamine significantly minimizes the strength decrease of dopamine independently.

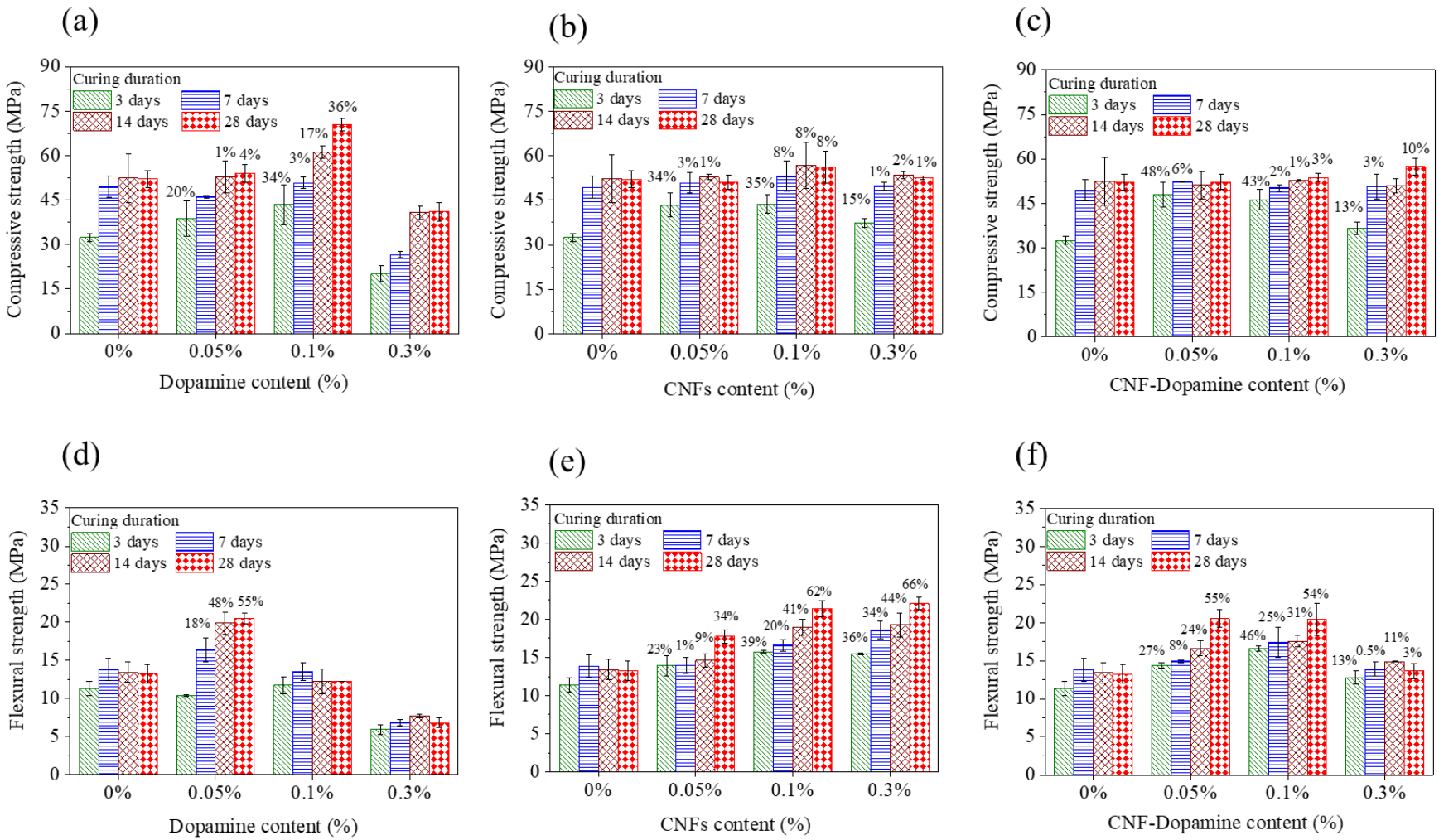

Figure 3.1: (a), (b), and (c) represent compressive strength of different doses of Dopamine, CNF, and CNF-Dopamine. (d), (e), and (f) represent flexural strength of different doses of Dopamine, CNF, and CNF-Dopamine.

3.4.2 Drying shrinkage

The results of the length change in the slag-OPC blended system are shown in Figure 3.2. It can be shown that the carbonation of the OPC-slag blend increased the length by a maximum of 0.02%. Transformation of $Ca(OH)_2$ to $CaCO_3$ yields an 11.4% increase in solid volume [46]. The addition of CNF and dopamine reduces length change by slowing the carbonation reaction. Less carbonation yields less transformation of portlandite to $CaCO_3$. Despite the fact that the length change is less than the OPC hydrated system recorded by other researchers, who reported a 0.08% length increase [82–84]. Therefore, the carbonation of the OPC-slag system, with or without bio-additives, helps to decrease the length change.

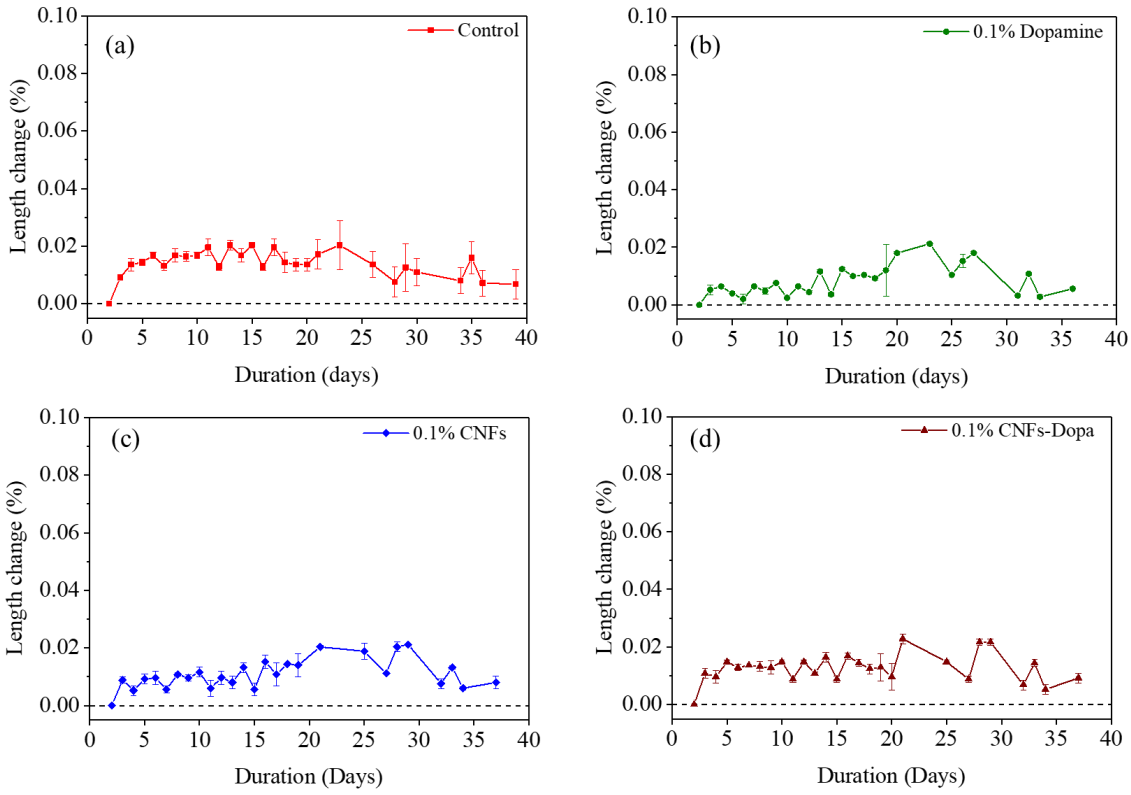

Figure 3.2: Length change of (a) Control, (b) 0.1% Dopamine, (c) 0.1% CNFs, and (d) 0.1% CNFs-Dopamine

3.4.3 Chemical analysis of carbonated matrix using thermal analysis

TGA analysis was performed for the control batch and 0.1% bio-additives batches of all curing durations. The amount of $CaCO_3$ and the relative proportion of metastable $CaCO_3$ were determined from the TGA and are presented in Figure 3.3. Several prior research discovered that $CaCO_3$ decomposes between 200 and 750 degrees Celsius [53,85,86]. The gradual weight loss from 200 deg C to 600 deg C is due to the decomposition of amorphous $CaCO_3$, aragonite, and vaterite (those polymorphs are commonly known as 'metastable $CaCO_3$') [70]. The sharp weight loss from 600 to 750 deg C is due to the decomposition of stable $CaCO_3$, known as calcite [53]. For the determination of the $CaCO_3$ amount, weight loss from 450 deg C to 750 deg C was considered in this study. Weight loss at temperatures ranging from 200 to 450 degrees Celsius is caused by the decomposition of chemically bound water and $Ca(OH)_2$. To avoid this overlapping weight loss, weight loss from 200 to 450 deg C was not taken into account while calculating the amount of $CaCO_3$. It is worth noting that polydopamine decomposes between 620 and 700 degrees Celsius [71].

Figure 3.3 (a) shows the amount of total CaCO3 for different doses of bio-additives. Previous studies show that dopamine stabilizes the unstable metastable $CaCO_3$ and blocks the transition of the calcite phase [71]. They have shown that the strong adhesive property due to the catechol group in dopamine keeps the metastable $CaCO_3$ together, and the affinitive interaction between calcium ion and catechols prevents the dissolution of metastable $CaCO_3$ and the recrystallization of calcite. This Ca^{2+} ion affinity with catechol also hinders the formation of $CaCO_3$ during the carbonation process. That is why the 0.1% Dopamine containing batch has a lower $CaCO_3$ amount than the control batch.

CNF has hydroxyl and carboxyl surface groups [87]. This hydroxyl and carboxyl group has oxygen atoms with unpaired electrons. Those unpaired electrons bind with the Ca^{2+} ion, resulting in a decrease in carbonation reaction in the earlier stage of curing. That is why it has lower $CaCO_3$ formation in the earlier curing days, as shown in Figure 3.3 (a). Due to the above-mentioned reasons, the 0.1% CNF-Dopa batch has a lower amount of $CaCO_3$.

The relative proportion of metastable $CaCO_3$ was calculated from the ratio of the weight loss due to the metastable $CaCO_3$ (450~600 deg C) and calcite (600~750 deg C). Figure 3.3 (b) shows the relative proportion of metastable $CaCO_3$. Dopamine-containing batches have higher amounts of metastable $CaCO_3$ as dopamine hinders the formation of calcite. With carbonation curing duration, the amount of metastable $CaCO_3$ decreases, and the amount of calcite increases. Previous research shows that higher metastable $CaCO_3$ has higher mechanical performance [70].

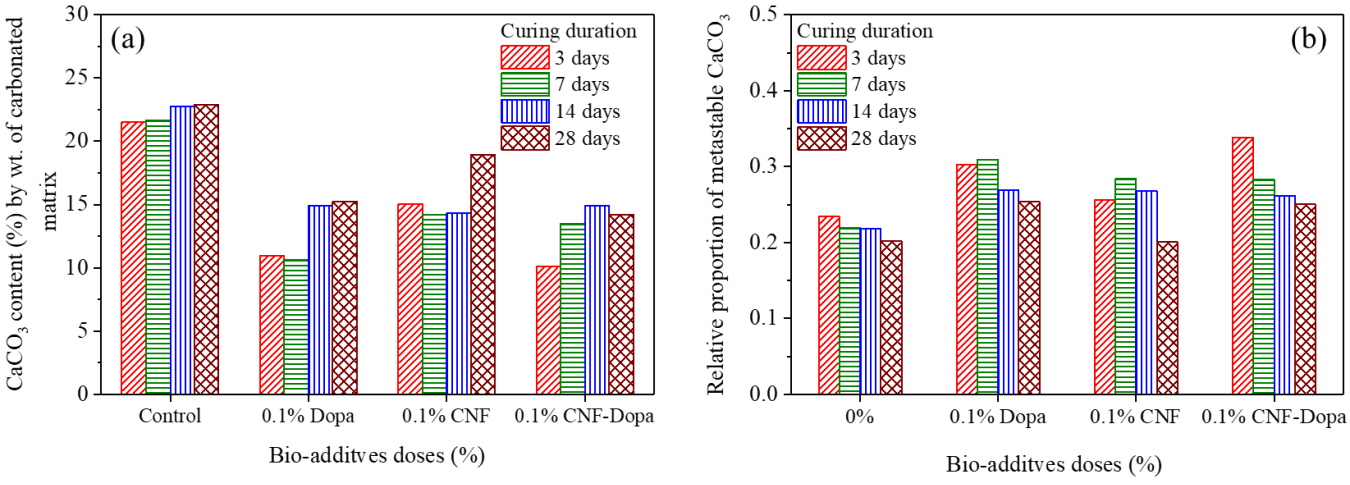

Figure 3.3: TGA analysis of OPC-slag carbonated composite, (a) $CaCO_3$ content (%) with bio additives doses, (b) Relative proportion of metastable $CaCO_3$ with bio additives doses.

3.4.4 Identifying different minerals formed during carbonation reaction

The peaks in the wavenumber, ranging from 800 cm^{-1} to 1200 cm^{-1}, were due to the asymmetric and stretching vibration (ν_3) of the Si-O bond [17,50]. The exact location of these peaks depends on the Ca/Si ratio [17]. The band of calcium silicate hydrate (C-S-H) gel can be observed at around 950 cm^{-1} and this was due to the Si-O stretching vibration (ν_3) of the Q^2 tetrahedron [17,41,51,52]. Hydrated OPC primarily contains a C-S-H gel consisting of Q^1 and Q^2 tetrahedrons in ^{29}Si NMR [8]. The band range from 1400 cm^{-1} to 1500 cm^{-1} was due to asymmetric stretching (ν_3) of CO_3^{2-} and the 872cm^{-1} and 856 cm-1 bands were due to out-of-plane and in-plane bending vibration (ν_2) of CO_3^{2-}, respectively [50,53]. The bending peak vibration at around 1639 cm^{-1} was due to the $Ca(OH)_2$ and chemically bound water [50,54]. This peak was previously reported to shift a higher wavenumber due to carbonation [50].

All the samples after 3 days of curing show the formation of calcite due to the presence of 712 and 872 cm^{-1} absorbance peaks. After 28 days of curing, the 0.1% dopamine-containing sample shows a peak at 856 cm^{-1}, which is a characteristic peak for aragonite. Batches containing CNF and CNF-Dopamine indicate a low level of aragonite content. The sharp absorbance peak at around 1414 cm^{-1} is due to the formation of calcite, and the split peaks/broad peak is due to the formation of metastable $CaCO_3$. The addition of dopamine formed metastable $CaCO_3$, which creates split peaks at around 1414 cm^{-1}.

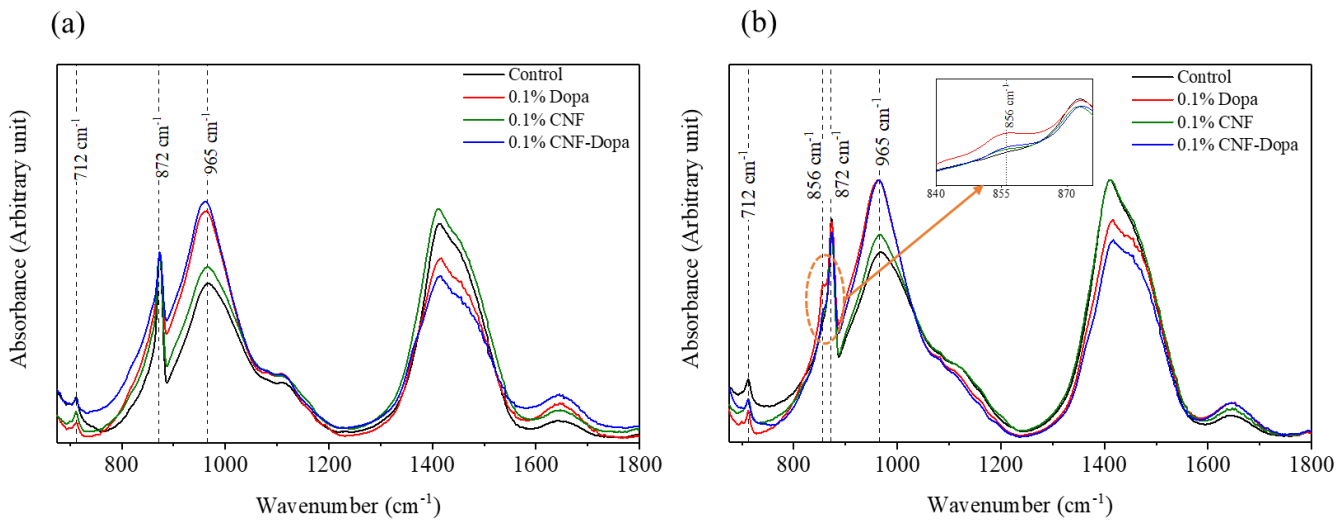

Figure 3.4: FTIR spectra after curing duration of (a) 3 days, and (b) 28 days

3.4.5 X-ray diffraction analysis

Figure 3.5 shows the XRD patterns of 28 days cured paste samples. Portlandite, calcite, and aragonite are the major crystal compositions in this carbonated system. The intensity of portlandite was higher for the batches containing dopamine, showing that incorporation of dopamine reduces the rate of carbonation. Also, the intensity of calcite was reduced with bio-additives addition. This postulates that bio-additives reduce the formation of calcite and increase the formation of metastable $CaCO_3$. Previous studies showed that the formation of metastable $CaCO_3$ increases the mechanical performance [70].

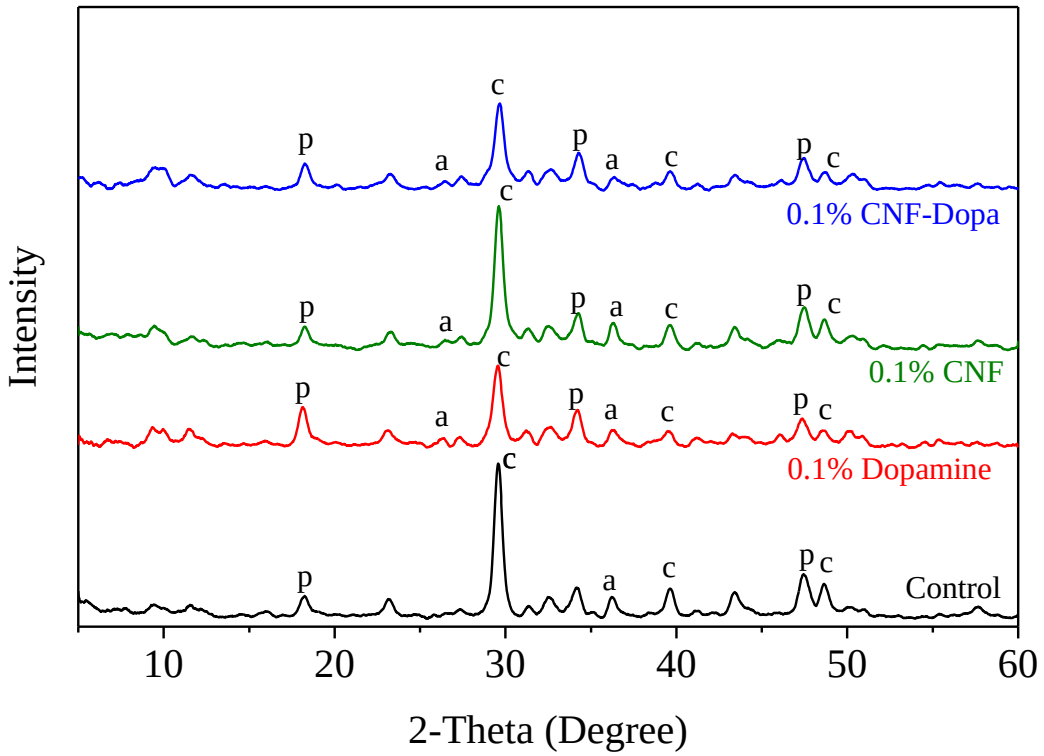

Figure 3.5: XRD patterns of 28 days cured paste samples. Here p: portlandite, c: calcite, a: aragonite

3.4.6 Porosity and pore size distribution

Pore structures of cement paste samples obtained by MIP are presented in Figure 3.6. The addition of bio-additives significantly reduces the porosity and average pore diameter. The total porosity of the paste samples was reduced by 13%, 20%, and 28% due to the addition of 0.1% Dopamine, 0.1% CNFs, and 0.1% CNFs-Dopa, respectively. Such a high reduction in porosity can lead to higher mechanical performance. Apart from the porosity, the average pore diameter also moves toward the lower diameter, due to the pore size refinement.

The pore size distribution of OPC-slag composites with the addition of CNFs and dopamine is shown in Figure 3.6. Figure 3.6 (a) shows that increased pore volume was observed with the

addition of CNFs and dopamine for pore diameters lower than 10 nm. After 10 nm pore diameter, pore volume was decreased with the addition of CNFs and dopamine. The control batch has a higher pore volume and 0.1% CNF-Dopa has a minimum pore volume. It can be postulated that the catechol group of polydopamine has strong adhesion and affinity interaction with calcium ions and offers Ca2+ binding sites for nucleation, which leads to a denser microstructure [79].

Table 3-2: Effects of CNFs and dopamine on pore structure of OPC-slag

Sample Name	Porosity (%)	Total Pore area (m^2/g)	Med. Pore Diam. vol (nm)	Avg. Pore diam (4V/A) (nm)
Control	20.4505	21.973	38.18	20.70
0.1% Dopa	17.9282	24.514	19.74	16.52
0.1% CNFs	16.4665	27.157	13.57	13.41
0.1% CNFs-Dopa	14.7408	28.159	10.99	11.59

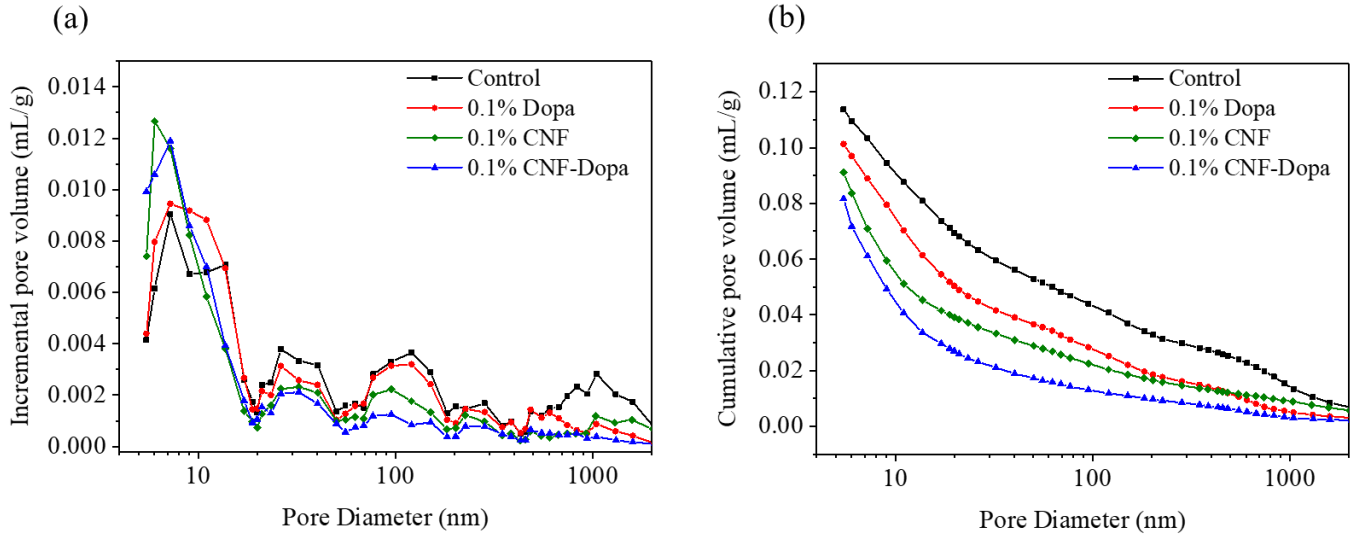

Figure 3.6: Effects of CNFs and Dopamine hydrochloride on pore size distribution of OPC-slag blended carbonated composites

3.4.7 Image analysis of carbonated OPC-slag composites

Figure 3.7 shows the pore distribution by SEM images. The control batch shows a higher number of pores than the other batches where CNF and Dopamine were added. These results also aligned

with the pore size distribution through MIP. Figure 3.8 (a) shows the formation of $Ca(OH)_2$ and $CaCO_3$. Figure 3.8 (b) shows the formation of Ca-modified silica gel and vaterite formation. Figure 3.8(c) shows the presence of CNF inside the microstructure. Figure 3.8(d) shows the formation of vaterite and other $CaCO_3$.

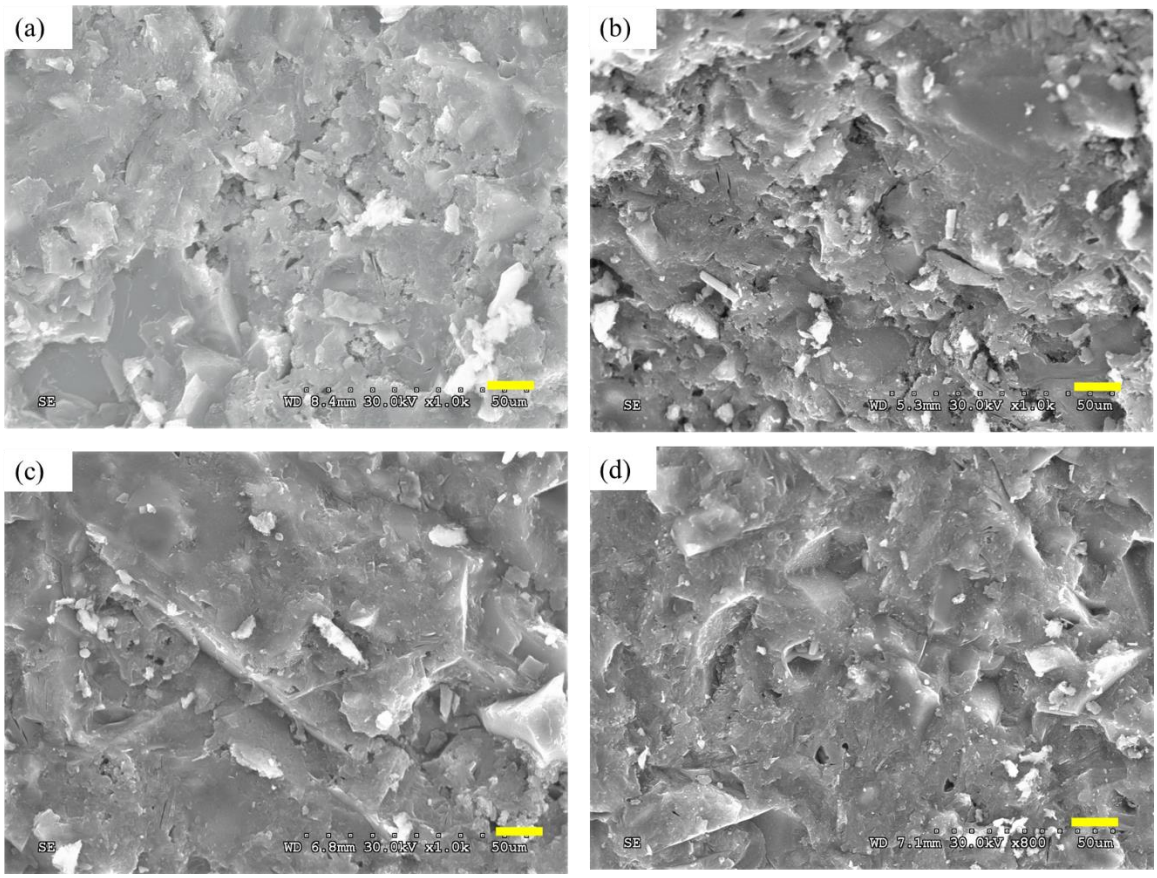

Figure 3.7: Porosity distribution through SEM images of (a) control, (b) 0.1% Dopamine, (c) 0.1% CNF, and (d) 0.1% CNF-Dopa. The scale bar represents 10 µm.

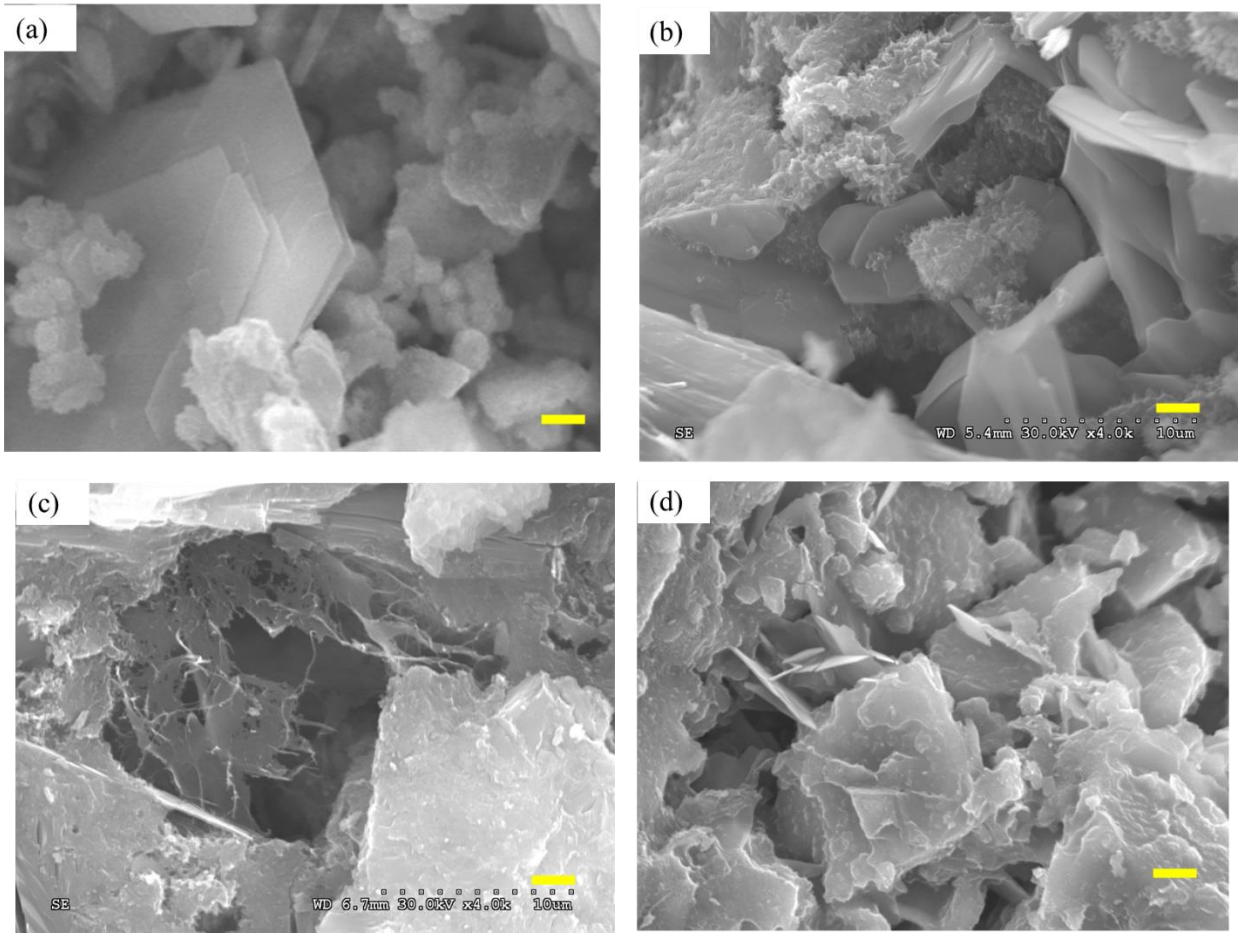

Figure 3.8: Mineral formation in slag-OPC composites of (a) control, (b) 0.1% Dopamine, (c) 0.1% CNF, and (d) 0.1% CNF-Dopa. The scale bar represents 2 µm

3.5 Conclusion

Based on this research, the following conclusion can be drawn,

(i) Dopamine helps to increase the formation of metastable $CaCO_3$ in CO_2-cured composites and reduce the carbonation rate.

(ii) A small dosage (0.05%) of dopamine can increase the flexural strength by nearly 50%. However, a dopamine dosage of more than 0.05% drastically reduced the flexural strength of the composites by reducing the degree of carbonation

(iii) The application of CNF as an additive can increase the flexural strength of the composites by 66%. The application of only CNF did not show any significant influence on the compressive strength of the carbonated composites. The flexural strength enhancement of the composite containing CNF was expected due to the reinforcing effect of these nanofibers.

(iv) Carbonated composite containing CNF have high amounts of nano porosity compared to the control batch, indicating a denser microstructure of these composites.

(v) The addition of the selected biopolymer did not affect the dimensional stability (i.e., length change) of the carbonated composites. The results indicated that the CO_2 cured composites do not experience any significant shrinkage as also observed in Chapter 4.

In summary, this study revealed that the application of either dopamine or CNF biopolymer in carbonated composites can be beneficial in two aspects: (i) to improve early age (i.e., 3 days) compressive and flexural strengths, and (ii) to improve the flexural strength of the composites.

Chapter 4: Effects of MgO in a semi-hydraulic and non-hydraulic system during carbonation curing

This work will be submitted for publication as bellow:

Rakibul I. Khan, Warda Ashraf, "Effects of MgO in a semi-hydraulic and non-hydraulic system during carbonation curing".

4.1 Abstract

This study presented an insight into the mechanical and microstructural properties of carbonated composites produced using slag, wollastonite, and MgO. Different batches containing 100% Wollastonite, 100% MgO, 100% slag, 50% Wollastoniote-50% MgO, 50% slag-50% MgO, 75% wollastonite-25% MgO, and 75% slag-25% MgO were subjected to carbonation curing at a concentration of 20% CO_2, 50°C temperature, and 80% relative humidity. The microstructure of the samples was evaluated using scanning electron microscopy (SEM), thermogravimetric analysis (TGA), Fourier transformed infrared spectroscopy (FTIR), and X-ray diffraction. TGA with mass spectroscopy (MS) was used for the identification of volatile gas during the decomposition of minerals. It was observed from dynamic vapor sorption (DVS) that the formation of hydrated magnesium carbonates (HMCs), i.e., needle-shaped nesquehonite and Rosset-like hydromagnesite, have increased the carbonated matrix density due to its expansive nature and by forming an interconnected network. The change in total and critical pore size distribution was observed with the addition of MgO. The compressive strength was also observed to increase by 309% when 50% MgO was incorporated into wollastonite and slag composites.

Keywords: Slag, wollastonite, MgO, carbonation, Hydro-magnesite

4.2 Introduction

Slag is known as green cement due to its lower CO_2 footprint during the production process [88]. It has superior durability as represented by good resistance against chemicals and chloride penetration. On the other hand, MgO can be a potentially sustainable alternative cementitious material to ordinary Portland cement due to its ability to absorb CO_2 when cured in a CO_2-rich environment [89]. MgO cement can also be produced at a lower calcination temperature [90]. Some researchers showed that MgO in slag improves the hydration reaction and increases CO_2 sequestration [88]. Increasing amounts of MgO in combination with slag increase the formation of CSH gel in a hydrated system and increase compressive strength. Apart from slag and MgO, wollastonite, which is a calcium silicate mineral, can also be a potential alternative cementitious material. Wollastonite is a non-hydraulic material that will act as inert material in the hydration system. But it can be activated by carbonation curing.

Carbonation curing is a different type of curing system, where casted samples are kept in a CO_2-rich environment. During this carbonation curing process, Ca and Si-rich materials (e.g., slag, wollastonite) will react with CO_2 in the presence of moisture and produce $CaCO_3$ and Ca-modified silica gel. Those two are the main binding phases in this curing system. In this study, the effects of MgO in slag and wollastonite systems under CO_2 curing were investigated through various nano-to-macro scale experimental techniques.

The carbonation of MgO also increased the strength of the matrix. In such formulations, carbonation is preceded by hydration, during which the dissolution of MgO is associated with an increase in the pH of the pore solution. The increased pH then promotes the dissolution of CO_2 for

the subsequent carbonation process. During carbonation-curing, dissolved CO_2 reacts with $Mg(OH)_2$ to form hydrated magnesium carbonates (HMCs). The formation of HMCs is associated with their expansive formation that reduces the porosity and establishes an interconnected network to provide binding ability, thereby increasing the strength of these binders. The most common HMCs in carbonated MgO are rosette-like hydro-magnesite ($Mg_5(CO_3)_4.(OH)_2.4H_2O$)) and needle-like nesquehonite ($MgCO_3.3H_2O$). The above findings on the carbonation of MgO and its effects on mechanical and microstructural performance have been confirmed by several studies [91–95].

The current study focuses on the comparative analysis between the effects of MgO in the semi-hydraulic system (i.e., slag) and non-hydraulic system (i.e., wollastonite). The objectives of this study are to (i) Investigate the formation of carbonation products in semi-hydraulic and non-hydraulic systems in the presence of MgO, (ii) Monitor the effects of MgO addition on the pore size distributions of the carbonated composites, and (iii) Evaluate the mechanical performances of the carbonated composites produced using a slag-MgO-wollastonite system.

4.3 Materials and methods

4.3.1 Materials

Ground granulated blast furnace slag (addressed as slag), Wollastonite ($CaSiO_3$), and Magnesium oxide (MgO) were utilized as raw materials in this research. Cemex provided the grade 120 slag, while Nico Minerals provided the wollastonite. MgO was purchased from VWR. It is worth noting that slag is a semi-hydraulic material, but wollastonite is a non-hydraulic substance.

4.3.2 Sample preparation

For this study, two types of samples were prepared. The thin plate samples without compaction belonged in the first category, while the compacted paste cube and beam samples were classified into the second. The mechanical performance and microstructural analysis were determined using the second category of samples. The pore size distribution analysis was determined using the first category of samples.

Five distinct batches of the first category of samples were prepared using a 0.80 w/b ratio. These batches are 100% slag, 100% MgO, 100% wollastonite, 50% slag-50% MgO, and 50% wollastonite-50% MgO. A relatively high w/b ratio was required for this system to achieve adequate workability. Different binders were mixed with water at a ratio of 0.80 w/b for all batches and then mixed for 3 minutes at 400 rpm using a 'Renfert Twister Evolution mixer'. After mixing, the paste samples with a thickness of 1 mm were placed on a glass plate and exposed to carbonation-curing. Carbonation-curing was performed at 80% RH, 20% CO_2 concentration, 50 deg C, and at atmospheric pressure. A commercially available 'VWR air jacket CO_2 incubator' was used to control these environmental parameters. Carbonated samples were collected after 300 hours, 600 hours, and 1200 hours of carbonation curing in the carbonation chamber. Before the experiments, the samples were maintained in a laboratory sealed environment for 24 hours after being collected from the carbonation chamber.

The second category of samples included 100% slag, 75% slag-25% MgO, 50% slag-50% MgO, 100% wollastonite, 75% wollastonite-25% MgO, 50% wollastonite-50% MgO, and 100% MgO. 100% MgO was used for microstructure analysis purposes. For the rest of this article, 50% slag and 50% MgO will be referred to as slag-MgO and 50% wollastonite, and 50% MgO will be referred to as wollastonite-MgO, respectively. Binder was mixed with water at a w/b ratio of 0.80

for 3 minutes in each batch using a commercially available Hobart rotatory mixture. The paste sample was placed into 25 mm cubes and 40 mm x 20 mm x 15 mm beam molds after mixing. A higher w/b ratio was chosen to maintain low viscosity so that it could be compacted easily. The cube and beam samples were immediately exposed to a CO_2-containing atmosphere after casting. The carbonation environment was identical to that of the category one samples. After 24 hours of carbonation, the samples were demolded and continued carbonation in the same condition as before. Compressive and flexural strength tests were performed on beam samples and cube samples taken from the carbonation chamber after 300, 600, and 1200 hours. Following testing, the samples were immersed in isopropanol for ~6 hours before being placed in a vacuum desiccator for 36 hours to prevent any additional hydration reactions. After that, those samples were used to perform Thermogravimetric analysis (TGA), Thermogravimetric analysis coupled with mass spectroscopy (TGA-MS), Fourier Transformed Infrared spectra (FTIR), X-ray diffraction (XRD), and scanning electron microscopy.

4.4 Results and discussion

4.4.1 Chemical analysis of carbonated matrix using thermal analysis

Wollastonite and slag react with CO_2 in the presence of water during the carbonation process, producing $CaCO_3$ and Ca-modified silica gel. Mechanical performance and microstructural hardness are determined by these two carbonated products. The mechanism of strength gain in carbonated MgO is dependent on the progression of hydration and subsequent carbonation. MgO is hydrated into brucite [$Mg(OH)_2$], which is then carbonated in the presence of moisture and CO_2, resulting in the creation of hydrated magnesium carbonates (HMCs). Nesquehonite ($MgCO_3.3H_2O$), hydro-magnesite [$4MgCO_3.Mg(OH)_2.4H_2O$], and dypingite [$4MgCO_3$.

$Mg(OH)_2.5H_2O$] are the most commonly observed HMCs. $Mg(OH)_2$ was preferentially carbonates to HMCs [96] as the ΔG of $MgCO_3.3H_2O$ generation (-38.7 kJ/mol) was lower than the energy of $MgCO_3$ generation (-30.2 kJ/mol). The strong and fibrous structures of HMCs present interlocking properties that decrease the initial porosity and provide binding strength within cement-based samples.

Chemically bound water decomposes in slag and wollastonite at temperatures ranging from 100 to 600°C [97–99]. $Ca(OH)_2$ decomposes to CaO and H_2O at around 450°C [97,99,100]. $CaCO_3$ decomposes to CaO and CO_2 at 600~800°C [97,99]. The evaporation of physically absorbed water and bonded water from hydrated magnesium carbonates (HMCs) can be attributed to the weight loss from 100 to 300 deg C. The sharp peaks at around 370°C and 390°C correspond to the dehydroxylation of $Mg(OH)_2$ and the decarbonization of HMCs respectively [89,100–102]. The gradual mass drop from 500 to 600°C is associated with the decomposition of metastable Ca, Mg-carbonates. The peak at around 600°C is due to well-crystallized stable $MgCO_3$ [89,100,103].

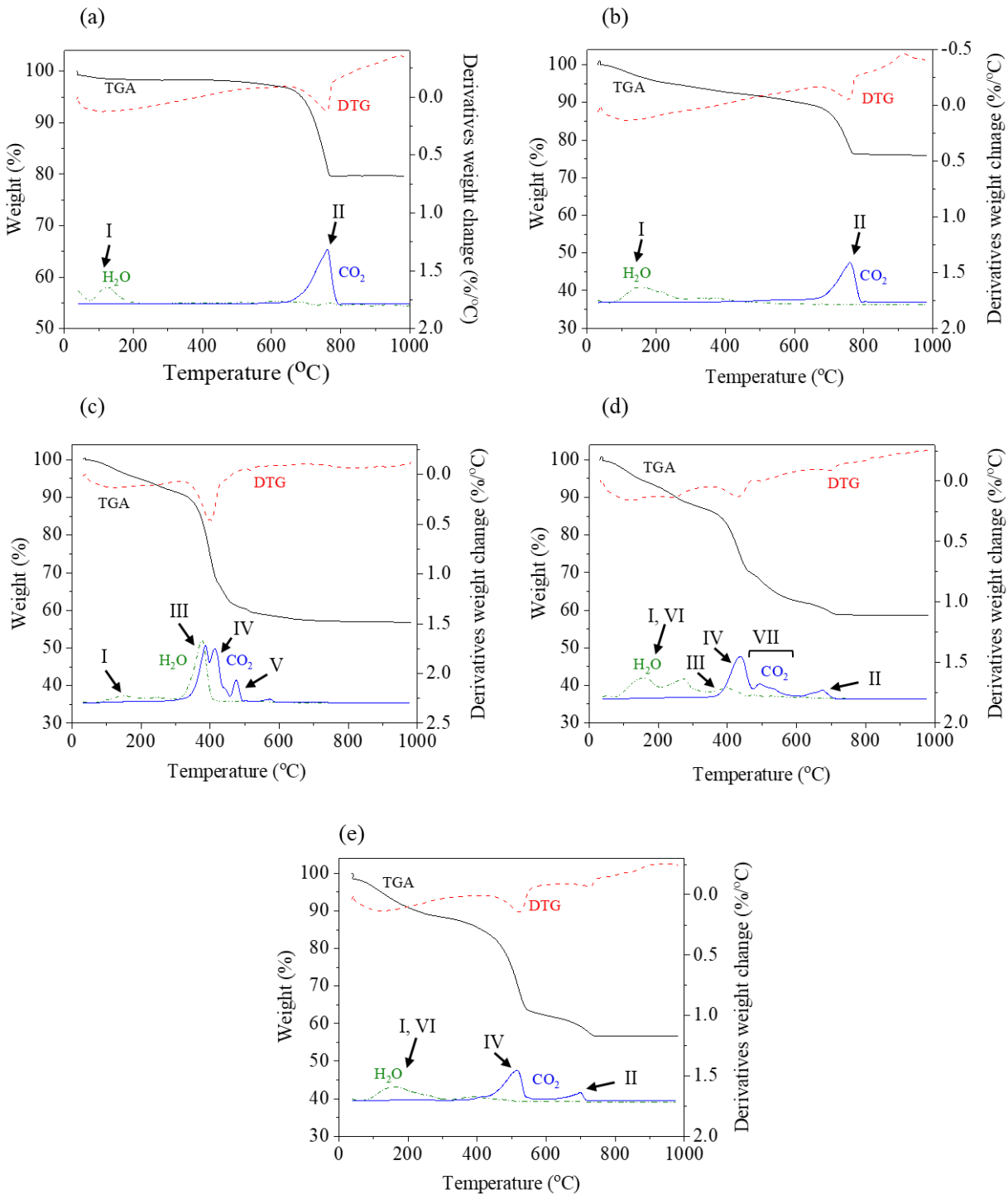

Figure 4.1: TGA-MS plots showing the releasee of H_2O and CO_2 gases from 300 hours carbonated matrixes: (a) wollastonite, (b) slag, (c) MgO, (d) 50% wollastonite-50% MgO, (e) 50% slag-50% MgO. Here, I: Physically absorbed & chemically bound water, II: Decomposition

TGA-MS plots of 300-hour carbonated matrixes are shown in Figure 4.1. The evaporation of H_2O and CO_2 from various minerals generated during carbonation curing at different temperatures is depicted in Figure 4.1. In the case of wollastonite, slag, and MgO, weight loss below 200°C was attributable to chemically bound water and physically absorbed water. Wang et al. showed that HMCs were also dehydrated at around 250°C [89,102]. After 200°C, there was no evaporated water in the case of carbonated MgO, as illustrated in Figure 4.1 (c). This indicates that the HMCs were not dehydrated or were not present in that region. As illustrated in Figure 4.1 (e), the same thing happened in the slag-MgO carbonated system. In the slag-MgO system, HMCs endured very little dehydration, or the presence of HMCs was negligible. However, the higher amount of H_2O has evaporated in wollastonite-MgO, as seen in Figure 4.1 (d), indicating a higher amount of HMCs. From 400 to 600 °C, there was a gradual weight loss due to H_2O and CO_2, indicating the development of metastable Ca, Mg-carbonates. Figure 4.1 (a-b) depicts a significant weight loss owing to CO_2 evaporation at around 750 °C. This weight loss was due to the decomposition of calcite ($CaCO_3$). Because $MgCO_3$ decomposes before 600°C, there was no weight loss in the case of carbonated MgO at this temperature. The gradual weight loss of slag-MgO and wollastonite-MgO from 600 to 750°C was noticed, which denotes the metastable $CaCO_3$ ($mCaCO_3$) decomposition [70].

According to the TGA-MS and DTG plots, more metastable $CaCO_3$ was generated when MgO was incorporated into slag and wollastonite. In a CO_2-cured environment, this metastable $CaCO_3$ provides better mechanical properties. It can therefore be inferred that a non-hydraulic system produces more HMCs than a semi-hydraulic system combined with MgO.

4.4.2 CO_2 sequestration

Carbonated activated binders, such as slag, wollastonite, and MgO, are known as carbon-negative cementitious materials due to their ability to sequester CO_2 and improve binding characteristics. The CO_2 sequestration capacity of MgO is 92.8 wt%, which is higher than the capacity of ordinary Portland cement (50.4 wt%) [102]. The carbonated matrix's CO_2 sequestration was calculated using thermogravimetric analysis (coupled with mass spectroscopy) in this investigation. Because $Ca(OH)_2$, $Mg(OH)_2$, and $MgCO_3$ decompose within a relatively narrow temperature range, calculating CO_2 sequestration solely from TGA was difficult in this study. As a result, TGA was utilized in conjunction with MS to identify and quantify the CO_2 gas released from the carbonated matrix.

The amount of CO_2 sequestration for 300 and 1200 hours of carbonation is shown in Figure 4.2. Wollastonite, slag, and MgO sequester 16%, 13%, and 88% (per gram of sample) CO_2 after 300 hours of carbonation, respectively. However, the addition of wollastonite-MgO and slag-MgO resulted in 60% and 50% CO_2 sequestration, respectively. Wollastonite-MgO sequestered significantly more CO_2 than slag-MgO. The possibility was that the wollastonite-MgO system produced more HMCs than the slag-MgO system. After 1200 hours of carbonation, wollastonite, slag, MgO, wollastonite-MgO, and slag-MgO sequestered 45%, 116%, 7%, 8%, and 5% more CO_2 than after 300 hours of carbonation, respectively. Based on these findings, it is possible to conclude that incorporating MgO into a non-hydraulic system resulted in greater CO_2 sequestration than a semi-hydraulic system.

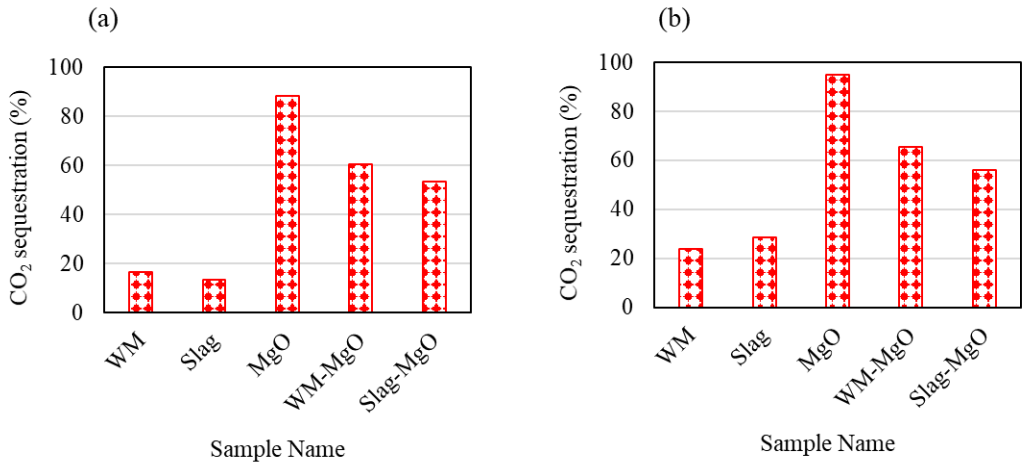

Figure 4.2: CO_2 sequestration after, (a) 300 hours, (b) 1200 hours carbonation. WM: denotes wollastonite, WM-MgO denotes: 50% wollastonite-50% MgO, Slag-MgO denotes: 50% slag-50% MgO

4.4.3 Identifying different minerals formed during carbonation reaction

From the thermal analysis, $CaCO_3$, HMCs were detected in the carbonated composites. However, distinct HMCs and different polymorphs of $CaCO_3$ in the carbonated system could not be distinguished using thermal analysis, and therefore FTIR spectra were used for this purpose. The absorbance at around 1420 cm^{-1} and 872cm^{-1} are due to the asymmetric stretching vibration (v_3 mode) and out-of-plane bending (v_2) of CO_3^{2-} [103], respectively. The broad peak or split peak at 1420 cm^{-1} denotes amorphous calcium carbonates (ACC), and on the other hand, the sharp peaks at 1420 and 872 cm^{-1} denote more stable $CaCO_3$ i.e., calcite. Figure 4.3 shows the FTIR spectra after 300 hours and 1200 hours of carbonation. In Figure 4.3 (a), wollastonite shows a broad peak at around 1420 cm^{-1} which becomes sharper after 1200 hours of carbonation (Figure 4.3 (b)). This shows the conversion of ACC to calcite in the case of wollastonite due to the longer duration of carbonation. Although in both cases, 872 cm^{-1} was present, which indicates that a lesser amount of calcite will form after 300 hours of carbonation. An extra aragonite v_2 bending peak at around

850 cm^{-1} absorbance was observed for slag after 300 hours of carbonation curing. For 300 hours of carbonation and 1200 hours of carbonation, the spectra of slag did not change. As a result, in the case of slag, no mineralogical change has occurred after 300 hours of carbonation.

The absorbance at 1423 and 1484 cm^{-1} corresponds to the antisymmetric stretching vibration (v_3 mode) of CO_3 for hydro-magnesite [89,94,104,105] and the shoulder at 1517 cm^{-1} is due to nesquehonite [89,94]. Low-intensity bands at 850 and 880 cm^{-1} correspond to the bending vibration of CO_3 represents the formation of hydro-magnesites [103][105]. 300 hours carbonated MgO contains 1423, 1484, 850, 879 cm^{-1} peaks of hydro-magnesite. The 1517 cm^{-1} peak for nesquehonite was only present for 1200 hours of carbonated MgO.

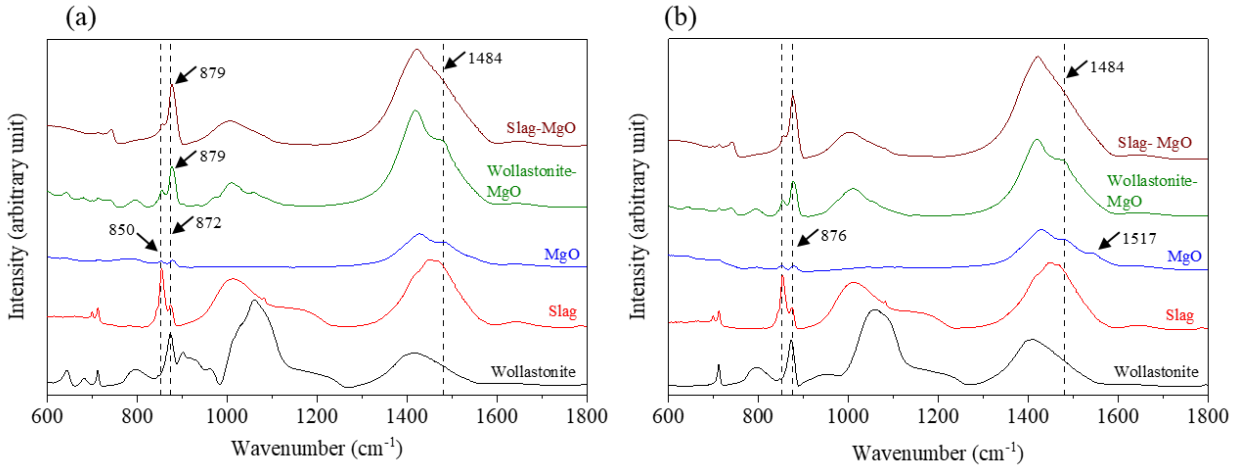

Figure 4.3: FTIR spectra, (a) 300 hours, (b) 1200 hours carbonation

Aragonite and hydro-magnesite both show an absorbance peak of 850 cm^{-1}. Carbonated wollastonite did not show this peak. However, wollastonite-MgO composite had this peak, indicating the presence of wollastonite and MgO in the carbonated environment could lead to the formation of aragonite or hydro-magnesite. This peak at 850 cm^{-1} exhibits a lower intensity in the slag-MgO carbonated system than in the slag carbonated system. This indicates the MgO inhibited aragonite development in a carbonated slag system, or it aided the conversion of aragonite to

calcite. The 1484 cm^{-1} hydro-magnesite peak was prominent for the wollastonite-MgO system but was absent or merged with $CaCO_3$ peaks for the slag-MgO carbonated system. This demonstrates that there was little or no hydro-magnetite in the slag-MgO system. This paved the path for the formation of other HMCs in the slag-MgO carbonated system. 1517 cm^{-1} absorbance peak of nesquehonite was absent in the slag-MgO and wollastonite -MgO systems after 1200 hours of carbonation. It's worth noting that after 1200 hours of carbonation, the absorbance peak at 879 cm^{-1} merges with the calcite peak and the form marge peak at 876 cm^{-1}.

Based on the presented FTIR spectral analysis, it is possible to conclude that the generation of hydro-magnesite is greater in non-hydraulic carbonated systems than in semi-hydraulic systems. These hydro-magnesites are responsible for the reduction in pore size in the MgO-included carbonated system. MgO also influences the polymorphic transition of $CaCO_3$ polymorphs.

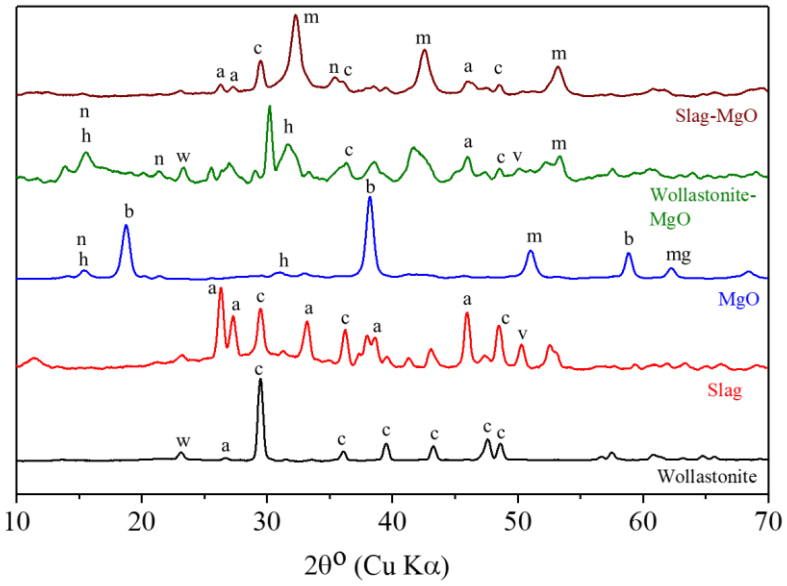

Figure 4.4: XRD plots of carbonated matrix after 1200 hours of carbonation. Here, a: aragonite, b: brucite, c: calcite, h: hydro-magnesite, m: magnesite, mg: MgO, n: nesquehonite, w: wollastonite

4.4.4 X-ray diffraction analysis

Figure 4.4 illustrates the XRD pattern of 1200 hour carbonated wollastonite, slag, MgO, wollastonite-MgO, slag-MO respectively. Carbonated wollastonite mostly has unreacted wollastonite and calcite phases. Although very small peaks of aragonite can be seen, this suggests that aragonite may be present in the composites. Carbonated slag mostly has aragonite and calcite in the system. The formation of vaterite was also seen in slag at 50 deg diffraction angle [88]. Carbonated MgO is primarily composed of brucite ($Mg(OH)_2$) and magnesite ($MgCO_3$). Hydro-magnesite and nesquehonite with very small intensities were observed as well. When MgO and wollastonite were combined, the amount of calcite and magnesite drastically decreased. Although there was no aragonite or vaterite in carbonated wollastonite, both phases were present when wollastonite and MgO were combined. There was no brucite in this mixture, which provides another important aspect of the increasing formation of HMCs from brucite with wollastonite incorporation. In the case of the slag-MgO carbonated system, the formation of calcite and magnesite are both reduced significantly. Magnesite was also formed in this case.

4.4.5 Pore structure analysis using dynamic vapor sorption

Vapor sorption analysis is usually performed for gel phase (C-S-H or Ca-modified silica gel) characterization. The advantages of using this technique rather than MIP or nitrogen sorption were discussed elsewhere [106]. A typical plot of the hysteresis loop of desorption and adsorption isotherm is shown in Figure 4.5 (a). The hysteresis loop between adsorption and desorption is found in all the matrixes and it contributes to the complex nature of pore connectivity [107][108]. The specific surface area (SBET) of the matrixes was determined using the BET method [109]. Pore size distribution was determined using the BJH model, incorporating the statical water layer thickness proposed by Hagymassy [110][111].

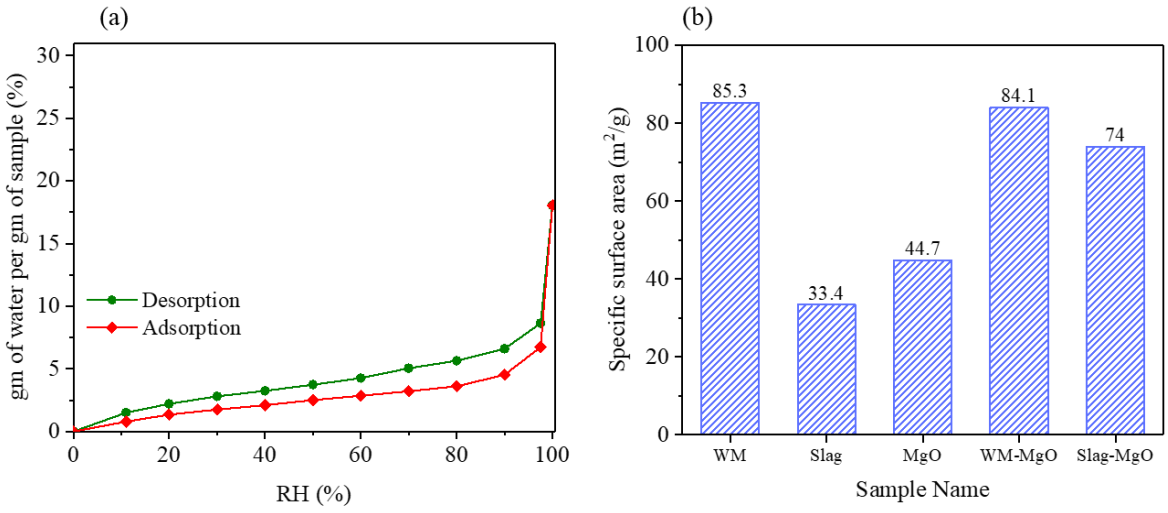

Figure 4.5: (a) A typical plots of vapor desorption and adsorption curves for wollastonite-MgO carbonated matrix, (b) specific surface area (S_{BET}) of 300 hours carbonated matrixes

The specific surface area of the carbonated matrix is given in Figure 4.5 (b). It can be observed from the figure that carbonated wollastonite has a higher surface area (85.3 m^2/g) than carbonated slag (33.4 m^2/g) and MgO (44.7 m^2/g). However, the inclusion of MgO in slag and wollastonite yielded 74 m^2/g and 84.1 m^2/g specific surface area, respectively. This indicates that higher crystalline carbonated products were formed when MgO was added in the slag system as well as the wollastonite system.

Figure 4.6 shows the pore size distribution of the carbonated calcium silicate matrixes. Carbonated wollastonite and slag show a major peak before 1 nm and another peak at around 1.5 nm. On the other hand, carbonated MgO shows three peaks, i.e., before 1 nm, 1.5 nm, and 3 nm. However, when MgO was added with wollastonite or slag, all the peaks merged into one large peak before 1 nm. This concludes that when MgO was added with slag and wollastonite, it formed more carbonated products which reduced the large pore size and formed smaller pores.

Based on the previous study, the pores in the carbonated matrix were divided into the following groups (based on the pore diameter), (i) inter-cluster spaces (diameter: < 2 nm), (ii) gel pores (diameter: 2-10 nm), (iii) capillary pores (diameter: 10 -41 nm), and large pores (diameter: >41 nm) [112][106]. The pore diameter below 2 nm is assumed to contain physiosorbed and chemisorbed water within an outer layer of Ca-modified silica gel clusters [106]. From Figure 4.7, it can be observed that carbonated wollastonite has a minimum volume of large pores and capillary pores, and carbonated slag has a maximum volume of large pores and carbonated MgO has a maximum volume of capillary pores. Carbonated Wollastonite-MgO contains the highest volume of inter particle porosity, and carbonated MgO has the minimum volume of inter-particle porosity. The reason behind those variations may be their pore size distribution and extent of carbonation.

Previous studies show that lower specific surface areas containing carbonated matrixes have higher amounts of metastable $CaCO_3$ and lower crystallinity [106]. From an FTIR study, it was observed that carbonated slag has a higher amount of aragonite and wollastonite has a higher amount of calcite. From the DVS results, it was observed that carbonated wollastonite has a higher SBET than carbonated slag. Carbonated minerals with higher crystallinity have higher SBET. The addition of MgO to slag and wollastonite increased the crystallinity.

Agglomeration between particles will also reduce the interparticle porosity. Here, interparticle porosity has increased, and this was due to less agglomeration of interparticle porosity. The gel pores are attributed to the pores between Silica, MgO, and $CaCO_3$. As the inclusion of MgO increases the crystallinity, it also increases the pores between carbonate and silica.

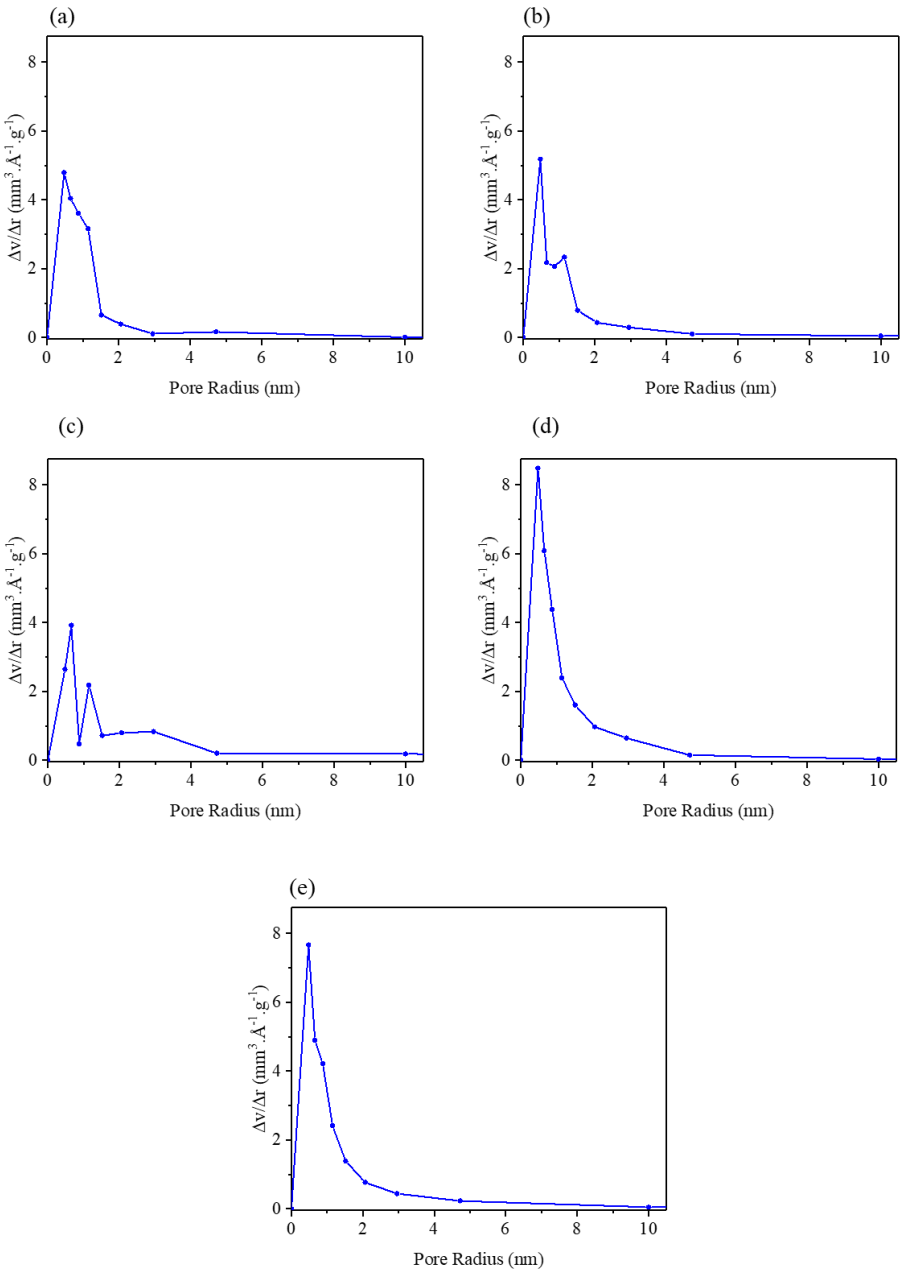

Figure 4.6: Pore size distribution of 300 hours carbonated matrixes: (a) wollastonite, (b) slag, (c) MgO, (d) Wollastonite-MgO, (e) slag-MgO.

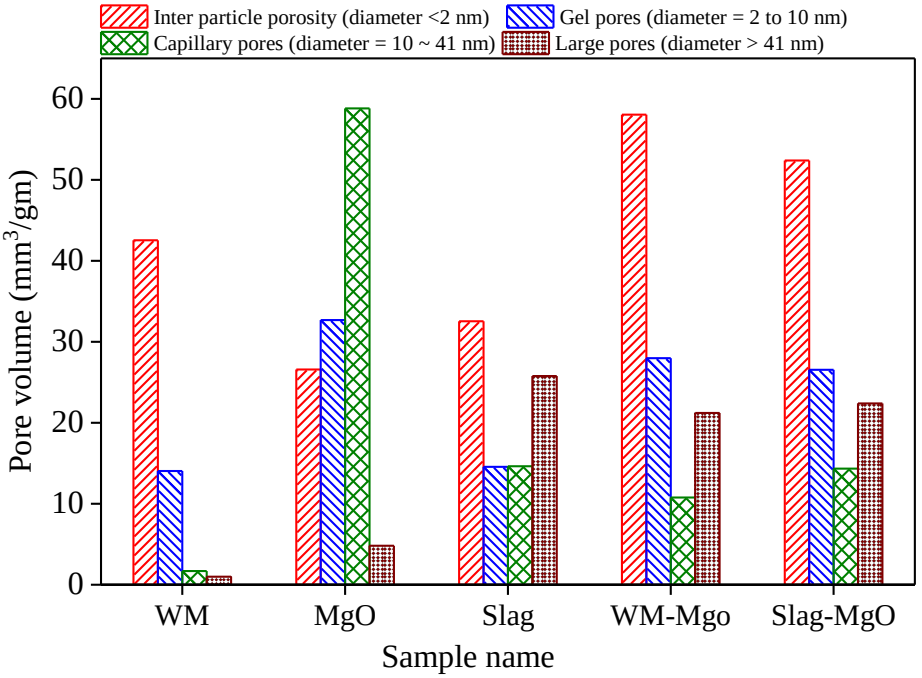

Figure 4.7: Pore size distribution of 300 hours carbonated matrixes

4.4.6 Image analysis of carbonated slag-wollastonite with MgO incorporation

Figure 4.8 reveals the microstructures of wollastonite, slag, and MgO subjected to carbonation curing for 300 hours and 1200 hours. Carbonated wollastonite mostly contained calcite (Figure 8 (a-b)). No $mCaCO_3$ was found in the wollastonite matrix. Aragonite was found in a carbonated slag system. Most of the magnesite was found in the carbonated MgO system. The carbonated wollastonite-MgO system has mostly hydro-magnesite and $CaCO_3$. Slag-MgO has few hydro-magnesite and $mCaCO_3$.

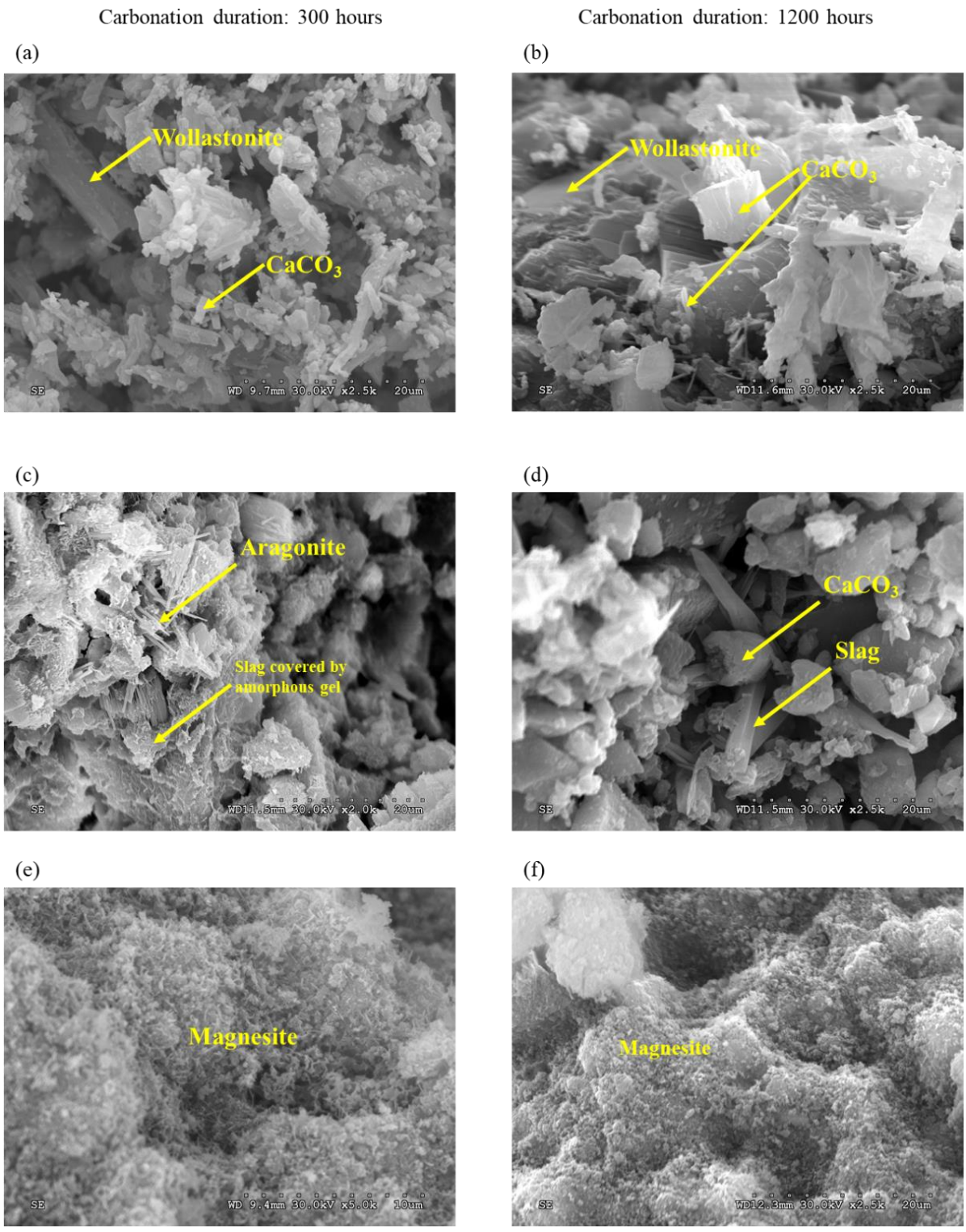

Figure 4.8: SEM images of carbonated matrixes, (a-b) wollastonite, (c-d) slag, (e-f) MgO

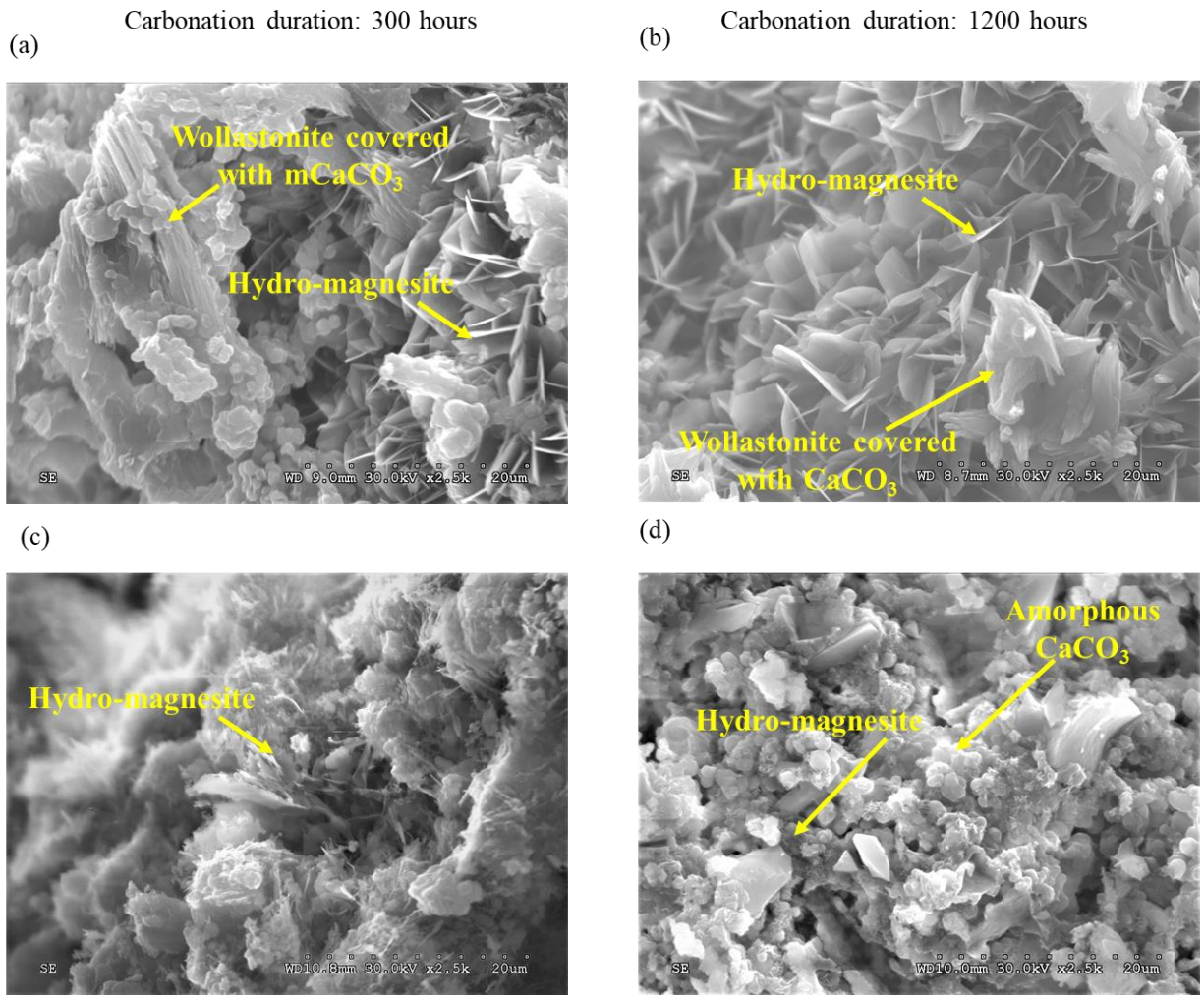

Figure 4.9: SEM images of carbonated matrixes: (a-b) wollastonite-MgO, (c-d) slag-MgO

4.4.7 Mechanical performances

The compressive strength of wollastonite and slag with different MgO content for different curing conditions was shown in Figure 4.10. The use of higher carbonation duration significantly improved the compressive strength. There was a significant increase in compressive strength from 300 hours of carbonation duration to 600 hours of carbonation duration. There was not any significant difference in compressive strength from 600 hours of carbonation duration to 1200

hours of carbonation duration. So, in this system, a maximum of 600 hours of carbonation duration was found to be the maximum for achieving the highest compressive strength.

The inclusion of MgO in the wollastonite system has significant effects on increasing compressive strength. 25% MgO increased compressive strength by 56%, 55%, and 48% after 300 hours, 600 hours, and 1200 hours of carbonation curing respectively. On the other hand, 50% MgO in the wollastonite system increased compressive strength by 626%, 326%, and 304% after 300 hours, 600 hours, and 1200 hours of carbonation duration. In the case of slag, MgO has increased compressive strength significantly. 25% of MgO in slag increased compressive strength by 174, 164%, and 188% after 300 hours, 600 hours, and 1200 hours of carbonation, respectively. 324%, 290%, and 309% increased compressive strength was observed for 50% MgO for 300 hours, 600 hours, and 1200 hours of carbonation.

The compressive strength of mortar samples shows a significant increase in strength after 600 hours of carbonation. 25% inclusion of MgO in wollastonite provided a 27.5 MPa compressive strength, which is 44% higher than only wollastonite. In the case of slag, 25% MgO gave a 26.5 MPa compressive strength, which is 26% higher than the only slag batch. The higher mechanical performance in the case of mortar was due to the higher diffusion of CO_2 inside the core structure.

A significantly increased flexural strength was also observed in this system. 25% MgO increased flexural strength by 141% and 108% after 300 hours of carbonation for wollastonite and slag, respectively. A 248% and 108% increase in flexural strength were observed at 50% MgO in wollastonite and slag after 300 hours of carbonation. A 5% and 47% increase in strength was observed for 25% and 50% MgO in the wollastonite system after 600 hours of carbonation. 224% and 232% increase in flexural strength was observed after 600 hours of carbonation for 25% and 50 % MgO in slag. There was a significant increase in flexural strength for more than 25% of MgO

in the slag system, whereas, in the wollastonite system, an increasing amount of MgO increased the flexural strength. The possible reason is that the increasing amount of MgO in wollastonite will increase the production of Patel like hydro-magnesite which gives reinforcing ability in this system. On the other hand, the production of hydro-magnesite is lower in the case of slag, that's why flexural strength did not increase after 25% of MgO.

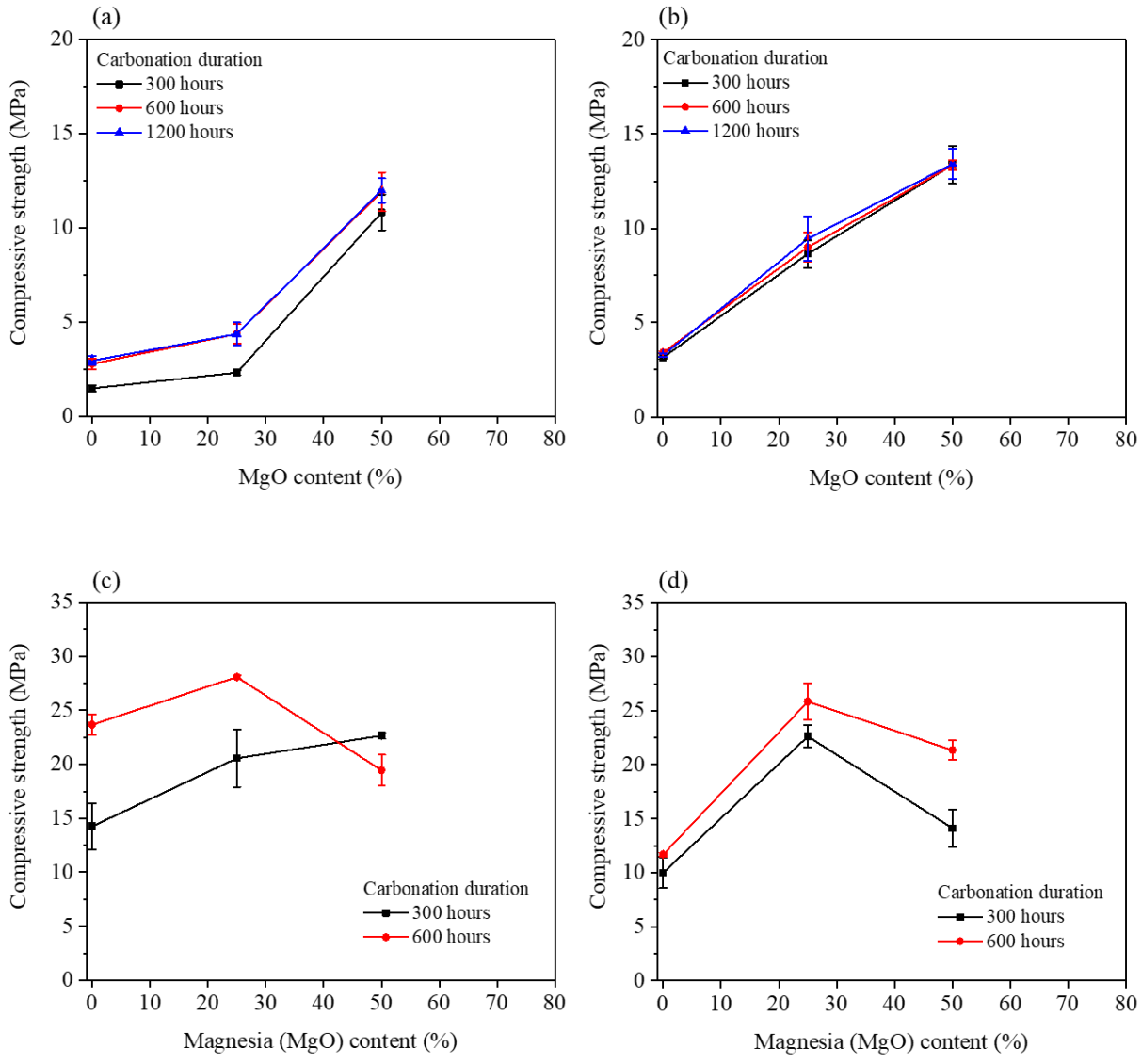

Figure 4.10: Compressive strength: Carbonated (a, c) wollastonite, and (b,d) slag with different MgO content. Plot (a,b) are of paste samples and (c,d) are of mortar samples.

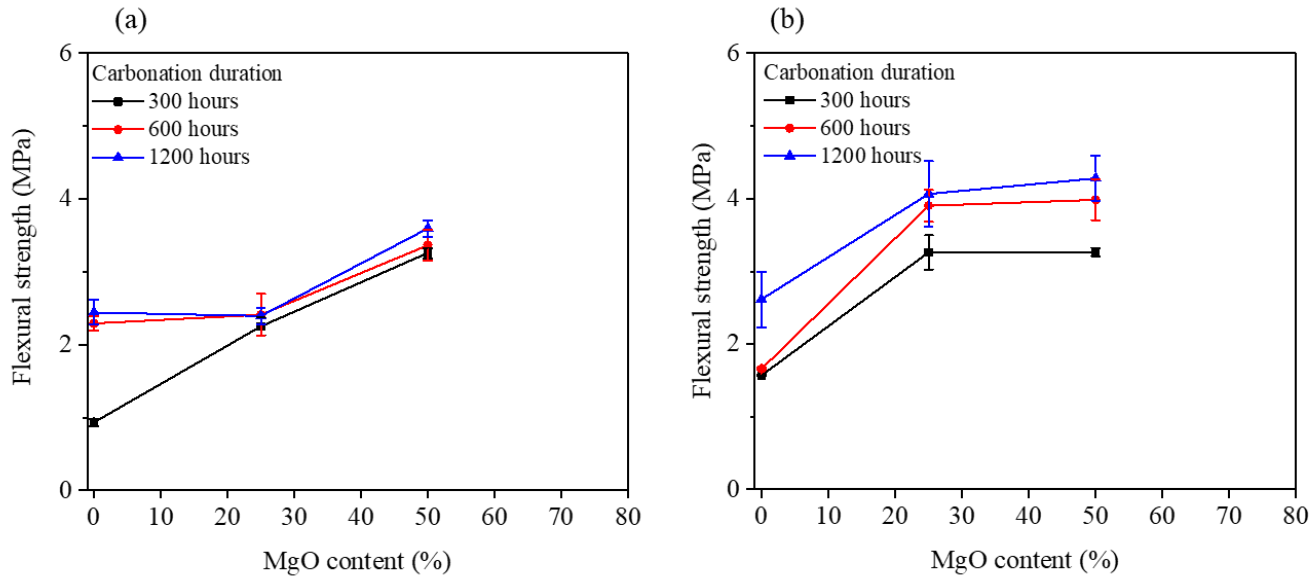

Figure 4.11: Flexural strength: Carbonated (a) wollastonite, and (b) slag with different MgO content

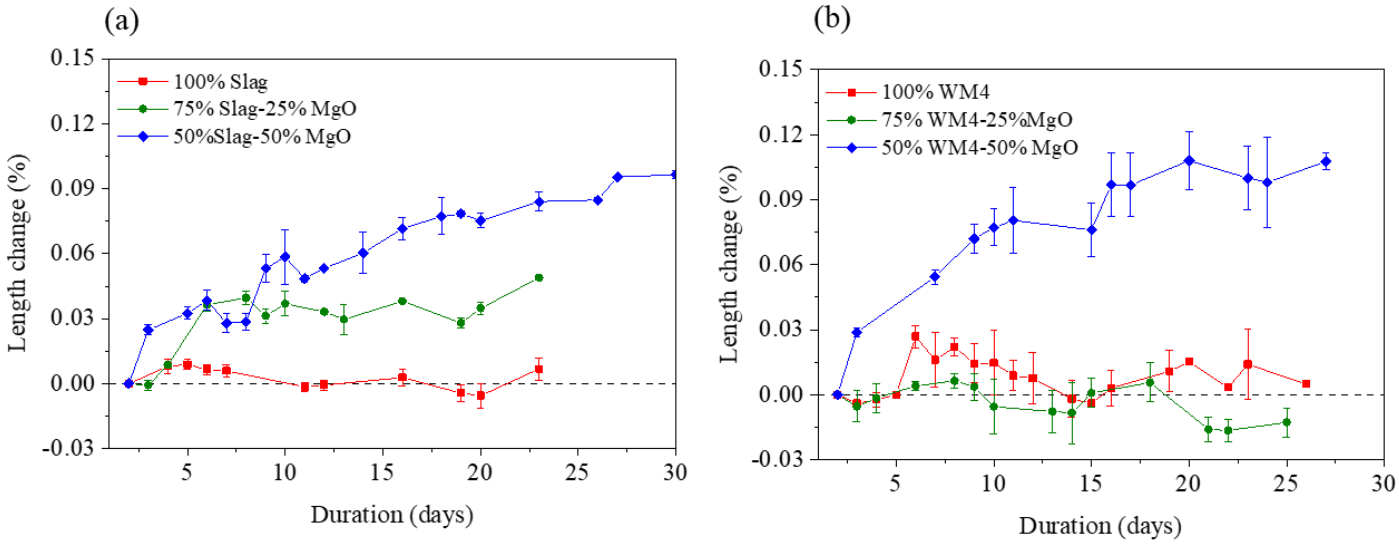

Figure 4.12: Length changes with carbonation duration, (a) slag blended with magnesia, (b) wollastonite blended with magnesia

4.4.8 Drying shrinkage

The results of the length change in the slag-magnesia blended system are shown in Figure 4.12 (a). Adding magnesia to a slag system increases the length change significantly due to the development of hydrated magnesium carbonate. Transformation of $Ca(OH)_2$ to $CaCO_3$ yields an 11.4% increase in solid volume. Transformation of MgO to $Mg(OH)_2$ and $MgCO_3.3H_2O$ yield 131.4% and 614.3% solid volume increase respectively [46]. Despite the fact that the length change is within the OPC hydrated system, recorded by other researchers, who reported a 0.08% length increase [82][83][84]. The length change of the wollastonite-magnesia blended system is depicted in Figure 4.12 (b). Wollastonite, for example, shrinks at first and then expands after 7 days of carbonation. Despite the fact that the length expansion was less than 0.01%. The addition of magnesia to wollastonite results in a 0.08% increase in length. Overall, this finding suggests that typical shrinkage cracking, as observed in traditional hydraulic cement, is not a concerning factor for carbonated composites. Nevertheless, due to the increasing trend in the expansion, such measurements will be continued for a longer duration in the future.

4.5 Conclusion

From this study, the following concluding points can be drawn,

(i) The dosage of MgO can significantly affect the carbonate phases formed in the CO_2 cured cementitious composites. Specifically, it was observed that the addition of MgO increased the formation of HMCs in carbonated wollastonite and slag composites. change the $CaCO_3$ polymorphs in the wollastonite carbonated system.

(ii) Formation of HMCs in carbonated composites was found to refine the pore size distribution by reducing the critical pore diameter. The relative amounts of nano-porosity were also found to

be higher in MgO-slag and MgO-wollastonite binary systems compared to those present in a single type of binder.

(iii) The addition of MgO in carbonated calcium silicates (either slag or wollastonite) was found to increase the compressive and flexural strengths of the composites by more than 200%. Such a drastic increase in the mechanical performances of the composites was attributed to the pore size refinement due to the addition of MgO in these systems.

(iv) The addition of MgO was observed to increase the expansion of the carbonated composites produced using either slag or wollastonite. The increase in the dosage of MgO also increased the expansion. Such expansion of the composites was expected due to the formation of expansive HMCs in these matrixes. The maximum expansion of the samples remained below 0.1% for the tested duration. However, for the future study, a longer measurement duration is recommended.

The most interesting finding of this study is that for carbonation cured composites, the combination of calcium silicates with MgO binders offer significantly better mechanical and microstructural characteristics compared to the composites produced using a singly type of binder (i.e., calcium silicates or MgO). Therefore, MgO offers a potential pathway to significantly improve the performance of the carbonation cured composites when used as an additive.

Chapter 5: Conclusions, future direction, and practical application

5.1 Concluding Remarks

The outcomes of specific tasks accomplished during this research are listed at the end of each chapter (Chapter 2 to Chapter 4). The significant findings of this study are summarized below:

(I). According to the results provided in Chapter 2, the combination of hydraulic and semi-hydraulic calcium silicate produces cementitious composites with improved mechanical performance under carbonation curing. Semi hydraulic calcium silicate produced a denser and less porous microstructure with higher durability due to enhanced carbonation kinetics. Semi hydraulic calcium silicate has a stronger affinity for the carbonation reaction, resulting in increased CO_2 sequestration. The amount of semi hydraulic calcium silicates and the degree of carbonation affect the polymerization of silica gel. All of the research findings contribute to the achievement of the first research objective, as mentioned in Chapter 1.

(II). Biopolymers (e.g., dopamine hydrochloride, cellulose nanofibers) have a considerable impact on calcium silicate carbonation kinetics. They were able to generate an organic-inorganic hybrid composite with improved mechanical properties. CSH polymerization is also increased by these biopolymers. By lowering critical pore size distribution and offering crack-bridging capacity, cellulose nanofibers significantly enhance flexural strength. These findings corresponded to the second research objective indicated in Chapter 1.

(III). According to the results presented in Chapter 4, adding MgO-based cement to semi/non-hydraulic calcium silicate has a substantial impact on the development of $CaCO_3$ polymorphs. Previous studies have demonstrated the influence of $CaCO_3$ polymorphs on mechanical performance. MgO-based cement produces hydrated magnesium-based carbonates during the carbonation curing process, which has a 600% larger solid volume than MgO. The critical and total porosity of the composite fluctuates as the solid volume increases. This also aids in the reduction of shrinkage caused by carbonation curing. These findings backed up the third research goal indicated in Chapter 1.

5.2 Suggested future research directions

This research uncovered numerous elements of carbonation and CO_2-activated binders. A number of potential study directions can be identified based on the findings and limitations.

Carbonation curing is a diffusion process. Relying entirely on an external source of CO_2 for carbonation may not result in consistent carbonation of the entire cross-section. Existing chemical engineering techniques, such as the use of gas absorption polymers, microcapsules, and zeolite impregnated with CO_2, should be fully investigated for internal carbonation of the matrix. These materials/polymers have the ability to store CO_2 and release it when admixed with concrete. To obtain the same results, inorganic salts with a higher dissolving rate might be utilized.

There was not enough mix design/standard for concrete carbonation curing, to the best of the author's knowledge. To establish a standard or mix design technique for this system, several sets of experiments with varied w/b ratios, CO2 concentrations, temperature, and RH can be used for hydraulic, semi-hydraulic, and non-hydraulic materials. A data-driven approach can be used for proposing a CO2 mix design using thermodynamics modeling and machine learning.

5.3 Practical applications

Novacem is one of the companies that uses a magnesium oxide material to make a cement-free binder that captures CO_2 when combined with water in a CO_2 atmosphere. Novacem's binder's main product was magnesium carbonate, which was responsible for its strength [113]. Solidia uses carbonation curing to activate non-hydraulic Solidia cement, resulting in calcite and silica as binding materials. When compared to OPC, this Solidia cement can reduce carbon footprint by 70%. Calera is yet another company that manufactures a calcium carbonate CO_2-activated binder system for concrete products. Its cement contains no traditional Portland cement and has a higher compressive strength. The carbon cure company extracted CO_2 from manufacturing processes and inflated it into an OPC and water mixture.

For concrete paver blocks, efflorescence is a prevalent issue. Carbonation at an early age can help to minimize or eradicate efflorescence [114]. This slag carbonation technology can be utilized to make environmentally friendly paver blocks with a minimal CO2 footprint.

Carbonation curing can be used on a wide range of precast structures, including concrete pipes, blocks, masonry units, and reinforced concrete. Carbonation can be utilized as an auxiliary curing regime for concrete pipes to minimize steam curing time, increase durability, and investigate the feasibility of using concrete pipes to sequester carbon dioxide [115]. Furthermore, regulated carbonation curing can improve the long-term durability of concrete pipes. Carbonating agents can be made from CO2 captured at industrial point sources. Because carbonation is essentially a lime-consuming process, carbonated concrete pipes made in this manner are believed to be more durable due to a reduction in reactive lime.

Cement blocks are frequently utilized and manufactured in large quantities. The annual production of 200-mm block equivalents in the United States and Canada is around 4.3 billion units. The annual use of Portland cement is estimated to be around 6 Mt. Clean production could make major contributions to sustainable development if this volume of cement could be substituted by slag activated by carbon dioxide [29].

Concrete masonry units (CMUs) have long been utilized as load-bearing and non-load-bearing walls in construction. In 2014, the North American market for concrete blocks and bricks is expected to grow to 4.3 billion units. Compared to cast-in-place concrete, masonry block construction not only functions better due to its precast quality, but also has a lower environmental impact. In North America, CMUs are commonly steam cured. While steam curing increases strength and shortens the production cycle, it is an energy-intensive procedure. It is estimated that atmospheric pressure steam curing consumes 0.59 GJ/m^3 (12.3 ft-lb/ft^3) of concrete and autoclave curing consumes 0.71 GJ/m3 (14.7 ft-lb/ft^3) of concrete for 1 m3 (35.3 ft^3) of concrete in block form. Carbonation curing, which uses high-purity carbon dioxide (99.5% CO_2) or low-purity flue gas (14% CO_2) for rapid hydration and durability improvement, is an alternate curing process for CMU manufacture [116].

Carbonation is thought to be harmful to reinforced concrete. However, if carbonation is done at a young age by curing, the process may be advantageous. Carbonation curing was created for precast reinforced concrete carbonation curing at an early age to maximize performance improvement and carbon storage capacity. Early carbonation curing differs from weathered carbonation. It is added to fresh concrete within 24 hours of casting. As a result, additional hydration will occur following early carbonation [117].

References

[1] F. Lea, Lea's Chemistry of Cement and Concrete by Peter Hewlett, 2004. https://doi.org/10.1016/B978-0-7506-6256-7.50031-X.

[2] G.J.-M. (Ies-J. Jos G.J. Olivier (PBL), J. a. H.W.P. (Pbl) Marilena Muntean (IES-JRC), Trends in Global CO2 Emissions: 2013 Report, 2013.

[3] S. Tsivilis, J. Tsantilas, G. Kakali, E. Chaniotakis, A. Sakellariou, The permeability of Portland limestone cement concrete, Cem. Concr. Res. (2003). https://doi.org/10.1016/S0008-8846(03)00092-9.

[4] M. Ghrici, S. Kenai, M. Said-Mansour, Mechanical properties and durability of mortar and concrete containing natural pozzolana and limestone blended cements, Cem. Concr. Compos. (2007). https://doi.org/10.1016/j.cemconcomp.2007.04.009.

[5] M.B. Mohd Salahuddin, M. Norkhairunnisa, F. Mustapha, A review on thermophysical evaluation of alkali-activated geopolymers, Ceram. Int. (2015). https://doi.org/10.1016/j.ceramint.2014.11.119.

[6] I. Mehdipour, A. Kumar, K.H. Khayat, Rheology, hydration, and strength evolution of interground limestone cement containing PCE dispersant and high volume supplementary cementitious materials, Mater. Des. 127 (2017) 54–66. https://doi.org/10.1016/j.matdes.2017.04.061.

[7] B. Alsubari, P. Shafigh, M.Z. Jumaat, Utilization of high-volume treated palm oil fuel ash to produce sustainable self-compacting concrete, J. Clean. Prod. (2016). https://doi.org/10.1016/j.jclepro.2016.07.133.

[8] W. Ashraf, J. Olek, S. Sahu, Phase evolution and strength development during carbonation of low-lime calcium silicate cement (CSC), Constr. Build. Mater. 210 (2019) 473–482. https://doi.org/10.1016/j.conbuildmat.2019.03.038.

[9] M. Auroy, S. Poyet, P. Le Bescop, J.M. Torrenti, T. Charpentier, M. Moskura, X. Bourbon, Comparison between natural and accelerated carbonation (3% CO2): Impact on mineralogy, microstructure, water retention and cracking, Cem. Concr. Res. 109 (2018) 64–80. https://doi.org/10.1016/j.cemconres.2018.04.012.

[10] C. Shi, B. Qu, J.L. Provis, Recent progress in low-carbon binders, Cem. Concr. Res. 122 (2019) 227–250. https://doi.org/10.1016/j.cemconres.2019.05.009.

[11] J.K. Hicks, M.A. Caldarone, E. Bescher, Opportunities from Alternative Cementitious Materials, Concr. Int. 37 (2015) 47–51.

[12] W. Ashraf, J. Olek, Carbonation activated binders from pure calcium silicates: Reaction kinetics and performance controlling factors, Cem. Concr. Compos. (2018). https://doi.org/10.1016/j.cemconcomp.2018.07.004.

[13] D. Zhang, Z. Ghouleh, Y. Shao, Review on carbonation curing of cement-based materials, J. CO2 Util. 21 (2017) 119–131. https://doi.org/10.1016/j.jcou.2017.07.003.

[14] Z. Liu, W. Meng, Fundamental understanding of carbonation curing and durability of carbonation-cured cement-based composites : A review, J. CO2 Util. 44 (2021) 101428. https://doi.org/10.1016/j.jcou.2020.101428.

[15] M. Fernández Bertos, S.J.R. Simons, C.D. Hills, P.J. Carey, A review of accelerated carbonation technology in the treatment of cement-based materials and sequestration of

CO2, J. Hazard. Mater. 112 (2004) 193–205. https://doi.org/10.1016/j.jhazmat.2004.04.019.

[16] Q. Liu, J. Liu, L. Qi, Effects of temperature and carbonation curing on the mechanical properties of steel slag-cement binding materials, Constr. Build. Mater. 124 (2016) 999–1006. https://doi.org/10.1016/j.conbuildmat.2016.08.131.

[17] W. Ashraf, J. Olek, Carbonation behavior of hydraulic and non-hydraulic calcium silicates: potential of utilizing low-lime calcium silicates in cement-based materials, J. Mater. Sci. 51 (2016) 6173–6191. https://doi.org/10.1007/s10853-016-9909-4.

[18] P. De Silva, L. Bucea, V. Sirivivatnanon, Chemical, microstructural and strength development of calcium and magnesium carbonate binders, Cem. Concr. Res. 39 (2009) 460–465. https://doi.org/10.1016/j.cemconres.2009.02.003.

[19] S.A. Walling, J.L. Provis, Magnesia-Based Cements: A Journey of 150 Years, and Cements for the Future?, Chem. Rev. 116 (2016) 4170–4204. https://doi.org/10.1021/acs.chemrev.5b00463.

[20] L. Mo, M. Deng, M. Tang, Effects of calcination condition on expansion property of MgO-type expansive agent used in cement-based materials, Cem. Concr. Res. 40 (2010) 437–446. https://doi.org/10.1016/j.cemconres.2009.09.025.

[21] T.S. Naidu, C.M. Sheridan, L.D. van Dyk, Basic oxygen furnace slag: Review of current and potential uses, Miner. Eng. 149 (2020). https://doi.org/10.1016/j.mineng.2020.106234.

[22] worldsteel 2016 Steel Statistical Yearbook now available online | worldsteel, (n.d.). https://www.worldsteel.org/media-centre/press-releases/2016/worldsteel-2016-steel-

statistical-yearbook-now-available-online.html (accessed April 30, 2021).

[23] J. Liu, D. Wang, Influence of steel slag-silica fume composite mineral admixture on the properties of concrete, Powder Technol. 320 (2017) 230–238. https://doi.org/10.1016/j.powtec.2017.07.052.

[24] S.Z. Carvalho, F. Vernilli, B. Almeida, M. Demarco, S.N. Silva, The recycling effect of BOF slag in the portland cement properties, Resour. Conserv. Recycl. 127 (2017) 216–220. https://doi.org/10.1016/j.resconrec.2017.08.021.

[25] S. Monkman, Y. Shao, Assessing the Carbonation Behavior of Cementitious Materials, J. Mater. Civ. Eng. 18 (2006) 768–776. https://doi.org/10.1061/(asce)0899-1561(2006)18:6(768).

[26] M. Mahoutian, Z. Ghouleh, Y. Shao, Carbon dioxide activated ladle slag binder, Constr. Build. Mater. 66 (2014) 214–221. https://doi.org/10.1016/j.conbuildmat.2014.05.063.

[27] Z. Ghouleh, R.I.L. Guthrie, Y. Shao, High-strength KOBM steel slag binder activated by carbonation, Constr. Build. Mater. 99 (2015) 175–183. https://doi.org/10.1016/j.conbuildmat.2015.09.028.

[28] F. Xi, S.J. Davis, P. Ciais, D. Crawford-Brown, D. Guan, C. Pade, T. Shi, M. Syddall, J. Lv, L. Ji, L. Bing, J. Wang, W. Wei, K.H. Yang, B. Lagerblad, I. Galan, C. Andrade, Y. Zhang, Z. Liu, Substantial global carbon uptake by cement carbonation, Nat. Geosci. 9 (2016) 880–883. https://doi.org/10.1038/ngeo2840.

[29] M. Mahoutian, Y. Shao, Production of cement-free construction blocks from industry wastes, J. Clean. Prod. 137 (2016) 1339–1346.

https://doi.org/10.1016/j.jclepro.2016.08.012.

[30] D. Xuan, B. Zhan, C.S. Poon, Development of a new generation of eco-friendly concrete blocks by accelerated mineral carbonation, J. Clean. Prod. 133 (2016) 1235–1241. https://doi.org/10.1016/j.jclepro.2016.06.062.

[31] E. Gruyaert, P. Van Den Heede, N. De Belie, Carbonation of slag concrete: Effect of the cement replacement level and curing on the carbonation coefficient - Effect of carbonation on the pore structure, Cem. Concr. Compos. 35 (2013) 39–48. https://doi.org/10.1016/j.cemconcomp.2012.08.024.

[32] S. Monkman, Y. Shao, Carbonation curing of slag-cement concrete for binding CO2 and improving performance, J. Mater. Civ. Eng. 22 (2010) 296–304. https://doi.org/10.1061/(ASCE)MT.1943-5533.0000018.

[33] V. Rostami, Y. Shao, A.J. Boyd, Carbonation Curing versus Steam Curing for Precast Concrete Production, J. Mater. Civ. Eng. 24 (2012) 1221–1229. https://doi.org/10.1061/(asce)mt.1943-5533.0000462.

[34] D. Zhang, Y. Shao, Effect of early carbonation curing on chloride penetration and weathering carbonation in concrete, Constr. Build. Mater. 123 (2016) 516–526. https://doi.org/10.1016/j.conbuildmat.2016.07.041.

[35] J.G. Jang, H.K. Lee, Microstructural densification and CO2 uptake promoted by the carbonation curing of belite-rich Portland cement, Cem. Concr. Res. 82 (2016) 50–57. https://doi.org/10.1016/j.cemconres.2016.01.001.

[36] X. Pan, C. Shi, X. Hu, Z. Ou, Effects of CO2 surface treatment on strength and permeability

of one-day-aged cement mortar, Constr. Build. Mater. 154 (2017) 1087–1095. https://doi.org/10.1016/j.conbuildmat.2017.07.216.

[37] H. El-Hassan, Y. Shao, Z. Ghouleh, Reaction Products in Carbonation-Cured Lightweight Concrete, J. Mater. Civ. Eng. 25 (2013) 799–809. https://doi.org/10.1061/(asce)mt.1943-5533.0000638.

[38] L. Mo, F. Zhang, M. Deng, Mechanical performance and microstructure of the calcium carbonate binders produced by carbonating steel slag paste under CO2 curing, Cem. Concr. Res. 88 (2016) 217–226. https://doi.org/10.1016/j.cemconres.2016.05.013.

[39] Q. Chen, W. Ding, H. Sun, T. Peng, Mineral carbonation of yellow phosphorus slag and characterization of carbonated product, Energy. 188 (2019) 116102. https://doi.org/10.1016/j.energy.2019.116102.

[40] M.A. Boone, P. Nielsen, T. De Kock, M.N. Boone, M. Quaghebeur, V. Cnudde, Monitoring of stainless-steel slag carbonation using X-ray computed microtomography, Environ. Sci. Technol. 48 (2014) 674–680. https://doi.org/10.1021/es402767q.

[41] N. Li, N. Farzadnia, C. Shi, Microstructural changes in alkali-activated slag mortars induced by accelerated carbonation, Cem. Concr. Res. 100 (2017) 214–226. https://doi.org/10.1016/j.cemconres.2017.07.008.

[42] P.S. Humbert, J. Castro-Gomes, CO2 activated steel slag-based materials: A review, J. Clean. Prod. 208 (2019) 448–457. https://doi.org/10.1016/j.jclepro.2018.10.058.

[43] T. Wang, H. Huang, X. Hu, M. Fang, Z. Luo, R. Guo, Accelerated mineral carbonation curing of cement paste for CO2 sequestration and enhanced properties of blended calcium

silicate, Chem. Eng. J. 323 (2017) 320–329. https://doi.org/10.1016/j.cej.2017.03.157.

[44] M.Á. Sanjuán, E. Estévez, C. Argiz, D. del Barrio, Effect of curing time on granulated blast-furnace slag cement mortars carbonation, Cem. Concr. Compos. 90 (2018) 257–265. https://doi.org/10.1016/j.cemconcomp.2018.04.006.

[45] L. Mo, F. Zhang, M. Deng, F. Jin, A. Al-Tabbaa, A. Wang, Accelerated carbonation and performance of concrete made with steel slag as binding materials and aggregates, Cem. Concr. Compos. 83 (2017) 138–145. https://doi.org/10.1016/j.cemconcomp.2017.07.018.

[46] L. Mo, D.K. Panesar, Accelerated carbonation - A potential approach to sequester CO2 in cement paste containing slag and reactive MgO, Cem. Concr. Compos. 43 (2013) 69–77. https://doi.org/10.1016/j.cemconcomp.2013.07.001.

[47] ASTM, ASTM C305/2014 - Standard Practice for, Astm. (2015) 1–3. https://doi.org/10.1520/C0305-14.2.

[48] ASTM, ASTM 6433 Standard Practice for Roads and Parking Lots Pavement Condition Index Surveys, (2007) 1–8. https://doi.org/10.1520/C0192.

[49] ASTM C143/C143M, Standard Test Method for Slump of Hydraulic-Cement Concrete, Astm C143. (2015) 1–4. https://doi.org/10.1520/C0143.

[50] P. Yu, R.J. Kirkpatrick, B. Poe, P.F. McMillan, X. Cong, Structure of Calcium Silicate Hydrate (C-S-H): Near-, Mid-, and Far-Infrared Spectroscopy, 2004. https://doi.org/10.1111/j.1151-2916.1999.tb01826.x.

[51] A. Puertas, F; Fernandez-Jimenez, Mineralogical and microstructural characterisation of alkali-activated fly ash/slag pastes, Environ. - MDPI. 4 (2017) 1–14.

https://doi.org/10.3390/environments4030044.

[52] K. Kupwade-Patil, S.D. Palkovic, A. Bumajdad, C. Soriano, O. Büyüköztürk, Use of silica fume and natural volcanic ash as a replacement to Portland cement: Micro and pore structural investigation using NMR, XRD, FTIR and X-ray microtomography, Constr. Build. Mater. 158 (2018) 574–590. https://doi.org/10.1016/j.conbuildmat.2017.09.165.

[53] J. Ihli, W.C. Wong, E.H. Noel, Y.Y. Kim, A.N. Kulak, H.K. Christenson, M.J. Duer, F.C. Meldrum, Dehydration and crystallization of amorphous calcium carbonate in solution and in air, Nat. Commun. 5 (2014) 1–10. https://doi.org/10.1038/ncomms4169.

[54] Z. Shi, C. Shi, S. Wan, N. Li, Z. Zhang, Effect of alkali dosage and silicate modulus on carbonation of alkali-activated slag mortars, Cem. Concr. Res. 113 (2018) 55–64. https://doi.org/10.1016/j.cemconres.2018.07.005.

[55] M. Thiery, G. Villain, P. Dangla, G. Platret, Investigation of the carbonation front shape on cementitious materials: Effects of the chemical kinetics, Cem. Concr. Res. (2007). https://doi.org/10.1016/j.cemconres.2007.04.002.

[56] A. Hidalgo, S. Petit, C. Domingo, C. Alonso, C. Andrade, Microstructural characterization of leaching effects in cement pastes due to neutralisation of their alkaline nature. Part I: Portland cement pastes, Cem. Concr. Res. 37 (2007) 63–70. https://doi.org/10.1016/j.cemconres.2006.10.002.

[57] S.A. Bernal, R.M. de Gutierrez, J.L. Provis, V. Rose, Effect of silicate modulus and metakaolin incorporation on the carbonation of alkali silicate-activated slags, Cem. Concr. Res. (2010). https://doi.org/10.1016/j.cemconres.2010.02.003.

[58] I. García Lodeiro, D.E. Macphee, A. Palomo, A. Fernández-Jiménez, Effect of alkalis on fresh C-S-H gels. FTIR analysis, Cem. Concr. Res. 39 (2009) 147–153. https://doi.org/10.1016/j.cemconres.2009.01.003.

[59] S.N. Costa, V.N. Freire, E.W.S. Caetano, F.F. Maia, C.A. Barboza, U.L. Fulco, E.L. Albuquerque, DFT Calculations with van der Waals Interactions of Hydrated Calcium Carbonate Crystals CaCO3·(H2O, 6H2O): Structural, Electronic, Optical, and Vibrational Properties, J. Phys. Chem. A. 120 (2016) 5752–5765. https://doi.org/10.1021/acs.jpca.6b05436.

[60] M. Sato, S. Matsuda, Structure of vaterite and infrared spectra, Zeitschrift Fur Krist. - New Cryst. Struct. 129 (1969) 405–410. https://doi.org/10.1524/zkri.1969.129.5-6.405.

[61] C. Shi, Steel Slag—Its Production, Processing, Characteristics, and Cementitious Properties, J. Mater. Civ. Eng. 16 (2004) 230–236. https://doi.org/10.1061/(asce)0899-1561(2004)16:3(230).

[62] G. Fang, W.K. Ho, W. Tu, M. Zhang, Workability and mechanical properties of alkali-activated fly ash-slag concrete cured at ambient temperature, Constr. Build. Mater. 172 (2018) 476–487. https://doi.org/10.1016/j.conbuildmat.2018.04.008.

[63] H. Jiang, Z. Qi, E. Yilmaz, J. Han, J. Qiu, C. Dong, Effectiveness of alkali-activated slag as alternative binder on workability and early age compressive strength of cemented paste backfills, Constr. Build. Mater. (2019). https://doi.org/10.1016/j.conbuildmat.2019.05.162.

[64] A.A.S. Javid, P. Ghoddousi, M. Jaberizadeh, B. Bozorgmehr, The comparison and introducing of plate test and electrical resistance methods of determining the setting time and thixotropy of self-consolidating concrete, J. Test. Eval. 48 (2020).

https://doi.org/10.1520/JTE20180326.

[65] S. Mindess, Developments in the formulation and reinforcement of concrete, 2019. https://doi.org/10.1016/C2017-0-03347-5.

[66] S.P. Zhang, L. Zong, Evaluation of relationship between water absorption and durability of concrete materials, Adv. Mater. Sci. Eng. 2014 (2014). https://doi.org/10.1155/2014/650373.

[67] G. De Schutter, K. Audenaert, Evaluation of water absorption of concrete as a measure for resistance against carbonation and chloride migration, Mater. Struct. Constr. 37 (2004) 591–596. https://doi.org/10.1617/14045.

[68] M.T. Bassuoni, M.L. Nehdi, T.R. Greenough, Enhancing the reliability of evaluating chloride ingress in concrete using the ASTM C 1202 rapid chloride penetrability test, J. ASTM Int. 3 (2006). https://doi.org/10.1520/jai13403.

[69] NT Build 492, Concrete, mortar and cement-based repair materials: Chloride migration coefficient from non-steady-state migration experiments, Measurement. (1999).

[70] R.I. Khan, W. Ashraf, J. Olek, Amino acids as performance-controlling additives in carbonation-activated cementitious materials, Cem. Concr. Res. 147 (2021) 1–39. https://doi.org/10.1016/j.cemconres.2021.106501.

[71] S. Kim, C.B. Park, Dopamine-induced mineralization of calcium carbonate vaterite microspheres, Langmuir. 26 (2010) 14730–14736. https://doi.org/10.1021/la1027509.

[72] P. Ziehl, F. Matta, N. Aich, N. Zohhadi, I.A. Khan, P. Ziehl, F. Matta, N. Aich, N. Zohhadi, I.A. Khan, R.U.S.A. Data, (12) United States Patent, 2 (2014).

[73] B. Cantaert, D. Kuo, S. Matsumura, T. Nishimura, T. Sakamoto, T. Kato, Use of Amorphous Calcium Carbonate for the Design of New Materials, Chempluschem. 82 (2017) 107–120. https://doi.org/10.1002/cplu.201600457.

[74] K.S. Kamasamudram, W. Ashraf, E.N. Landis, R.I. Khan, Effects of ligno– and delignified–cellulose nanofibrils on the performance of cement-based materials, J. Mater. Res. Technol. 13 (2021) 321–335. https://doi.org/10.1016/j.jmrt.2021.04.090.

[75] M.A. Akhlaghi, R. Bagherpour, H. Kalhori, Application of bacterial nanocellulose fibers as reinforcement in cement composites, Constr. Build. Mater. 241 (2020) 118061. https://doi.org/10.1016/j.conbuildmat.2020.118061.

[76] K.S. Kamasamudram, W. Ashraf, E.N. Landis, Cellulose nanofibrils with and without nanosilica for the performance enhancement of portland cement system, Constr. Build. Mater. 285 (2021) 121547. https://doi.org/10.1016/j.conbuildmat.2020.121547.

[77] T.F.R. Claramunt J, Ardanuy M, Arevalo R, Pares F, Mechanical performance of ductile cement mortar composites reinforced with nanofibrillated cellulose, Strain Hardening Cem. Compos. (2011) 131–138.

[78] O.A. Hisseine, A.F. Omran, A. Tagnit-Hamou, Influence of cellulose filaments on cement paste and concrete, J. Mater. Civ. Eng. 30 (2018) 1–14. https://doi.org/10.1061/(ASCE)MT.1943-5533.0002287.

[79] Y. Fang, J. Wang, X. Qian, L. Wang, G. Lin, Z. Liu, Bio-inspired functionalization of very fine aggregates for better performance of cementitious materials, Constr. Build. Mater. 241 (2020) 118104. https://doi.org/10.1016/j.conbuildmat.2020.118104.

[80] ASTM:C157/C157M-08, Standard Test Method for Length Change of Hardened Hydraulic-Cement Mortar and Concrete, ASTM Int. 08 (2008) 1–7. https://doi.org/10.1520/C0157.

[81] B.P. Lee, P.B. Messersmith, J.N. Israelachvili, J.H. Waite, Mussel-inspired adhesives and coatings, Annu. Rev. Mater. Res. 41 (2011) 99–132. https://doi.org/10.1146/annurev-matsci-062910-100429.

[82] M.S. Eisa, M.E. Basiouny, E.A. Fahmy, Effect of metakaolin-based geopolymer concrete on the length of rigid pavement slabs, Innov. Infrastruct. Solut. 6 (2021) 1–9. https://doi.org/10.1007/s41062-021-00465-5.

[83] M. Hsie, C. Tu, P.S. Song, Mechanical properties of polypropylene hybrid fiber-reinforced concrete, Mater. Sci. Eng. A. 494 (2008) 153–157. https://doi.org/10.1016/j.msea.2008.05.037.

[84] J.J. Heckman, R. Pinto, P.A. Savelyev, 済無No Title No Title No Title, Angew. Chemie Int. Ed. 6(11), 951–952. 27 (1967) 1357–1364.

[85] I.M. Weiss, C. Muth, R. Drumm, H.O.K. Kirchner, Thermal decomposition of the amino acids glycine, cysteine, aspartic acid, asparagine, glutamic acid, glutamine, arginine and histidine Ingrid M. Weiss*, Christina Muth, Robert Drumm & Helmut O.K. Kirchner, (2017) 1–23.

[86] W. Ashraf, J. Olek, Elucidating the accelerated carbonation products of calcium silicates using multi-technique approach, J. CO2 Util. 23 (2018). https://doi.org/10.1016/j.jcou.2017.11.003.

[87] L. Jiao, M. Su, L. Chen, Y. Wang, H. Zhu, H. Dai, Natural cellulose nanofibers as

sustainable enhancers in construction cement, PLoS One. 11 (2016). https://doi.org/10.1371/journal.pone.0168422.

[88] N.K. Lee, K.T. Koh, M.O. Kim, G.H. An, G.S. Ryu, Physicochemical changes caused by reactive MgO in alkali-activated fly ash/slag blends under accelerated carbonation, Ceram. Int. 43 (2017) 12490–12496. https://doi.org/10.1016/j.ceramint.2017.06.119.

[89] N.T. Dung, R. Hay, A. Lesimple, K. Celik, C. Unluer, Influence of CO2 concentration on the performance of MgO cement mixes, Cem. Concr. Compos. 115 (2021). https://doi.org/10.1016/j.cemconcomp.2020.103826.

[90] J.J. Thomas, S. Musso, I. Prestini, Kinetics and activation energy of magnesium oxide hydration, J. Am. Ceram. Soc. 97 (2014) 275–282. https://doi.org/10.1111/jace.12661.

[91] P. Ballirano, C. De Vito, V. Ferrini, S. Mignardi, The thermal behaviour and structural stability of nesquehonite, MgCO3·3H2O, evaluated by in situ laboratory parallel-beam X-ray powder diffraction: New constraints on CO2 sequestration within minerals, J. Hazard. Mater. 178 (2010) 522–528. https://doi.org/10.1016/j.jhazmat.2010.01.113.

[92] M. Merlini, F. Sapelli, P. Fumagalli, G.D. Gatta, P. Lotti, S. Tumiati, M. Aabdellatief, A. Lausi, J. Plaisier, M. Hanfland, W. Crichton, J. Chantel, J. Guignard, C. Meneghini, A. Pavese, S. Poli, High-temperature and high-pressure behavior of carbonates in the ternary diagram CaCO3-MgCO3-FeCO3, Am. Mineral. 101 (2016) 1423–1430. https://doi.org/10.2138/am-2016-5458.

[93] W. Cheng, C. Zhang, H. Cheng, Z. Chen, H. Liao, F. Cheng, Effect of ethanol on the crystallization and phase transformation of MgCO3·3H2O in a MgCl2–CO2–NH3·H2O system, Powder Technol. 335 (2018) 164–170.

https://doi.org/10.1016/j.powtec.2018.04.063.

[94] V. Ferrini, C. De Vito, S. Mignardi, Synthesis of nesquehonite by reaction of gaseous CO2 with Mg chloride solution: Its potential role in the sequestration of carbon dioxide, J. Hazard. Mater. 168 (2009) 832–837. https://doi.org/10.1016/j.jhazmat.2009.02.103.

[95] S. GERDEMANN, D. DAHLIN, W. OCONNOR, Carbon Dioxide Sequestration by Aqueous Mineral Carbonation of Magnesium Silicate Minerals, Greenh. Gas Control Technol. - 6th Int. Conf. (2003) 677–682. https://doi.org/10.1016/b978-008044276-1/50108-2.

[96] L. Wang, S.S. Chen, D.C.W. Tsang, C.S. Poon, K. Shih, Recycling contaminated wood into eco-friendly particleboard using green cement and carbon dioxide curing, J. Clean. Prod. 137 (2016) 861–870. https://doi.org/10.1016/j.jclepro.2016.07.180.

[97] G. Villain, M. Thiery, G. Platret, Measurement methods of carbonation profiles in concrete: Thermogravimetry, chemical analysis and gammadensimetry, Cem. Concr. Res. 37 (2007) 1182–1192. https://doi.org/10.1016/j.cemconres.2007.04.015.

[98] W. Deboucha, N. Leklou, A. Khelidj, M.N. Oudjit, Hydration development of mineral additives blended cement using thermogravimetric analysis (TGA): Methodology of calculating the degree of hydration, Constr. Build. Mater. 146 (2017) 687–701. https://doi.org/10.1016/j.conbuildmat.2017.04.132.

[99] K. Scrivener, R. Snellings, B. Lothenbach, A Practical Guide to Microstructural Analysis of Cementitious Materials, 2018. https://doi.org/10.1201/b19074.

[100] L. Mo, D.K. Panesar, Effects of accelerated carbonation on the microstructure of Portland

cement pastes containing reactive MgO, Cem. Concr. Res. 42 (2012) 769–777. https://doi.org/10.1016/j.cemconres.2012.02.017.

[101] R. Zhang, N. Bassim, D.K. Panesar, Characterization of Mg components in reactive MgO - Portland cement blends during hydration and carbonation, J. CO2 Util. 27 (2018) 518–527. https://doi.org/10.1016/j.jcou.2018.08.025.

[102] L. Wang, L. Chen, J.L. Provis, D.C.W. Tsang, C.S. Poon, Accelerated carbonation of reactive MgO and Portland cement blends under flowing CO2 gas, Cem. Concr. Compos. 106 (2020). https://doi.org/10.1016/j.cemconcomp.2019.103489.

[103] N.T. Dung, C. Unluer, Carbonated MgO concrete with improved performance: The influence of temperature and hydration agent on hydration, carbonation and strength gain, Cem. Concr. Compos. 82 (2017) 152–164. https://doi.org/10.1016/j.cemconcomp.2017.06.006.

[104] L. Hopkinson, K. Rutt, G. Cressey, The transformation of nesquehonite to hydromagnesite in the system CaO-MgO-H2O-CO2: An experimental spectroscopic study, J. Geol. 116 (2008) 387–400. https://doi.org/10.1086/588834.

[105] R. Hay, N.T. Dung, A. Lesimple, C. Unluer, K. Celik, Mechanical and microstructural changes in reactive magnesium oxide cement-based concrete mixes subjected to high temperatures, Cem. Concr. Compos. 118 (2021) 103955. https://doi.org/10.1016/j.cemconcomp.2021.103955.

[106] W. Ashraf, J. Olek, Elucidating the accelerated carbonation products of calcium silicates using multi-technique approach, J. CO2 Util. 23 (2018) 61–74. https://doi.org/10.1016/j.jcou.2017.11.003.

[107] A. Kumar, S. Ketel, K. Vance, T. Oey, N. Neithalath, G. Sant, Water Vapor Sorption in Cementitious Materials-Measurement, Modeling and Interpretation, Transp. Porous Media. 103 (2014) 69–98. https://doi.org/10.1007/s11242-014-0288-5.

[108] M.B. Pinson, T. Zhou, H.M. Jennings, M.Z. Bazant, Inferring pore connectivity from sorption hysteresis in multiscale porous media, J. Colloid Interface Sci. 532 (2018) 118–127. https://doi.org/10.1016/j.jcis.2018.07.095.

[109] S. Brunauer, P.H. Emmett, E. Teller, Adsorption of gases in multimolecular layers, J. Am.Chem.Soc. 60 (1938) 309–319.

[110] P.P. Barrett, Elliott; Joyner, Leslei G; Halenda, The determination of pore volume and area distributions in porous substances. I. Computations from nitrogen isotherms, (1951).

[111] J. Hagymassy, S. Brunauer, R.S. Mikhail, Pore structure analysis by water vapor adsorption. I. t-Curves for water vapor, J. Colloid Interface Sci. 29 (1969) 485–491. https://doi.org/10.1016/0021-9797(69)90132-5.

[112] H.M. Jennings, A. Kumar, G. Sant, Quantitative discrimination of the nano-pore-structure of cement paste during drying: New insights from water sorption isotherms, Cem. Concr. Res. 76 (2015) 27–36. https://doi.org/10.1016/j.cemconres.2015.05.006.

[113] S.M. Evans, Novacem – carbon negative cement to transform the construction industry, Innov. Invest. Oppor. Carbon Capture Storage Carbon Capture Storage. (2008) 2–14.

[114] S. Zhang, Z. Ghouleh, Y. Shao, Effect of Carbonation Curing on Efflorescence Formation in Concrete Paver Blocks, J. Mater. Civ. Eng. 32 (2020) 04020127. https://doi.org/10.1061/(asce)mt.1943-5533.0003210.

[115] V. Rostami, Y. Shao, A.J. Boyd, Durability of concrete pipes subjected to combined steam and carbonation curing, Constr. Build. Mater. 25 (2011) 3345–3355. https://doi.org/10.1016/j.conbuildmat.2011.03.025.

[116] H. El-Hassan, Y. Shao, Z. Ghouleh, Effect of initial curing on carbonation of lightweight concrete masonry units, ACI Mater. J. 110 (2013) 441–450. https://doi.org/10.14359/51685791.

[117] D. Zhang, Y. Shao, Early age carbonation curing for precast reinforced concretes, Constr. Build. Mater. 113 (2016) 134–143. https://doi.org/10.1016/j.conbuildmat.2016.03.048.

[118] ASTM C39, Compressive Strength of Cylindrical Concrete Specimens, ASTM Stand. (2015) 1–7. https://doi.org/10.1520/C0039.

[119] ASTM C1202, Standard Test Method for Electrical Indication of Concrete's Ability to Resist Chloride Ion Penetration, Am. Soc. Test. Mater. (2012) 1–8. https://doi.org/10.1520/C1202-12.2.

[120] C. Elements, U. Drilled, C. Cores, C.C. Specimens, H. Concrete, B. Statements, Astm C42/C42M−16, ASTM Int. (2012).

[121] N. Otsuki, S. Nagataki, K. Nakashita, Evaluation of the AgNO3 solution spray method for measurement of chloride penetration into hardened cementitious matrix materials, Constr. Build. Mater. 7 (1993) 195–201. https://doi.org/10.1016/0950-0618(93)90002-T.

[122] L. Li, M. Cao, H. Yin, Comparative roles between aragonite and calcite calcium carbonate whiskers in the hydration and strength of cement paste, Cem. Concr. Compos. 104 (2019). https://doi.org/10.1016/j.cemconcomp.2019.103350.

[123] M. Hambach, H. Möller, T. Neumann, D. Volkmer, Portland cement paste with aligned carbon fibers exhibiting exceptionally high flexural strength (> 100 MPa), Cem. Concr. Res. 89 (2016) 80–86. https://doi.org/10.1016/j.cemconres.2016.08.011.

Appendix: Experimental Methods

Thermogravimetric analysis (TGA)

The commercially available TGA 550 TA instrument was used in this study. Thin carbonated plate samples (category 1) were used for this test. The thin carbonated sample was first ground using a mortar pestle. Approximately 35 ~ 40 mg of ground power sample was loaded into a platinum pan and kept in an isothermal condition at around 25°C for 5 minutes. Afterwards, the temperature of the TGA chamber was increased to 980°C with a ramp of 15°C per minute. N_2 gas was purged in the entire process. Initially, for a few batches, three replicate samples were tested through TGA to validate for any deviation in carbonation across samples. The test result deviations were less than 2% by weight of total carbonated samples. Due to the low deviation, TGA was performed only with one sample for the remainder of the batches. The following decomposition temperatures were used for analysis of TGA data in this current study. Chemically bound water decomposes from 100~600°C [97–99]. $Ca(OH)_2$ decomposes to CaO and H_2O at around 450°C [97,99]. $CaCO_3$ decomposes to CaO and CO_2 at 600~800°C [97,99]. The amount of CaO content in the paste was calculated from the summation of CaO from $Ca(OH)_2$ and from $CaCO_3$.

Fourier transform infrared spectroscopy (FTIR)

Thin carbonated plate samples (category 1) were ground for this measurement. The commercially available Nicolet iS50 FTIR from Thermo Scientific was used for this test. The spectra were collected using the Attenuated Total Reflection (ATR) mode with 4 cm^{-1} resolution and 32 scans per sample.

TGA with coupled mass spectrometer (TGA-MS)

For few samples TGA was coupled with a mass spectrometer (MS). This coupled TGA-MS system enabled the separation and identification of any volatile species coming off the sample during the heating process. In this case, TGA was performed using a Netzsch STA 449 F3 Jupiter Simultaneous Thermal Analysis (STA) instrument. All samples were measured under ultra-high purity helium gas (flow of 50 ml/min). The temperature was increased at a rate of 10 ºC/min and gases were transferred to the GC/MS instrumentation via a heated (250 ºC) transfer line. An Agilent Technologies 7890A GC system equipped with a non-polar capillary column (Agilent J&B HP-5 packed with [5%-Phenyl-methylpolysiloxane]) coupled with a 5975 MSD spectrometer was used for the analyses of the gases released from the samples. A gas injection was triggered every minute (60 sec) from the beginning of the heating cycle, and 0.25 ml of gas was sampled from the gases released by the compound and carrier gas (He).

X-ray Diffraction (XRD)

X-ray diffraction patterns were collected via Bruker D-500 spectrometer using a Cu Kα radiation (40 kV, 30 mA). The diffraction patterns were obtained for the 2θ range of 5° to 80° using a step size of 0.02 (2θ) per second.

XRD analysis was performed using commercially available software (Match! Phase Analysis using Powder Diffraction). The used PDF card numbers were PDF #96-900-1298, PDF #96-901-5894, PDF #96-900-2349, PDF #96-900-7621, PDF #96-901-2402, PDF #96-900-2821, PDF #96-101-1118, and PDF #96-900-5779 for calcite, aragonite, brucite, hydro-magnesite, nesquehonite, magnesite, MgO, and wollastonite respectively.

Dynamic vapor sorption (DVS)

Commercially available DVS equipment (TA instrument, Q5000) was used to obtain adsorption-sorption isotherm of carbonated samples prepared in section 2.2 (category one). The samples were soaked in DI water for 48 hours before testing to ensure full saturation. After soaking approximately 15~20 mg of sample was loaded in a quartz pan. The sample was first equilibrated at 97.5% RH for 5760 seconds. After this point, the RH was gradually reduced (with 5~10% RH steps) to obtain the desorption isotherm. After reaching 0% RH, the RH was gradually increased (with 5 to 10% RH steps) up to 97.5% to obtain adsorption isotherms. Mass equilibrium was reached at each RH when the mass fluctuation was less than 0.001% for 15 minutes. Throughout the experiment, the temperature was kept constant at 23 deg Celsius. During the experiment, N2 gas was purged.

Scanning electron microscope (SEM)

The microstructures of 300 hours and 1200 hours carbonated cured samples were evaluated using Hitachi 3000N SEM. The instrument was operated in high vacuum mode with a 30 kV accelerated voltage and a working distance of about 10 mm. The cement paste sample was coated with Platinum (Pt) before capturing the SEM images.

Mercury intrusion porosimetry (MIP)

Mercury intrusion porosimetry is used to determine the meso-porous (pore radius 2~50 nm) and macro-porous (> 50 nm) structure of cementitious materials. The MIP test was performed on control batch, and binder paste samples containing 0.1% CNF, 0.1% Dopamine, and 0.1% CNF-Dopamine dosages after 28 days of carbonation curing. The sample size was around 15 ×15×15

mm. The surface tension γ of mercury is 0.485 N/m, and the average contact angle θ between mercury and the pore wall is 130°. MIP tests were conducted on an AutoPore IV 9500 V2.03.01, from Micrometrics Instrument Corporation, under a maximum pressure of 413 MPa to reach pores with a diameter of 3.02 nm.

Mechanical performances

The compressive and flexural strength of 25 mm x 25 mm cube and 40 mm x 20 mm x 15 mm beam samples prepared from paste were measured after 300 hours, 600 hours and 1200 hours of carbonation curing. The compressive strength was measured via MTS Landmark servo hydraulic test system using a displacement rate of 0.02mm/sec. The flexural strength was measured via MTS Criterion Model 43 using displacement rate of 0.2 mm/min.

Compressive strength test

The compressive strength of the concrete cylinders (sample category 2) was measured using ASTM C39/C39M after 3 days, 7 days and 28 days of curing [118]. The average compressive strength of the four cylinders was used for each test data presented in this study. A loading rate of 1780~2670 N/s was used during the compressive strength test.

Length change

The length change was measured using the mortar samples indicated in the sample preparation section in accordance with the ASTM C 157 standard [80]. The length was calculated using the following equation in accordance with ASTM C157,

$$Length\ chnage\ (\%) = \frac{CRD_f - CRD_i}{250} \times 100 \qquad \text{eqn. A1}$$

Where, CRD=difference between the comparator reading of the specimen and the reference bar at any age.

Rapid chloride penetration test (RCPT)

To perform the rapid chloride penetration test, the ASTM C1202 standard test method was followed [119]. The diameter and thickness of the sample specimens were 100 mm and 50 mm, respectively. First, sample specimens of corresponding curing conditions were collected from the core of the cylinder specimens (category 2) following the ASTM C42 standard [120]. Coring was done with a drilling rig equipped with a diamond dressed core bit so that the microstructure would be undisturbed. Once the specimen was ready, it went through the conditioning process as per the standard before starting the test. To conduct the rapid chloride penetration test, a commercially available device called Giatec-Perma was used. The test specimen was placed between two cells containing 3% NaCl solution and 0.3 N NaOH solution.

Figure 0.1: Measurements of chloride penetration depth

Upon completion of the 6-hour test, the specimens were removed from the test setup, split in the middle, and then an $AgNO_3$ solution was sprayed on the wet specimens after cutting them. This helped to form a white AgCl layer which indicated the chloride penetration into the system [121]. The thickness of the AgCl layer was measured for further analysis in which the correlation between the chloride penetration depth and the durability of the supplementary cementitious materials was investigated. For determining the chloride ion penetration depth, at least four measurements were taken from each half (Figure 0.1); so, a total of 8 measurements were taken from each specimen to find the average.

Beam failure criteria

To determine the flexural capacity of carbonation cured composites, the author performed a 3-point bending test of paste samples as shown in Figure 0.2. The beam size for this test was 40 x 20 x 15 mm. The beam depth was 20 mm, which satisfied the ACI minimum beam depth criteria (ACI 9.3.1.1). Figure 0.2 (a) shows that the beam has maximum shear force at support and moment at its center. Shear failure occurs at the support with an inclined crack and flexural failure occurs at mid-span with a vertical crack [122,123]. Based on the crack pattern, it was assumed that the beam failure was due to the flexure as the beam failed at the center. ACI shear capacity equations will not be applicable in this case as those ACI equations are based on concrete samples. Hence, the author assumed the beam failure of the 3-point bending test was due to flexure.

(a)

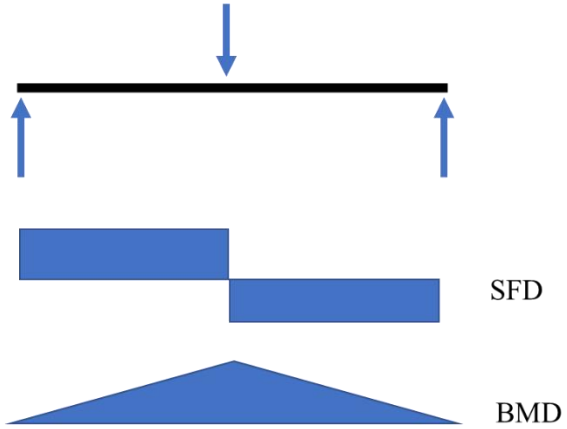

(b)

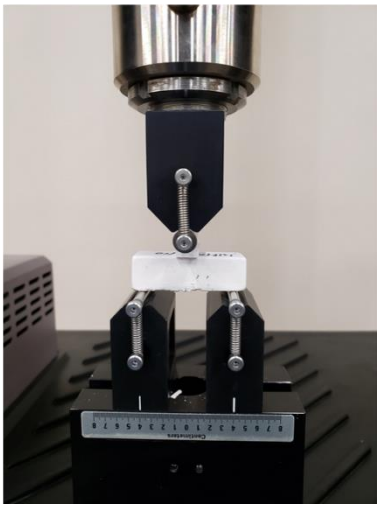

Figure 0.2: (a) Shear force and bending moment diagram, (b) experimental setup for 3-point bending test